INVESTIGATING ANTHOCYANIN PROFILE, LOCALIZATION, AND TRANSPORT IN *APONOGETON MADAGASCARIENSIS*

by

Georgia Lee Denbigh

Submitted in partial fulfillment of the requirements
for the degree of Master of Science

at

Dalhousie University
Halifax, Nova Scotia
July 2020

I dedicate this thesis to former and future self. Let this thesis be a reminder of all your hardships and accomplishments. You are strong, smart, and capable. I am so proud of you!

TABLE OF CONTENTS

LIST OF TABLES

LIST OF FIGURES

ABSTRACT

Lace plant *(Aponogeton madagascariensis)* forms perforations throughout its leaves via developmental programmed cell death (PCD). Newly emerged 'pre-perforated' lace plant leaves are filled with anthocyanin pigmentation, and the first visible sign of cell death is the disappearance of anthocyanins in 'window' leaves, which generates a unique PCD gradient. Due to the conspicuous pattern of anthocyanin loss at an early stage, it is evident that anthocyanins play an important role in lace plant PCD. Previous research on anthocyanins in lace plants has identified highly condensed bodies, named anthocyanin vacuolar inclusions (AVIs), that are visible in the apex of window leaves using light microscopy, however, the structure of AVIs and their function in leaf development and PCD remains unclear. Further, the intracellular transport of anthocyanins from the endoplasmic reticulum (ER; biosynthesis site) to the vacuole (accumulation site) is unknown in lace plant. Three models have been proposed: vesicular, ligandin, or autophagic transport. Even though the involvement of the ER is well-documented in animal PCD, little is known about ER dynamics in lace plant PCD. Therefore, the objectives of the study are (1) to isolate and identify anthocyanin species present in different lace plant tissues, (2) to investigate anthocyanins and AVIs in lace plant leaves by (i) determining the ultrastructure and localization of anthocyanins and AVIs, (ii) determining the mode of intracellular transport of anthocyanins, and (iii) investigating ER changes across the PCD gradient, and (3) to determine the role of anthocyanins in lace plant PCD.

Ultra-pressure liquid-chromatography (UPLC) and mass-spectrometry (MS) were utilized to profile anthocyanins in lace plant leaves and inflorescences. A combination of long-term, live-cell imaging and transmission electron microscopy (TEM) were used to determine the localization of AVIs in lace plant leaves. A protocol was optimized for 3,3'-dihexyloxacarbocyanine iodide, a fluorescent dye, to observe ER changes in lace plant leaves across the PCD gradient using confocal laser scanning microscopy (CLSM). TEM was also used to compare ER in healthy and dying cells. Lastly, pharmacological experimentation was performed with anthocyanin modulators, methyl jasmonate (a biosynthesis promoter) and phenidone (a biosynthesis inhibitor), to determine the effect on perforation formation in lace plant leaves. Results indicated that anthocyanin profiles differ among the various developmental leaf stages and inflorescences. Microscopic observations determined that AVIs are more visible in the apex of window leaves compared to the mid-regions. Based on CLSM results, two forms of anthocyanin bodies that differed at the leaf apex and mid-regions were observed: a large, singular spherical body (approximately 1-2 μm in size) located in cells at the window apex and multiple small, spherical bodies (less than 1 μm) located in vasculature and NPCD cells in the mid-regions. Transmission electron microscopy of areoles in the mid-regions of window stage leaves revealed that AVIs are deposited in ER-derived vesicles for transportation to the vacuole, which supports the vesicular transport model. CLSM provided evidence of ER changes between developmental leaf-stage, as well as across the PCD gradient. Addition of anthocyanin modulators significantly increased (methyl jasmonate treatment) and decreased (phenidone treatment) anthocyanin content in lace plant leaves, but the anthocyanin modulators did not significantly affect perforation number at the concentrations used. The results of the study suggest the differential occurrence of anthocyanin species and their potential role at specific stages of lace plant leaf development and contributes to the understanding of AVIs and anthocyanin transport, as well as corresponding structural changes taking place in the ER, an organelle involved in the transport mechanism of anthocyanins.

LIST OF ABBREVIATIONS USED

a.u.	Absorbance units
AAFC	Agriculture and Agri-Food Canada
ABC	ATP-binding cassette
ACT	Acyltransferases
ANOVA	Analysis of variance
ANS	Anthocyanidin synthase
AVI	Anthocyanin vacuolar inclusion
Ca^{2+}	Calcium ions
CHI	Chalcone isomerase
CHS	Chalcone synthase
CLSM	Confocal laser scanning microscopy
CMXRos	Mitotracker Red CMXRos
DAD	Diode array detector
DFR	Dihydroflavonol 4-reductase
dH_2O	Distilled water
DIC	Differential interference contrast
DiOC6(3)	3,3'-Dihexyloxacarbocyanine iodide
DMSO	Dimethyl sulfoxide
DNA	Deoxyribonucleic acid
EPCD	Early-programmed cell death
ER	Endoplasmic reticulum
ESI	Electrospray ionization

F3H	Flavanone 3-hydroxylase
FA	Formic acid
H^+DT	Proton-gradient-dependent transporter
HPLC	High-pressure liquid chromatography
L0	Leaf zero
L1	Leaf one
L2	Leaf two
LC	Liquid chromatography
LDOX	Leucoanthocyanidin dioxygenase
LPCD	Late-programmed cell death
MeJA	Methyl jasmonate
MRM	Multiple reaction monitoring
MS	Mass spectrometry
MS/MS	Tandem mass spectrometry
NMR	Nuclear magnetic resonance
NPCD	Non-programmed cell death
PCD	Programmed cell death
PV	Pre-vacuolar vesicle
ROS	Reactive oxygen species
SE	Standard error
TEM	Transmission electron microscopy
UFGT	Anthocyanin 3-O-glucosyltransferase
UPLC	Ultra-pressure liquid chromatography

UPR	Unfolded protein response
UV	Ultraviolet

ACKNOWLEDGEMENTS

I would like to thank my supervisors, Arunika Gunawardena and Christian Lacroix, for their guidance and support in the completion of my thesis. Thank you to Patrice Coté, Shawna MacKinnon, and Harrison Wright for serving on my committee and answering my innumerable questions. Thank you to the Gunawardena lab members for making the lab a stimulating and enjoyable environment – working with all of you has been a pleasure! I appreciate the assistance of Cassandra Hirte in the completion of the pharmacological experiments.

I want to thank the biology graduate students for their continuous encouragement and moral support. I have never met a group of more caring, inspiring, and motivated students. I cannot wait to see the future of academia and science with you all at the forefront. I am extremely appreciative of Nathan Hoffmann (my biggest cheerleader) for his endless emotional support.

I am grateful for the graduate scholarships provided that funded the project, namely the Natural Sciences and Engineering Research Council of Canada (NSERC) Graduate Scholarship, the Nova Scotia Research and Innovation Graduate Scholarship, and Dr. Gunawardena's NSERC Discovery Grant.

CHAPTER 1: INTRODUCTION

1.1. PLANT METABOLITES

Plants produce a wide range of organic molecules that participate in growth, development and survival (Croteau et al. 2000; Tiwari and Rana 2015). These organic compounds can be broadly generalized into two main groups based on functionality: primary and secondary metabolites (Croteau et al. 2000; Crozier et al. 2008). Primary metabolites are essential for metabolism, growth, development, and reproduction in plants (Croteau et al. 2000; Hanson 2003; Katerova et al. 2012). They are low molecular weight compounds, such as nucleic acids, amino acids, carbohydrate, and lipids, that are common to all plants and occur in all cells (Rhodes 1994; Hanson 2003; Aldred 2009a; Kabera et al. 2014). Secondary metabolites are traditionally defined as a diverse and complex set of organic compounds that are not directly involved in fundamental life processes but are important for interactions between the plant and its environment (Namdeo 2007; Crozier et al. 2008; Aldred 2009a; Kabera et al. 2014; Tiwari and Rana 2015; Guerriero et al. 2018). The absence of primary metabolites may result in the immediate death of the plant, whereas the absence of secondary metabolites may only reduce the survivability or fecundity of the plant (Tiwari and Rana 2015; Arimura and Maffei 2016). Certain classes of secondary metabolites are often restricted to a limited range of families or genera within the plant kingdom (Hanson 2003; Crozier et al. 2008; Tiwari and Rana 2015; Arimura and Maffei 2016). They are not found uniformly throughout the plant, and instead are limited to particular cells, organs or tissues (Rhodes 1994). Secondary metabolites were initially defined as waste products or errors resulting from primary metabolism (Bennett and Wallsgrove 1994; Rhodes 1994); however, the importance for secondary metabolites for the success of a plant has long been recorded and recognized.

Secondary metabolites can contribute to specific colours, odours and tastes in plants (Bennett and Wallsgrove 1994). These organic compounds play a deterrent or combative role in defense against herbivores, pests, and pathogens (Bennett and Wallsgrove 1994; Guerriero et al. 2018). They also contribute to physiological functions, such as attracting pollinators, prompting symbiosis, or providing structural components to vascular tissues (Guerriero et al. 2018). For example, anthocyanins (a type of flavonoid) are widely recognized for their contribution in floral and fruit pigmentation, which is crucial for reproductive success, but have also been found to play a crucial role in leaf morphogenesis in *Aponogeton madagascariensis* (Dauphinee et al. 2017). For these reasons, many have argued to rename "secondary metabolites," which imply a secondary, less important role in plants, to "specialized metabolites" as their minor function is no longer accepted (Arimura and Maffei 2016).

Plant secondary metabolites can be categorized based on chemical structure, composition, solubility in various solvents, or, most commonly, their biosynthetic pathway (Tiwari and Rana 2015). The classification of secondary metabolites is outlined in Figure 1. Recent categorization has grouped secondary metabolites into four broad classes: nitrogen- and sulphur-containing compounds, terpenes, and phenolics (Guerriero et al. 2018; Jamwal et al. 2018). Nitrogen- and sulphur-containing compounds are derived from common amino acids. Terpenes consist of five-carbon isopentanoid units, whereas phenolic compounds are synthesized via the shikimic acid pathway (Bennett and Wallsgrove 1994; Jamwal et al. 2018).

Phenolic compounds are a structurally diverse group of secondary metabolites that collectively possess hydroxylated aromatic rings (Bennett and Wallsgrove 1994; Aldred 2009b; Kabera et al. 2014; Shitan 2016). Most phenolic compounds polymerize to form larger molecules

termed polyphenols, which can be further subdivided into two classes: flavonoids and non-flavonoids (Crozier et al. 2008; Kabera et al. 2014).

Flavonoids are comprised of fifteen carbons, with two aromatic rings connected by a three-carbon bridge (Taylor and Grotewold 2005; Harborne 2007; Kabera et al. 2014). Because of their polar hydroxyl groups, they are often water-soluble and localized in the vacuole of plant cells (Crozier et al. 2008; Kabera et al. 2014). Various studies have identified high concentrations of flavonoids present in flowers, fruits, and leaves where they play central roles in plant development and environmental response (Taylor and Grotewold 2005; Crozier et al. 2008). Over 10,000 flavonoids have been identified and categorized into several classes, including flavones, flavanones, isoflavones, flavanonols, flavonols, chalcones, and anthocyanins (Taylor and Grotewold 2005; Crozier et al. 2008; Feng et al. 2017; Santos et al. 2017).

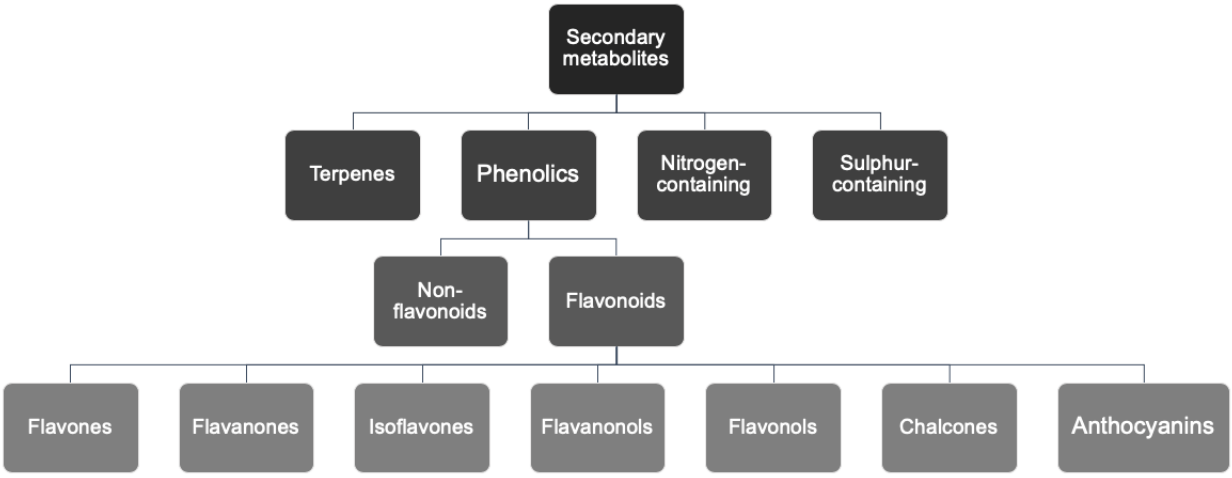

Figure 1. Classification of secondary metabolites. Secondary metabolites can be divided into four broad groups: terpenes, phenolics, nitrogen-containing, and sulfur-containing compounds. Phenolics can be subdivided into non-flavonoids or flavonoids. The flavonoids can be further categorized into flavones, flavanones, isoflavones, flavanonols, flavonols, chalcones, and anthocyanins. Information for the classification of secondary metabolites was gathered from Bennet and Wallsgrove (1994), Taylor and Grotewold (2005), Crozier et al. (2007), Kabera et al. (2014), Tiwari and Rana (2015), Guerriero et al. (2018), and Jamwal et al. (2018).

1.2. ANTHOCYANINS

1.2.1. Anthocyanin biosynthesis

Anthocyanins are found in numerous plant species and are responsible for the orange, red, blue, and purple pigments prominently seen in fruits and flowers (Chanoca et al. 2015; de Brito Francisco and Martinoia 2018). They are also present in the roots, shoots, stems, leaves, and seeds of plants. Over 600 different anthocyanin species have been identified in nature. However, their biosynthesis and regulation are highly conserved in plants (de Brito Francisco and Martinoia 2018; Liu et al. 2018). Anthocyanins are formed by the coupling of an anthocyanidin molecule with sugar and acyl conjugates (Crozier et al. 2008; Liu et al. 2018). The anthocyanidins differ from each other based on the number and position of the hydroxyl or methyl-ether group. A majority of the naturally occurring anthocyanins are derivatives of six widespread anthocyanidins: pelargonidin, cyanidin, delphinidin, peonidin, petunidin and malvidin (Crozier et al. 2008; Ananga et al. 2013). Common conjugated sugars are monosaccharides, such as glucose, galactose, arabinose, rhamnose, xylose and glucuronic acid (Ananga et al. 2013).

The anthocyanin biosynthetic pathway is an extension of the general flavonoid synthesis via the shikimate pathway (Ananga et al. 2013; Jaakola 2013; Liu et al. 2018). A general outline of the anthocyanin pathway is presented in Figure 2. Chalcone synthase (CHS) produces a naringenin chalcone from 4-coumaroyl-CoA and malonyl-CoA. Chalcone isomerase (CHI) isomerizes naringenin chalcone to naringin, which is then converted to dihydroflavonol by flavanone 3-hydroxylase (F3H). Dihydroflavonol 4-reductase (DFR) converts three dihydroflavonols to leucoanthocyanidins. Leucoanthocyanidin dioxygenase/anthocyanidin

synthase (LDOX/ANS) converts the colourless leucoanthocyanidins into coloured anthocyanidins, and a sugar is attached by anthocyanin 3-O-glucosyltransferase (UFGT). The anthocyanin may eventually be acylated with an aromatic acyl group by acyltransferases (ACT).

Anthocyanin biosynthesis and accumulation may be enhanced or reduced by external factors or internal stimuli (Solfanelli et al. 2006; Jaakola 2013; Liu et al. 2018). Anthocyanin production is modulated by light intensity and quality, temperature, and nutrient availability (Solfanelli et al. 2006; Jaakola 2013; Liu et al. 2018). High light intensity, UV and blue light increase anthocyanin synthesis and accumulation (Akula and Ravishankar 2011; Jaakola 2013; Liu et al. 2018). Low temperatures increase anthocyanin production, whereas high temperatures (30–35 °C) have been shown to decrease anthocyanin content (Jaakola 2013; Liu et al. 2018). The low anthocyanin abundance seen in plants grown at high temperatures is also thought to result from its interaction with reactive oxygen species (ROS) as opposed to reduced production (Liu et al. 2018). Sugar is a well-known stimulator of anthocyanin production, in addition to nitrogen and phosphorous starvation, whereas potassium starvation decreases anthocyanin (Hodges and Nozzolillo 1996; Das et al. 2012). Plant hormones also play a crucial role in regulating anthocyanin biosynthesis. Ethylene, abscisic acid, cytokinins and jasmonates stimulate anthocyanin production and accumulation, whereas auxin and gibberellin lower anthocyanin biosynthesis (Das et al. 2012; Jaakola 2013).

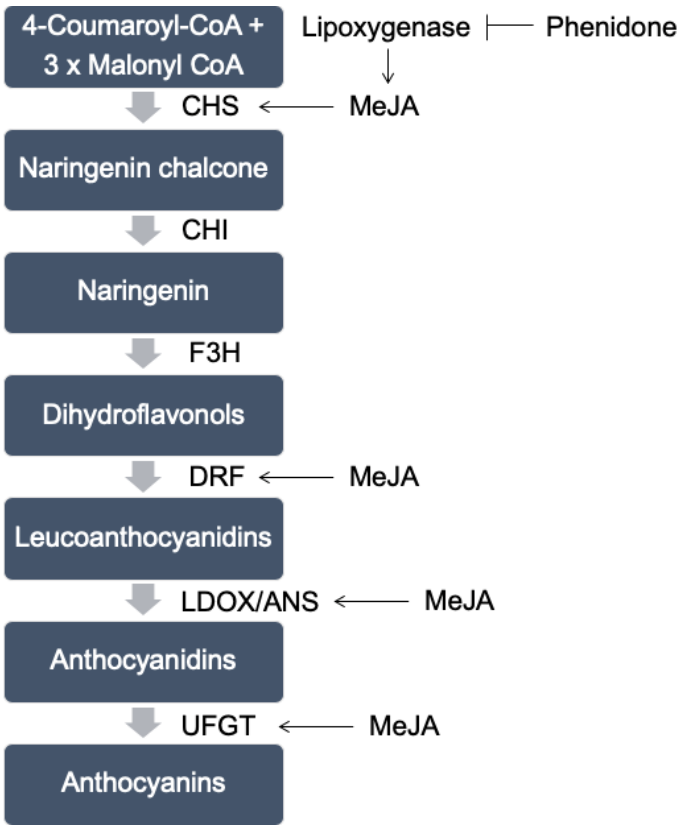

Figure 2. Anthocyanin biosynthesis pathway. Chalcone synthase (CHS) produces a naringenin chalcone from 4-coumaroyl-CoA and three malonyl-CoA. Chalcone isomerase (CHI) isomerizes naringenin chalcone to naringin, which is then converted to dihydroflavanols by flavanone 3-hydroxylase (F3H). Dihydroflavonol 4-reductase (DFR) then converts three dihydroflavonols to leucoanthocyanidins. Leucoanthocyanidin dioxygenase/anthocyanidin synthase (LDOX/ANS) converts the colourless leucoanthocyanidins into coloured anthocyanidins, and a sugar is attached by anthocyanin 3-O-glucosyltransferase (UFGT) to produce anthocyanins. Information on anthocyanin biosynthesis was gathered from Ananga et al. (2013), Jaakola (2013), and Liu et al. (2018). Methyl Jasmonate (MeJA) promotes CHS, DRF, LDOX/ANS, and UFGT activity (Saniewski et al. 2003; Shan et al. 2009; Qi et al. 2011). Phenidone is a lipoxygenases inhibitor, which prevents the synthesis of jasmonates in plant cells (Cucurou et al. 1991).

1.2.2. Anthocyanin translocation

Anthocyanins are synthesized in the cytosol by a multi-enzyme complex anchored onto the cytoplasmic face of the endoplasmic reticulum (ER; Zhang et al. 2006; Grotewold and Davies 2008; Pourcel et al. 2010; Sun et al. 2012). The compounds are then transported from the cytoplasm into vacuoles for storage. The translocation is necessary to prevent oxidation of

anthocyanin and to enable the pigments to accumulate and provide visible colouration (Zhang et al. 2006; Pourcel et al. 2010). There has been much debate about how anthocyanins are transported from sites of synthesis to sites of accumulation (Bassham 2015). Three non-exclusive models have been proposed for the intracellular transport of anthocyanin: the ligandin transporter (Marrs et al. 1995; Mueller et al. 2000; Conn et al. 2008; Grotewold and Davies 2008; Gomez et al. 2011), vesicular transport (Zhang et al. 2006; Poustka et al. 2007; Grotewold and Davies 2008; Conn et al. 2010; Gomez et al. 2011), and autophagic transport models (Pourcel et al. 2010; Bassham 2015; Chanoca et al. 2015).

According to the ligandin transporter model, anthocyanins are escorted to the tonoplast (vacuolar membrane) by glutathione *S*-transferase (GST) enzymes (Bassham 2015). Mutations in GST genes prevents the accumulation of anthocyanins within the vacuole (Poustka et al. 2007; Sun et al. 2012). This model differs from vesicular transport, which suggests that anthocyanins first translocate to the interior of the ER, are deposited in ER-derived membrane-bound vesicles, and are transported to the vacuole (Pourcel et al. 2010; Bassham 2015; Chanoca et al. 2015). The vesicular model was based on observations of anthocyanin bodies or aggregates accumulating in discrete cytoplasmic structures (Grotewold and Davies 2008; Pourcel et al. 2010). The third model involves an autophagic-like pathway. In this model, anthocyanins produced in the cytoplasm press against the tonoplast, where the vacuolar membrane extends and engulfs the anthocyanins, releasing the membrane-bound materials into the vacuole (Bassham 2015; Chanoca et al. 2015). This process resembles one form of autophagy, called microautophagy, but interestingly does not depend on autophagy-related gene *ATG5* (Pourcel et al. 2010; Bassham 2015; Chanoca et al. 2015).

Two additional translocation routes for the movement of anthocyanin across the tonoplast have been suggested for the ligandin transporter model, including ATP-binding cassette (ABC) protein transporters or proton-gradient-dependent transporters (H^+DT). The ABC family is a large, ubiquitous group of transmembrane proteins that transport metabolites across membranes via ATP hydrolysis (Grotewold and Davies 2008; Chanoca et al. 2015; Shitan 2016). This method differs from H^+DT that rely on the differential proton gradient present across the cytoplasm and vacuolar lumen (Grotewold and Davies 2008).

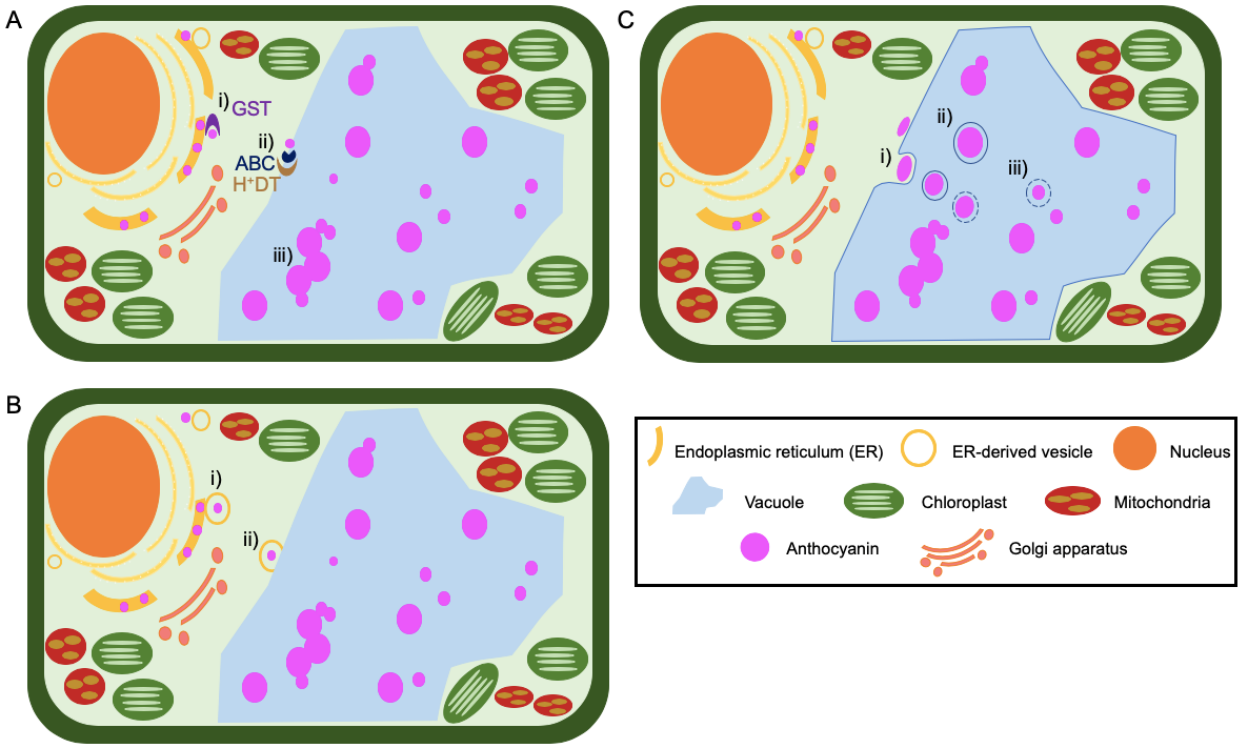

Figure 3. Methods of intracellular anthocyanin transport. Three methods for intracellular transport of anthocyanin from the site of biosynthesis (cytosolic face of the endoplasmic reticulum; ER) to the site of storage (vacuole): the ligandin transporter (Marrs et al. 1995; Mueller et al. 2000; Conn et al. 2008; Grotewold and Davies 2008; Gomez et al. 2011), vesicular transport (Zhang et al. 2006; Poustka et al. 2007; Grotewold and Davies 2008; Conn et al. 2010; Gomez et al. 2011), and autophagic transport models (Pourcel et al. 2010; Bassham 2015; Chanoca et al. 2015). In the ligandin transport model (A), anthocyanins bind to specific glutathione S-transferases (GST) in the cytoplasm (i) and are escorted to the tonoplast. ATP-binding cassette (ABC) protein transporters or proton-gradient-dependent transporters (H^+DT) translocate anthocyanins into the vacuole (ii). Inside the vacuolar lumen, anthocyanins can be uniformly distributed or agglomerate as compact pigmented bodies, called anthocyanin vacuolar inclusions (iii). (B) The vesicular transport method suggests that anthocyanins first translocate to the interior of the ER, are deposited into ER-derived membrane-bound vesicles (i) and are transported to the vacuole. The anthocyanin-containing vesicle binds to the tonoplast and releases the anthocyanin into the lumen for storage (ii). (C) In the autophagic model, anthocyanins produced in the cytoplasm press against the tonoplast, where the vacuolar membrane extends and engulfs the anthocyanins (i), releasing the membrane-bound materials into the vacuole (ii). The tonoplast-derived membrane eventually disintegrates (iii).

1.2.3. Anthocyanin vacuolar inclusions

Inside the vacuolar lumen, anthocyanins can be uniformly distributed or agglomerate as compact pigmented bodies, called anthocyanin vacuolar inclusions (AVIs; Pourcel et al. 2010;

Ananga et al. 2013; Bassham 2015; Chanoca et al. 2015). AVIs have been found in numerous plant species, without any phylogenetic association (Zhang et al. 2006). AVIs were previously defined as “anthocyanoplasts” and were described as membrane-bound organelles that synthesize anthocyanin (Small and Pecket 1982; Nozue et al. 1993). More recent findings have recognized that the condensed anthocyanin bodies lack an internal structure and consist of a proteinaceous matrix onto which anthocyanins are non-covalently bound (Markham et al. 2000; Pourcel et al. 2010).

Two morphological manifestations of AVIs have been observed in plants. The first type is spherical and exhibits a mobile, liquid-like behaviour, whereas the second type is fibrous, rigid and insoluble (Bae et al. 2006; Zhang et al. 2006; Grotewold and Davies 2008). There are inconsistencies in the literature regarding the presence of an immediate enclosing membrane surrounding the condensed anthocyanin body (Nozue et al. 1993; Markham et al. 2000; Bae et al. 2006; Conn et al. 2010). Previous research on the composition of the membrane enclosing AVIs suggests that the lipids are derived from ER and tonoplast membranes, which is indicative of vesicular transport (Conn et al. 2010). In the literature, anthocyanins (with or without an enclosing membrane) contained in cytoplasmic vesicles are termed “anthocyanin bodies or aggregates” and then are exclusively termed “AVIs” after delivery into the vacuole (Zhang et al. 2006; Chanoca et al. 2015). Transmission electron microscopy (TEM) revealed the AVI structures as electron-dense, osmiophilic bodies ranging in size from less than 1 μm in diameter in sweet potato protoplasts (Nozue et al. 1993), to 3 to 10 μm in leaves of *Arabidopsis* 5*gt* mutants that increase the density of AVIs when grown with naringenin (Chanoca et al. 2015), and 200 nm to 10 μm in lisianthus (*Eustoma grandiflorum*) petal cells (Zhang et al. 2006; Chanoca et al. 2015).

AVIs extracted from lisianthus petals, grape and tobacco cells possess a high proportion of acylated anthocyanins (Conn et al. 2003; Grotewold and Davies 2008; Kallam et al. 2017). The acylation process consists of adding an acyl group via ACT, which increases the stability of anthocyanin and alters its colouration (Conn et al. 2003; Ananga et al. 2013; Liu et al. 2018). The accumulation or sequestration of modified anthocyanins suggests that specific species of anthocyanins may be selected for a particular role or function (Pourcel et al. 2010). AVIs have been recorded at various stages of plant development, including seed coat formation, leaf morphogenesis, corolla development, and fruit ripening, and their role has been suggested in leaf senescence (Ougham et al. 2005; Bae et al. 2006; Zhang et al. 2006; Grotewold and Davies 2008; Conn et al. 2010; Nozzolillo et al. 2010; Kovinich et al. 2011; Fletcher 2017). However, the specific function of the condensed anthocyanin bodies remains elusive.

1.2.4. Anthocyanin functions and uses

Anthocyanins are found in the fruits, flowers, seeds, and vegetative tissues (including roots, hypocotyls, sheath, stems, tubers, rhizomes, runners, bulbs, corms, phylloclades, axillary buds, and leaves) in numerous plant species (Hatier and Gould 2008a; Tanaka et al. 2008; Landi et al. 2015). Foliar anthocyanins may be present throughout the leaf blade or be confined to certain areas of the leaf lamina, such as the margins, adaxial or abaxial surfaces. They have also been recorded in the epidermal and/or mesophyll cell layers (Hatier and Gould 2008a). Many plant species produce anthocyanin in response to stressful environmental conditions. However, some species synthesize anthocyanins under optimal growth conditions as a part of normal development (i.e. reproduction and senescence; Hatier and Gould 2008a).

Anthocyanins are produced in plants under stressful external conditions, such as intense light, UV radiation, temperature extremes, drought, pathogen pressure, wounding, herbivory,

herbicide spraying and heavy metal pollution (Gould 2004; Hatier and Gould 2008b; Tanaka et al. 2008; Conn et al. 2010; Landi et al. 2015; Liu et al. 2018). Up-regulation of anthocyanin in response to excess visible and UV light has been well characterized in leaves. Anthocyanins accumulate in young developing tissues to protect the cells from photoinhibition and photobleaching without compromising photosynthesis (Hatier and Gould 2008a; Conn et al. 2010). These pigments protect the photosynthetic apparatus by filtering visible light (in the yellow-green wavelengths), absorbing UV radiation, and scavenging harmful ROS and free-radicals due to their antioxidant capacity (Gould 2004; Liu et al. 2018). Filtration of yellow-green light reduces the excitation of chlorophyll, which is a major source of ROS production (Gould 2004). Some anthocyanins, especially those that are acylated, can absorb UV-A and UV-B that produce harmful ROS and cause DNA damage (Gould 2004; Landi et al. 2015). Interestingly, anthocyanins have been recorded in the internal mesophyll cell layers as opposed to the epidermal layers where light and UV interception would be most effective, which suggests an additional role of anthocyanin apart from excess light radiation (Gould 2004).

Anthocyanins are produced in certain plant species as a normal feature of growth and development. The colourful pigment is synthesized in flowers and fruits as visual attractants for pollinators and seed dispersers (Gould 2004; Tanaka et al. 2008; Conn et al. 2010; Pourcel et al. 2010; Liu et al. 2018). Some plant species produce anthocyanin pigmentation in leaves as a source of camouflage, by producing a brown/black colouration that mimics dead or decaying tissues (Gould 2004). Anthocyanins accumulate in the leaves of deciduous trees and shrubs during senescence to combat oxidative stress resulting from nutrient recycling and reabsorption (Lee et al. 2003). Thus, anthocyanins play a crucial role in plant development as both colourful pigments and effective antioxidants.

The antioxidant capacity of anthocyanins are also thought to regulate developmental processes by controlling signalling cascades (Taylor and Grotewold 2005; Landi et al. 2015). The pigment efficiently scavenges free radicals and ROS produced mainly in the chloroplast and mitochondria in plant cells by donating an electron and stabilizing the highly reactive molecules (Gould 2004; Hatier and Gould 2008b). ROS are actively produced in plant cells to function as signalling molecules for various growth and developmental processes, including stomatal closure, hypersensitive response, and programmed cell death (Hatier and Gould 2008b; Landi et al. 2015; Dauphinee et al. 2017). Additionally, anthocyanins have an affinity for a range of proteins that control or contribute to signalling cascades (Taylor and Grotewold 2005; Landi et al. 2015).

1.3. ANTHOCYANINS AND LACE PLANT

Programmed cell death (PCD) is a genetically encoded method for cellular destruction and is required in eukaryotes for normal development and defence (Fuchs and Steller 2015; Van Hautegem et al. 2015; Daneva et al. 2016). Plant PCD may be environmentally induced by external stimuli or developmentally regulated by internal factors. Environmentally induced PCD occurs in response to external stressors, such as hypoxia (Gunawardena et al. 2001; Drew et al. 2004) and pathogen invasion (Coll et al. 2011). In contrast, developmentally regulated PCD occurs at precise times and locations during plant growth. Examples include xylem differentiation, leaf morphogenesis, and leaf senescence (Gunawardena et al. 2004; Van Hautegem et al. 2015; Maizel 2015). An interesting example of developmentally regulated PCD in plants is the formation of perforations during leaf morphogenesis, which exclusively occurs in two distantly related plant families: Araceae and Aponogetonaceae (Gunawardena et al. 2006; Dauphinee and Gunawardena 2015).

Lace plant (*Aponogeton madagascariensis*) is an aquatic monocot belonging to the family Aponogetonacea, which consists of over 50 species mainly distributed in the tropical and subtropical regions of the world (Chen et al. 2015). *Aponogeton madagascariensis* is endemic the river systems in Madagascar and the Comoros Islands and can be found in a variety of freshwater environments ranging from stagnant ponds to turbulent streams (van Bruggen, 1985). Lace plant receives its common name from its unique lattice-like leaf morphology, which is generated via developmentally regulated programmed cell death (PCD; Fig. 4A). Lace plants utilize this form of PCD to systematically delete distinct subpopulations of cells located equidistantly between longitudinal and transverse veins to produce perforations throughout the leaf blade (Fig. 4B; Gunawardena et al. 2004). Lace plant possesses outstanding potential as a model system for studying developmentally regulated PCD in plants due to: the accessibility and predictability of perforation formation (Fig. 4B), the ability to perform live-cell imaging of the thin and semi-transparent leaves (Fig. 4C), and the availability of an established sterile culture system for propagation and pharmacological experimentation (Fig. 4D-E; Gunawardena et al. 2004; Wright et al. 2009; Dauphinee and Gunawardena 2015).

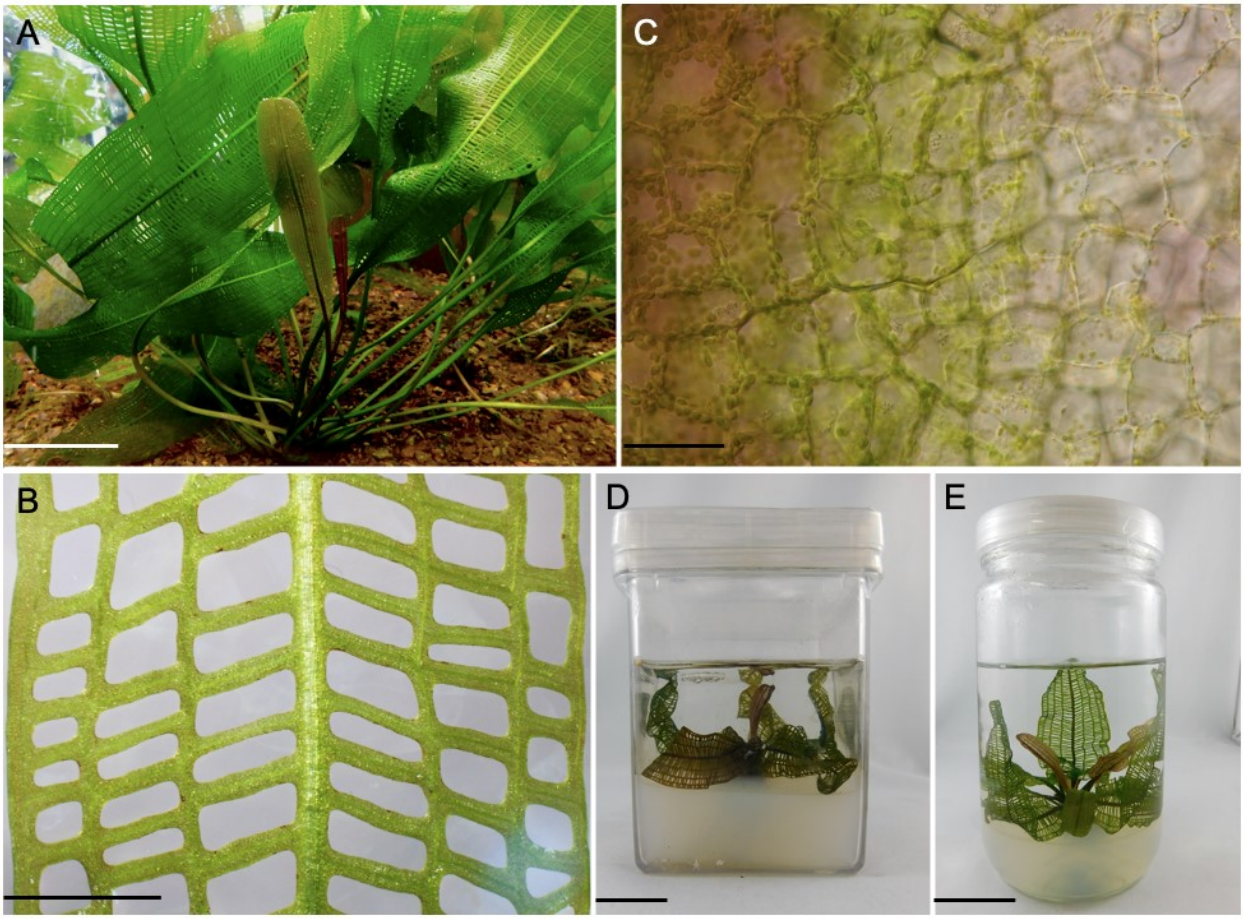

Figure 4. Lace plant (*Aponogeton madagascariensis*) possesses outstanding potential as a model for studying developmentally regulated programmed cell death (PCD). (A) *Aponogeton madagascariensis* is an aquatic monocot endemic to the river systems in Madagascar and the Comoros Islands and can be found in a variety of freshwater environments ranging from stagnant ponds to turbulent streams. The plant is commonly used in aquariums due to its rare perforated morphology. (B) Perforations formed in the lace plant leaf blade by PCD predictably occur equidistantly between longitudinal and transverse veins. (C) The thin and semi-transparent leaves are ideal for live-cell imaging. (D-E) Established axenic culture systems are used for efficient propagation and pharmacological experimentation. Scale bars: A = 5 cm, B = 0.5 cm, C = 50 µm, D = 2.5 cm, E = 4 cm.

Lace plant leaves emerge in a helical pattern of leaf initiation from a spherical corm bearing roots in a heteroblastic series (Fig. 5A; van Bruggen, 1985; Dauphinee and Gunawardena 2015). The first three to four leaves that emerge from the corm are termed "juvenile" and do not perforate or exhibit visible foliar anthocyanin. The successive leaves that

emerge are called “adult” and form perforations via developmental PCD (Fig. 5A). Five stages of perforation formation have been identified in lace plant leaves: pre-perforation, window, perforation formation, perforation expansion, and mature (Gunawardena et al. 2004). Newly emerged pre-perforated adult leaves are tightly furled and exhibit anthocyanin throughout (Fig. 5A). Microscopic observations indicate no visible signs of PCD at this stage in leaf development (Fig. 5C; Gunawardena et al. 2004). PCD is active during the window stage (Fig. 5A and D), where cell death can be visualized as a disappearance of anthocyanin in the center of a perforation site or areole (an area bounded by vasculature). A perforation will form and expand towards the leaf vasculature, consistently halting four to five cell-layers from the leaf vasculature. In the mature stage, perforation formation is complete, and anthocyanin completely disappears from the leaves (Fig. 5A and E). Under optimal growth conditions, purple or white inflorescences bloom on two spikes that emerge from the surface of the water (Fig. 5B; Van Bruggen 1985; Dauphinee and Gunawardena 2015).

The window stage leaf is of particular interest because the PCD process is visible at this stage of leaf development, and a unique gradient of cell death can be seen within one given areole (Fig. 5D; Lord et al. 2011). Non-PCD (NPCD) cells located at the periphery of the areole maintain anthocyanin pigmentation until maturity. Early PCD (EPCD) cells have lost their anthocyanin pigmentation but maintain chlorophyll pigmentation and are fated to die. Late PCD (LPCD) cells located in the center of the areole have lost their anthocyanin and chlorophyll pigmentation and are close to death. ‘PCD cells’ can be used to describe both early and late PCD cells that are fated to die during perforation formation in lace plant leaves.

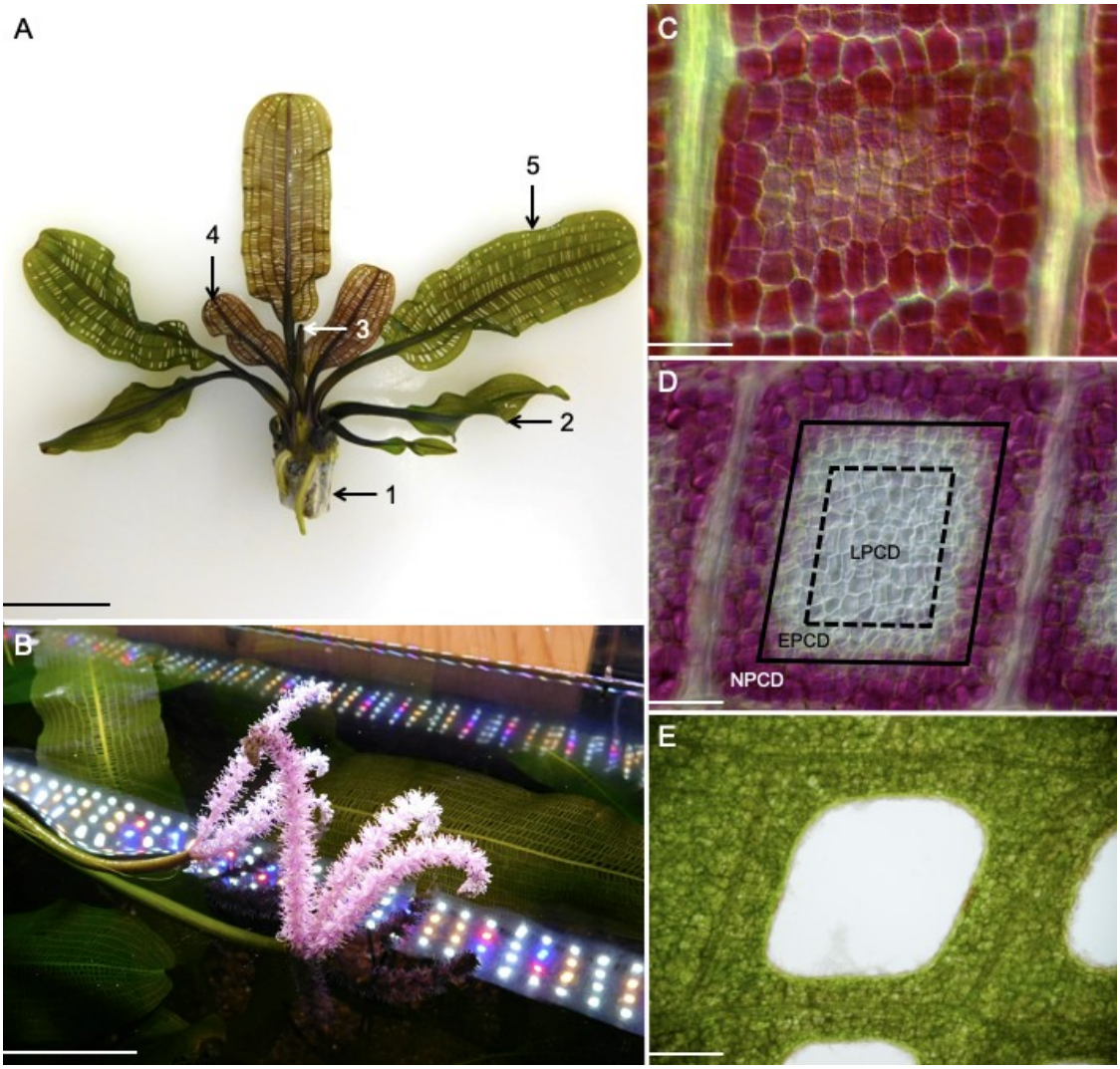

Figure 5. Lace plant development. (A) Lace plant leaves emerge from a spherical corm that bears roots (1) in a heteroblastic series. The first three leaves that emerge are called juvenile leaves (2) and they do not perforate or exhibit foliar anthocyanin. The successive leaves that emerge are called adult leaves that perforate via developmentally regulated PCD. Newly emerged pre-perforated leaves (3) are tightly furled and cells contain abundant anthocyanin. The cell death process is active in window stage leaves (4) and perforation formation completed in mature leaves (5). (B) Under optimal environmental conditions, inflorescences bloom on a long spike that emerges from the water surface. (C) Anthocyanin can be observed throughout the pre-perforated-stage areole (area bounded by vasculature). (D) PCD death can be visualized as a disappearance of anthocyanin in the center of the perforation site in window leaf areoles, and a unique gradient of cell death is produced within an areole. Non-PCD (NPCD) cells located at the periphery of the areole maintain anthocyanin pigmentation until maturity. Early PCD (EPCD) cells have lost their anthocyanin pigmentation but maintained chlorophyll pigmentation and are fated to die. Late PCD (LPCD) cells located in the center of the areole have lost their anthocyanin and chlorophyll pigmentation and are close to death. PCD cells = EPCD + LPCD cells. (E) Anthocyanin completely disappears in mature-stage areoles and PCD is complete. Scale bars: A = 2 cm, B = 5 cm, C = 25 µm, D = 100 µm, E = 300 µm.

Quantification of anthocyanin abundance using spectrophotometry reveals higher levels in window stage compared to mature stage lace plant leaves (Dauphinee et al. 2017).

Apart from a spectrophotometric analysis that quantifies anthocyanin abundance, anthocyanin can be characterized and profiled using liquid chromatography and mass spectrometry. Anthocyanins are typically extracted by acidified methanol or ethanol, then purified to isolate anthocyanin from co-extracted compounds (Castañeda-Ovando et al. 2009). High or ultra-pressure liquid chromatography (HPLC/UPLC) with UV-Vis or diode array detectors (DAD) are the most common methods for anthocyanin separation and are also used for quantification and identification (Castañeda-Ovando et al. 2009). UPLC, coupled with mass spectrometry (MS), has become a preferred technique to identify anthocyanins due to the inaccessibility of reference compounds or standards and the complexity of the anthocyanin profiles (Castañeda-Ovando et al. 2009).

Previous research on anthocyanin in lace plants has identified AVIs in lace plant leaves. The number of AVIs in window stage leaves increased under stressful growth conditions, including high pH, low light, and nutrient-deficient conditions (AVI morphologies in stressed leaves can be seen in Appendices 2-4 and in Fletcher 2017). Although the presence of AVIs has been recognized in lace plant leaves, characterization of their structure, localization and function is still lacking. Additionally, the anthocyanin transport mechanism from the site of biosynthesis (ER) to the site of accumulation (as soluble anthocyanin or AVIs) and storage has not been elucidated in the lace plant.

The ER is a major site for protein folding, signalling molecule storage (Ca^{2+}), and anthocyanin synthesis (Zuppini et al. 2004). During adverse or stressful cellular conditions

stimulated by internal (developmental) or external (environmental) factors, ER functioning and capacity are exceeded. This may result in an unfolded protein response (UPR), where adaptations such as upregulating chaperones that assist in correct protein folding or proteases that break down the misfolded proteins are employed to reestablish ER homeostasis (Kim et al. 2006; Liu and Howell 2010; Srivastava et al. 2018). Under chronic or severe stress conditions, PCD is induced to eliminate damaged cells (Watanabe and Lam 2008; Eichmann and Schäfer 2012; Howell 2013; Tian et al. 2014; Srivastava et al. 2018). Although the signalling pathways leading from UPR to PCD are recognized in plants, few core regulators and components of the process have been identified (Watanabe and Lam 2008; Liu and Howell 2010). Additionally, limited studies have identified the morphological changes that take place in the ER during developmentally regulated plant PCD.

Lastly, the conspicuous pattern of anthocyanin loss coordinated with developmental PCD in lace plant leaves indicates its crucial role in perforation formation. Numerous pharmacological whole-plant experiments using PCD modulators have recorded a coordinated reduction of anthocyanins with the inhibition of perforation formation (developmental PCD) in lace plant leaves. Modulators that decrease the incidence of perforation formation and anthocyanin abundance include aminoethoxyvinylglycine (AVG, an ethylene-biosynthesis inhibitor), cyclosporine A (CsA; a mitochondrial permeability transition pore antagonist), ascorbic acid and L-cysteine (antioxidants), ruthenium red (calcium channel blocker), chlorophenylethynylsulfonamide (PES-Cl, a heat shock protein 70 inhibitor), N-1-naphthylphthalamic acid and auxinole (auxin-signaling inhibitors) (Lord et al. 2011; Dauphinee et al. 2012; Dauphinee et al. 2017; Dauphinee et al. 2019; Denbigh et al. 2020; Fraser et al. 2020; Rowarth et al. 2020). Modulators that increase anthocyanin production, such as 1-

aminocyclopropane-1-carboxylic acid (ACC, an ethylene-biosynthesis promoter), and hydrogen peroxide (a type of ROS), do not alter perforation formation (Dauphinee et al. 2012; Dauphinee et al. 2017), unless used at a high concentration that hinders normal growth and development. These whole-plant pharmacological experiments differ from cell death rate experiments that used PCD modulators to analyze the rate of death following PCD induction (Dauphinee et al. 2019; Fraser et al. 2020). Preliminary pharmacological experiments using anthocyanin biosynthesis modulators, methyl jasmonate (MeJA) and phenidone, on lace plants resulted in leaves with altered anthocyanin content and perforation development compared to control plants (Fletcher 2017). Methyl jasmonate increases anthocyanin production by stimulating upregulation of various anthocyanin biosynthesis enzymes (Fig 2; Saniewski et al. 2003; Rudell et al. 2005; Shan et al. 2009; Qi et al. 2011). This differs from phenidone, which decreases anthocyanin by inhibiting jasmonate (a hormone that stimulates anthocyanin synthesis) production (Fig 2; Cucurou et al. 1991). Additional experimentation with MeJA and phenidone would further support the effects of anthocyanin modulation on perforation formation in lace plant leaves.

1.4. OBJECTIVES OF THE STUDY

The objectives of the study are:

(1) to identify anthocyanin species present in different lace plant tissues (collaboration with Dr. Shawna Mackinnon and Dr. Harrison Wright, Kentville Research and Development Centre, Agriculture and Agri-Food Canada [AAFC]);

(2) to investigate anthocyanins and AVIs in lace plant leaves by (i) determining the ultrastructure and localization of anthocyanins and AVIs; (ii) determining the mode of intercellular transport of anthocyanins; and (iii) investigating ER changes across the PCD gradient; and

(3) to determine the role of anthocyanin in lace plant PCD.

The above objectives were achieved using analytical chemistry, microscopic, histological, and pharmacological techniques. The following hypotheses derive from the objectives listed above:

(1) different anthocyanin profiles exist among the various lace plant tissues;

(2) (i) the presence of anthocyanin bodies varies across and within developmental leaf stages; (ii) the vesicular transport method for anthocyanin trafficking is prevalent in lace plant leaves; and (iii) ER ultrastructure changes exist across the PCD gradient;

(3) anthocyanin biosynthesis modulation regulates perforation formation and PCD in lace plant leaves.

CHAPTER 2: MATERIALS AND METHODS

2.1. LACE PLANT PROPAGATION

Aponogeton madagascariensis cultures were established and propagated according to the sterile tissue culture procedure described in Gunawardena et al. (2006). Lace plants that possessed brown, senescent leaves, and grew to fill the extent of the culture vessel area (about 3-4-month-old plants) were deemed overgrown and were selected for tissue culturing under sterile conditions. Dead and decaying plant tissues were excised from the lace plants, and corms were cut into 1 cm^3 cubes with 0.5 cm of healthy shoots surrounding the shoot apical meristem. Newly cultured lace plant corms were placed in autoclaved Magenta GA-7 boxes or 946 mL glass culture vessels (PhytoTechnology Laboratories, Lenexa, KS, USA) containing liquid Murashige and Skoog (MS) medium layered over solid MS medium (Fig. 6). Liquid MS medium consisted of the following chemicals dissolved in distilled water (dH_2O) adjusted to pH 5.7 with 1M NaOH: 30 g/L sucrose (BioShop Canada, Burlington, Canada), 2.15 g/L MS basal salts (PhytoTechnology Laboratories), 0.1 g/L myo-inositol (Sigma-Aldrich, Oakville, Canada), and 0.1 mg/L thiamine HCl (Sigma-Aldrich). Solid MS media consisted of liquid MS medium with 1% micropropagation grade agar (PhytoTechnology Laboratories). Lace plant corms were fully submerged into the solid MS substrate, onto which liquid MS medium was poured. The cultures were propagated under daylight fluorescent light bulbs (Philips, Daylight Deluxe, F40T12/DX, Markham, ON, Canada) that emitted 125 $\mu mol/m^2/s$ on 12-hour light/dark cycles and were maintained at 24 °C.

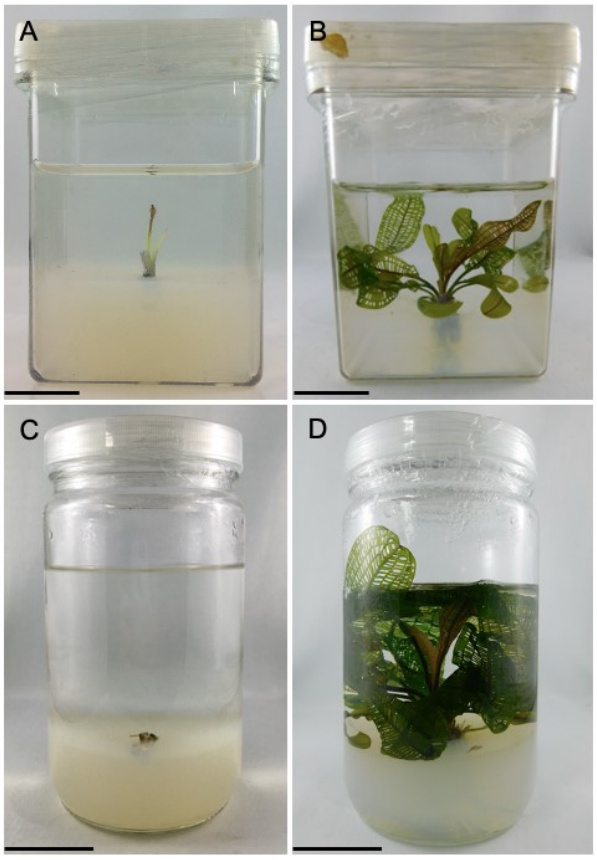

Figure 6. Lace plant sterile propagation. (A) Newly cultured lace plants are grown in sterile magenta GA7 boxes containing 150 mL liquid Murashige and Skoog (MS) medium and 100 mL solid MS medium substrate. (B) After 4-5 weeks of growth, lace plants develop three fully perforated leaves and can be used for whole plant treatment experiments. (C) Newly cultured lace plants propagated in sterile glass culture vessels containing 200 mL liquid MS medium and 450 mL solid MS medium substrate. (D) After two months of growth, the lace plant leaves can be harvested for crude anthocyanin extractions. Scale bars: A-B= 2.5 cm, C-D = 4 cm.

2.2. ANTHOCYANIN EXTRACTION

2.2.1. Sample preparation and crude anthocyanin extraction

Crude anthocyanin extractions were optimized, according to Li et al. (2010) and Dauphinee et al. (2017) with some modifications. Lace plant tissues (pre-perforated, window and mature stage leaves, and inflorescences) were excised from sterile cultures (Fig. 7A-B), blot-dried, weighed, and then flash frozen with liquid nitrogen. Frozen tissues were macerated on ice

with a mortar and pestle into a fine powder. An extraction solution consisting of 95% methanol, 5% formic acid (FA; v/v) was added (1 mL per gram of tissue) and then incubated on ice in the dark for 50 min, followed by centrifugation at 10,000 *g* for 10 min at 4 °C. The supernatant was collected (Fig. 7C), and 10 mL was filtered through an 80 µm mesh onto glass culturing plates to allow the solvents to evaporate at 25 °C overnight in the dark (Fig. 7D). The dry residue was scraped from the glass plate using a fresh razor, collected, and stored in a microcentrifuge tube at -20 °C (Fig. 7E). The crude anthocyanin extracts were then delivered to the MacKinnon lab (Kentville Research and Development Centre, AAFC, Kentville, NS, Canada) for reversed-phase fractionation, ultra-pressure liquid chromatography-diode array detection (UPLC-DAD) and liquid chromatography-mass spectrometry/mass spectrometry (LC-MS/MS) analysis.

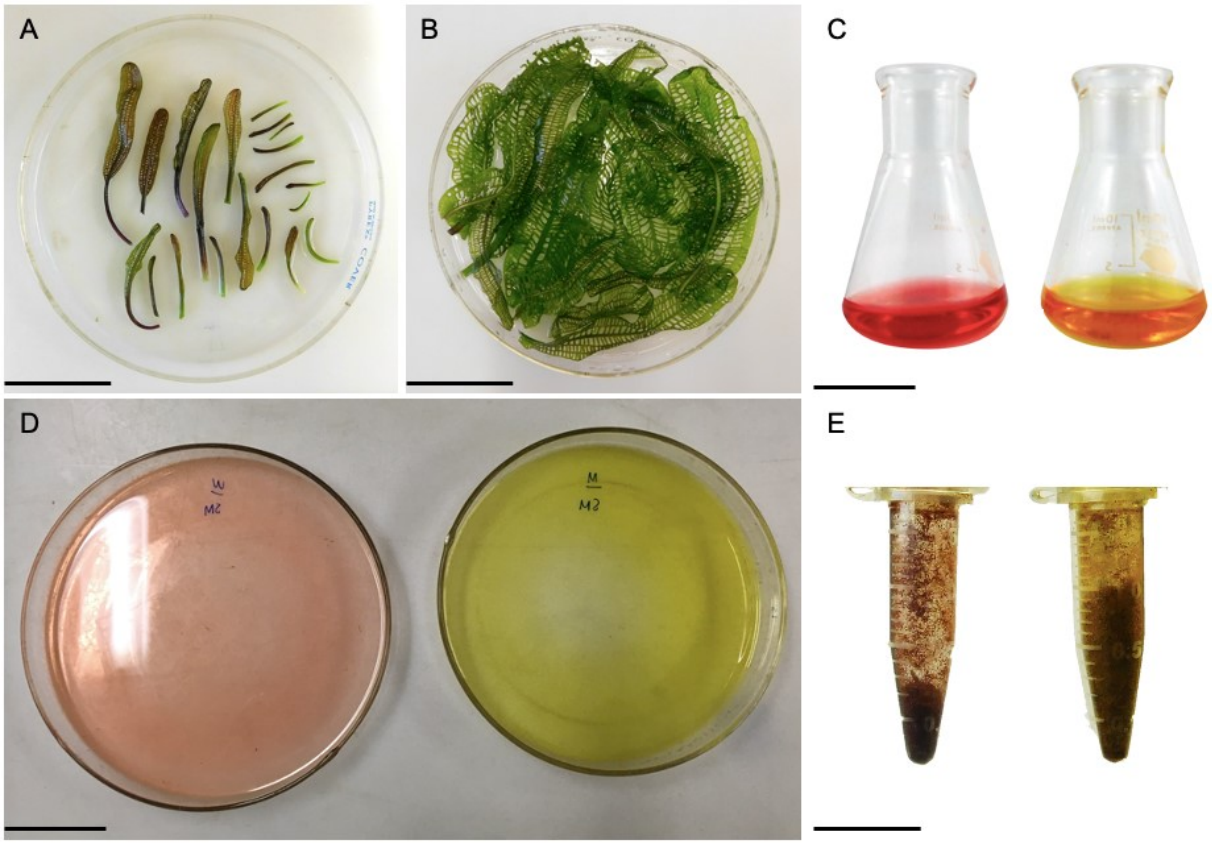

Figure 7. Crude anthocyanin extraction for lace plant tissues. (A) Window and (B) mature stage lace plant leaves were excised from sterile cultures, rinsed thoroughly, blot dried and weighed. (C) The crude anthocyanin extract solution is collected and poured onto glass Petri plates (D) to allow the solvent to evaporate overnight. The dried residue is collected and stored in microcentrifuge tubes (E) at -20 °C. Scale bars: A-B and D = 4 cm, C and E = 1.5 cm

2.2.2. Fractionation of lace plant anthocyanin

The crude anthocyanin extract (10 – 30 mg) was re-dissolved in 5 mL acidified dH_2O (5% FA) and run through a C18 Sep-Pak cartridge (6cc/1g, part#WAT036905, Waters Cooperation, Mississauga, Ontario, Canada) preconditioned in reverse eluent order, ending with non-acidified water. The cartridge was eluted with acidified water (5% FA) to remove sugars, followed by 15% methanol to remove phenolic acids, 100% ethyl acetate to remove flavanols, and then acidified methanol (5% FA) to remove anthocyanins. The cartridge was dried under

vacuum between each elution to remove all traces of the previous solvent. The anthocyanin-enriched fractions were collected in a microcentrifuge tube and stored at -20 °C.

2.3. QUANTIFICATION OF ANTHOCYANIN

2.3.1. Spectrophotometry

The anthocyanin extraction protocol is the same as the techniques described in Dauphinee et al. (2017), adapted from Li et al. (2010). Lace plant leaf samples (20 mg) were macerated in 200 µL of anthocyanin extraction solution (95% methanol, 5% FA v/v), then incubated on ice in the dark for 50 min. The leaf samples were centrifuged at 10, 000 *g* for 10 min at 4 °C and the supernatant was collected. The relative absorbance of the solutions was read in triplicate at 520 nm using a SmartSpec Plus Spectrophotometer (Bio-Rad Laboratories, Mississauga, ON, Canada) that was calibrated with the extraction solution as a baseline response.

2.3.2. Ultra-pressure liquid chromatography-diode array detection

The anthocyanin-enriched extracts from lace plant leaves and inflorescences were dissolved in 2% FA in water and filtered through a 0.22 mm syringe filter in preparation for ultra-pressure liquid chromatography (UPLC) analysis. A 10 µL sample was injected onto an Agilent 1290 Infinity II LC system (Agilent Technologies Inc., Santa Clara, CA, USA) equipped with a PFP Kinetix 2.6 µm column (2.1 × 50 mm) (Phenomenex, Torrance, CA, USA), an Agilent binary pump system, diode array detector (DAD), autosampler and column heater. The column was eluted with the following gradient method with decreasing proportions of solvent A to solvent B, where solvent A was 2% FA in water and solvent B was 2% FA in acetonitrile. The flow rate was 1.0 mL/min, the column temperature was 55 °C and the absorbance of the eluent was monitored at 280, 320, 360 and 520 nm. The UPLC parameters for profiling anthocyanin in lace plant tissues are listed in Table 1.

Table 1. Ultra-pressure liquid chromatography (UPLC) parameters for profiling anthocyanins in lace plant tissues.

UPLC analytical parameters	**Lace plant anthocyanin profiling settings**
Sample diluent	2% formic acid in water
Temperature	55 ºC
Injection volume	10 µL
Analytical column	2.6 µm column
Mobile phase solvent	2% formic acid in water (solvent A) and 2% formic acid in acetonitrile (solvent B)
Flow rate	1.0 mL/min
Solvent gradient (decreasing proportions of solvent A to solvent B)	0–3 min, 1.1% B; 3–34 min, 1.1–20.7% B; 34–40 min, 20.7–90.2% B; 40–43 min, 90.2% B; 43–47 min 90.2-1.1% B and 47-50 min 1.1% B
Stop time	50 min

2.3.3. Liquid chromatography-mass spectrometry and multiple reaction monitoring

The anthocyanin-enriched extracts from window and mature stage lace plant leaves were dissolved in 1.1% acetonitrile in water and filtered through a 0.22 mm syringe filter in preparation for triple quadrupole linear ion traps (QTrap) liquid chromatography-mass spectrometry-mass spectrometry (LC-MS/MS) analysis. A 25 µL volume of sample was injected into an Agilent 1200 Series HPLC (Agilent Technologies Inc.) equipped with a PFP Kinetix 2.6 µm column (2.1 × 50 mm) (Phenomenex, Torrance) set at 55 °C and operated at a flow rate of 400 µL/min. The column was eluted with the following gradient method where solvent A was 2% FA in water, and solvent B was 2% FA, 8% water, and 90% acetonitrile for 0−3 min, 1.2% B; 3−12 min, 1.2−6.2% B; 12−17 min, 6.2% B; 17−48 min, 6.2-21.2% B; 48−54 min 21.2-100% B; 54−59 min, 100% B; 59-61 min, 100-1.2% B; 61-66 min, 1.2% B. The HPLC was coupled to

an ABSciex QTrap 4000 (ABSciex, Concord, ON, Canada) linear ion trap equipped with a Turbospray (ABSciex) electrospray ionization (ESI) interface, which offered unit mass resolution (i.e., ±0.5 amu). The ESI/MS was carried out in positive ion mode using the following parameters: gas 1 80 psi and gas 2 60 psi; temperature, 700 °C; ion source 2000 V; curtain gas, 25 psi; declustering potential, 65 V; entrance potential, 10 V; collision energy, 26 V; and collision cell exit potential, 17 V. The LC-MS/MS parameters for profiling anthocyanin in lace plant leaves are listed in Table 2. Tandem mass spectrometry (MS/MS) was carried out for multiple reaction monitoring (MRM) corresponding to 80 previously identified anthocyanins that contained the following anthocyanin bases: pelargonidin, cyanidin, peonidin, delphinidin, petunidin, and malvidin. Parent and product ion combinations were used to scan for the presence of the 80 anthocyanins in leaf extracts.

Table 2. Liquid chromatography-mass spectrometry (LC-MS) parameters for profiling anthocyanins in lace plant leaves.

LC-MS/MS analytical parameters	**Lace plant anthocyanin profiling settings**
Ion source	Turbospray
Ion source gas	Nitrogen
Ion spray voltage	2000 V
Entrance potential	10 V
Declustering potential	65 V
Curtain gas	25 psi
Temperature	700 °C
Interface heater temperature	700 °C
Ion mode	Positive ion mode
Scan type	Multiple reaction monitoring
Multiple reaction monitoring (MRM) mode	Yes
Collision energy	26 V
Collision cell exit potential	17 V
Collision gas	Nitrogen (gas 1 = 80 psi) (gas 2 = 60 psi)

2.3.4. Anthocyanin standards used in lace plant anthocyanin quantification

Anthocyanin standards of cyanidin 3-glucoside, delphinidin 3-glucoside, malvidin 3-glucoside, peonidin 3-glucoside, pelargonidin 3-glucoside, petunidin 3-glucoside, and kaempferol 3-rhamnoside that were used for UPLC and LC-MS/MS analysis were purchased from Sigma-Aldrich. Standards of cyanidin 3-rhamnoside and cyanidin 3-sophoroside-5 glucoside were purchased from Shaanxi Pioneer Biotech Company (Lianhu District, Xi'an, China), delphinidin 3-rhamnoside was purchased from Indofine Chemical Company (Hillsborough, NJ, USA), and delphinidin 3-rutinoside was purchased from Biosynth Carbosynth (Berkshire, UK).

2.4. INVESTIGATION OF ANTHOCYANIN VACUOLAR INCLUSIONS (AVI)

2.4.1. Light microscopy

Window and mature stage lace plant leaves were excised from sterile cultures, thoroughly rinsed, and mounted in 400 µL of distilled water on a custom grooved slide. A coverslip was applied and sealed with melted VALAP (a mixture of Vaseline, lanolin, and paraffin wax in a 1:1:1 ratio). Leaves were completely scanned from tip to base at low magnification (Plan Fluor 4x objective; Nikon Instruments Inc., Mississauga, ON, Canada) using audio-video interleave to record the location and abundance of anthocyanin vacuolar inclusions (AVI). Leaf apices (top 10% of the total leaf blade length, or approximately 0.5 cm from the leaf tip) were further investigated at higher magnification (Plan Fluor 20x; Nikon Instruments Inc.) for a minimum of 4 hours. Micrographs of the leaf apices (Fig. 8A and B) and mid-regions (between the top 10 to 25% of the total leaf blade length, including midribs, longitudinal and transverse veins, and areoles; Fig. 8A and D) were captured at 20x magnification (Plan Fluor 20x; Nikon Instruments Inc.).

To observe anthocyanin in cross-sections of window stage leaves, the following procedure was followed: a baby carrot was longitudinally sectioned and window stage leaf was wedged between the two halves. The baby carrot was placed on a Petri plate containing water, and the carrot was cross sectioned with a scalpel. Thin cross-sections of the leaf apex and mid-region (Fig. 8C and E) were obtained and mounted on a slide with 100 µL of distilled water. A coverslip was gently placed on top of the wet-mount, and the slide was viewed under the microscope at 20x magnification.

The observation was replicated a minimum of three times for window stage leaves. Live cell imaging was performed using a Nikon 90i compound light microscope fitted with a DXM

1200C digital camera (Nikon Instruments Inc.). Micrographs and videos were acquired through NIS Elements AR 3.1 software (Nikon Instruments Canada). Images were prepared for publication using Adobe Illustrator and Adobe Photoshop (CC), (Adobe Systems Inc.).

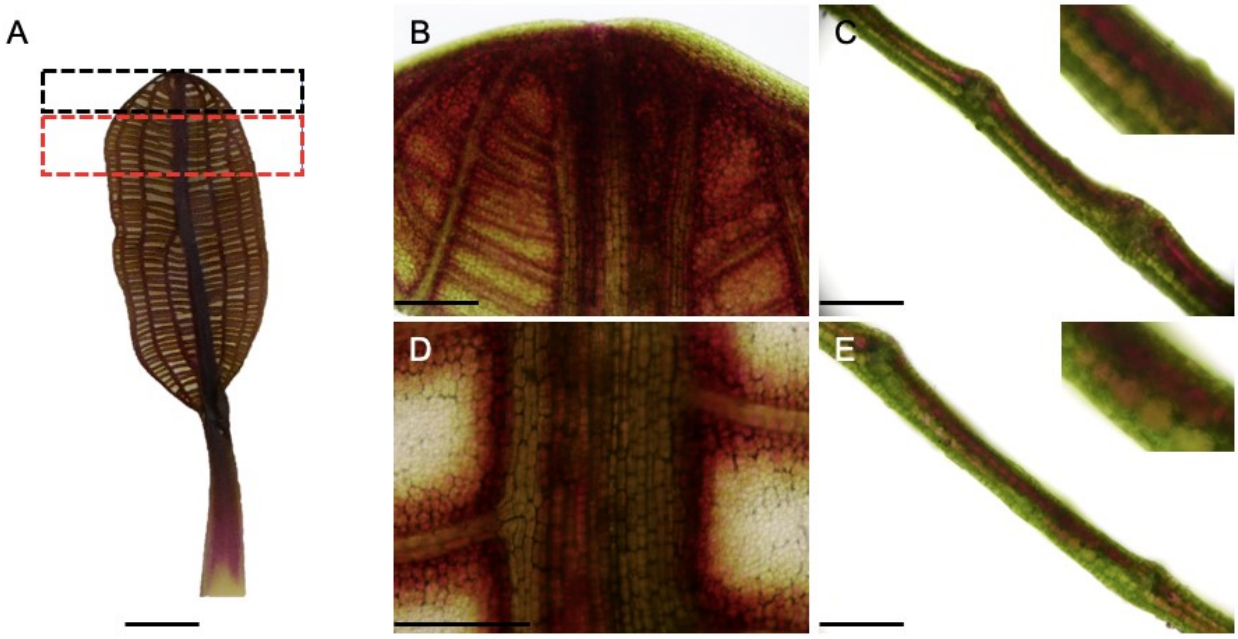

Figure 8. Area of interest for anthocyanin vacuolar inclusion (AVI) investigation. (A) Window stage leaves were excised from sterile cultures for microscopic examination of AVIs using live-cell imaging (compound light microscopy, confocal laser scanning microscopy) and transmission electron microscopy. Leaf apex (outlined in black) and mid-region (outlined in red) were further investigated. (B) Leaf apices are located in the top 10% of the total leaf blade length (or approximately 0.5 cm from the leaf tip). (C) Thin cross-sections of the leaf apex were obtained and observed as a wet mount (enlarged image in top-right corner). (D) Mid-regions are located between the top 10 to 25% of the total leaf blade length and include midribs, longitudinal and transverse veins, and areoles. (E) Thin cross-sections of the mid-region were obtained and observed (enlarged image in top-right corner). Bars: A = 0.5 cm, B-E = 0.05 cm.

2.4.2. Confocal laser scanning microscopy

Anthocyanin vacuolar inclusions were investigated at the leaf apex and mid-region of window stage leaves excised from sterile lace plant cultures. Leaf apices were sectioned and mounted on a slide with liquid media. The coverslip was sealed onto the slide with melted

VALAP, and then samples were viewed with using a Nikon Eclipse Ti C1 confocal laser scanning microscope (Nikon Instruments Inc.). Soluble anthocyanin and AVI autofluorescence were imaged at an excitation wavelength of 514 nm and an emission wavelength of 610-670 nm, in accordance with Chanoca et al. (2015). Time-lapse videos were recorded for 20 seconds with no fixed intervals, and z-stacks imaging was performed at a 1 μm step size. Videos and images were processed and analyzed using NIS Elements AR 3.1 software (Nikon Instruments Canada). A minimum of three experiments were performed for each leaf area (tip and mid-region).

2.4.3. Transmission electron microscopy (TEM)

Window stage leaves were excised from sterile cultures and rinsed thoroughly with distilled water. The leaves were placed on a slide (without a coverslip) with 500 μL of distilled water and examined under light microscopy at 20x magnification to determine the presence of anthocyanin and/or AVIs. The leaves were immediately transferred to a Petri plate containing fixative (2.5% glutaraldehyde diluted in a 0.1 M sodium cacodylate buffer), and the apex and areoles closest to the midrib (between the top 10 to 25% of the total leaf blade length) were cut into 0.25 cm^2 pieces (Fig. 8A). The samples were fixed for a minimum of 2 hours and then were washed three times for 10 min with the 0.1 M sodium cacodylate buffer. Secondary fixation was performed using 1% osmium tetroxide for 48 hours under vacuum infiltration at 20 psi. The samples were briefly washed with distilled water, then placed in 0.25% uranyl acetate overnight at 4°C. The samples were dehydrated by immersion in a series of acetone solutions of increasing concentration as follows: 50, 70, 70, 95, 95, 100 and 100% for 10 min each. The samples were infiltrated with Epon-Araldite resin solutions first at a 3:1 ratio of acetone to resin for 3 hours, followed by a 1:3 ratio of acetone to resin overnight. The samples were embedded in 100% Epon-Araldite resin and cured for 48 hours at 60 °C. Thin sections (100 nm thick) were cut using

an Ultracut E Ultramicrotome (Reichert-Jung, Vienna, Austria) with a diamond knife, and then were placed on formvar/carbon support film copper grids (FCF205-CU-25, Cedarlane Laboratories, Burlington, ON, Canada). Specimen grids were stained with 2% aqueous uranyl acetate for 10 min, followed by two 5-min rinses with distilled water, 4 min in lead citrate counterstain, and a final quick rinse with distilled water. The samples were viewed using a JEM 1230 Transmission Electron Microscope (JEOL, Peabody, MA, USA) at 80 kV and images were captured using a Hamamatsu ORCA-HR digital camera (Hamamatsu Photonics, Hamamatsu, Japan). The sample selection, preparation, and viewing procedure was repeated at least four times.

2.5. INVESTIGATION OF ENDOPLASMIC RETICULUM (ER)

2.5.1. Confocal microscopy

2.5.1.1. *Developing a staining protocol for 3,3'-dihexyloxacarbocyanine iodide (DiOC6[3])*

An endoplasmic reticulum (ER) stain, 3,3'-dihexyloxacarbocyanine iodide (DiOC6[3]), was optimized for lace plant leaves based on a study by Quader and Schnepf (1986), with some modifications. A 5 mg/mL stock solution dissolved in DMSO was diluted to 5 µg/mL with liquid MS medium. Window and mature stage leaves were excised from sterile cultures, rinsed thoroughly with liquid medium, cut into 0.5 cm^2 pieces, and placed onto small Petri plates (1 inch in diameter). The leaf pieces were completely submerged in the stain and then were vacuum infiltrated for 15 min at 10 psi, and were left to incubate at room temperature on a shaker in the dark for an additional 15 min. The samples were removed from the stain and placed on a shaker for 5 min in new Petri plates containing 3 mL of fresh media. The samples were rinsed two additional times with fresh media for 5 min, then were mounted onto a slide with 100 µL fresh media. A negative control consisting of leaves incubated in a similar volume

of DMSO dissolved in liquid media was prepared and viewed simultaneously. The samples were viewed with a Nikon Eclipse Ti C1 confocal system (Nikon Instruments Inc.) using an excitation light of 484 nm and recording fluorescence emission at 501 nm. ER networks were visualized within the various cell types (NPCD, EPCD, and LPCD) within an areole at low (Plan Fluor 20x; Nikon Instruments Inc.) and high magnification (Plan Fluor 40x, Plan Fluor 100x; Nikon Instruments Inc.). Time-lapse videos were recorded for 20 seconds with no fixed intervals, and z-stacks imaging was performed at a 1 μm step size. Micrographs captured ER networks in the cytoplasm closest to the outer face of the plasma membrane in epidermal cells. Videos and images were processed and analyzed using NIS Elements AR 3.1 software (Nikon Instruments Canada). A minimum of three replicate experiments were performed.

2.5.1.2. *Co-localizing endoplasmic reticulum and mitochondria*

To ensure the selective binding of DiOC6 to the ER at the optimized concentration used to stain lace plant cells, onion scale cells were stained with the optimized concentration of DiOC6(3) and then compared to onion cells stained with mitochondrial stain Mitotracker Red CMXRos (CMXRos). CMXRos staining was similar to Lord et al. (2011) with minor modifications. A thin layer of tissue was peeled from the onion blub scales using fine-pointed forceps. The thin membrane was sliced into 0.5 cm^2 pieces, then fully submerged in a 1:1 ratio of 5 μg/mL DiOC6(3) and 0.6 μM CMXRos dissolved in liquid MS medium. The pieces were vacuum infiltrated and rinsed similarly to the previous staining protocol, then mounted onto a slide for visualization with a Nikon Eclipse Ti C1 confocal system (Nikon Instruments Inc.) using an excitation light of 577 nm and recording fluorescence emission at 599 nm for CMXRos and an excitation light of 484 nm and recording fluorescence emission of 501 nm for DiOC6(3). Time-lapse videos were recorded for 20 seconds, and z-stack imaging was performed at a 1 μm

step size (Supplementary material 6-7). Videos and images were processed via NIS Elements AR 3.1 software (Nikon Instruments Canada). A minimum of three independent experiments were performed.

2.5.2. Transmission electron microscopy (TEM)

Window stage lace plant leaves were excised from plants in sterile cultures and rinsed thoroughly with distilled water. The leaves were placed in a Petri plate containing fixative (2.5% glutaraldehyde diluted in a 0.1 M sodium cacodylate buffer) and areoles were cut into 0.25 cm^2 pieces. The samples were fixed, embedded, sectioned, and stained as described above. Micrographs of NPCD and PCD cells were recorded using a Hamamatsu ORCA-HR digital camera (Hamamatsu Photonics). This procedure was repeated a minimum of three times.

2.6. PHARMACOLOGICAL EXPERIMENTS WITH ANTHOCYANIN MODULATORS

2.6.1. Whole plant experiments

Lace plants grown in magenta boxes that possessed a minimum of three perforated mature leaves (4-5-week-old plants; Fig. 9A) and similar corm sizes were randomly assigned to a treatment group (control, MeJA, or phenidone). Concentrations of MeJA and phenidone were based on previous experiments by Fletcher (2017). A gradient of the compound (0, 1, 2.5, or 5 µM MeJA [Sigma-Aldrich], or 0, 10, 100, or 200 µM phenidone [1-phenyl-3-pyrazolidinone; Sigma-Aldrich] dissolved in 95% ethanol) was added to the liquid medium of individual magenta boxes, and the effects on plant growth were monitored over 14 days. The last leaf with fully developed perforations before treatment was designated leaf 0 (L0; Fig. 9A and C) and the leaves that emerged after treatment (L1, L2, etc.; Fig. 9C) were excised, laid out in chronological order and photographed using a Nikon L110 digital camera (Nikon Instruments Canada, Mississauga, ON, Canada). The leaves of control and treated plants were then used for post-

harvest analyses of leaf morphology and anthocyanin content. A minimum of four independent samples were analyzed for each treatment type.

2.6.2. Post-harvest analysis of treated lace plants

2.6.2.1. *Leaf morphology*

Leaf lamina length and width, and the number of perforations were used to assess the effects of the treatment on the development of leaves that emerged over the 14 days. The morphology of various leaf stages (L0, L1, L2, L3, etc.) of treated plants were compared to their respective control leaf stages.

2.6.2.2. *Anthocyanin spectrophotometry*

The anthocyanin extraction protocol used to compare relative anthocyanin abundance in control and treated leaves is the same as the techniques described in Dauphinee et al. (2017), as described above. Relative anthocyanin abundance in the various leaf stages was compared to the respective control leaf stages (Fig. 9D).

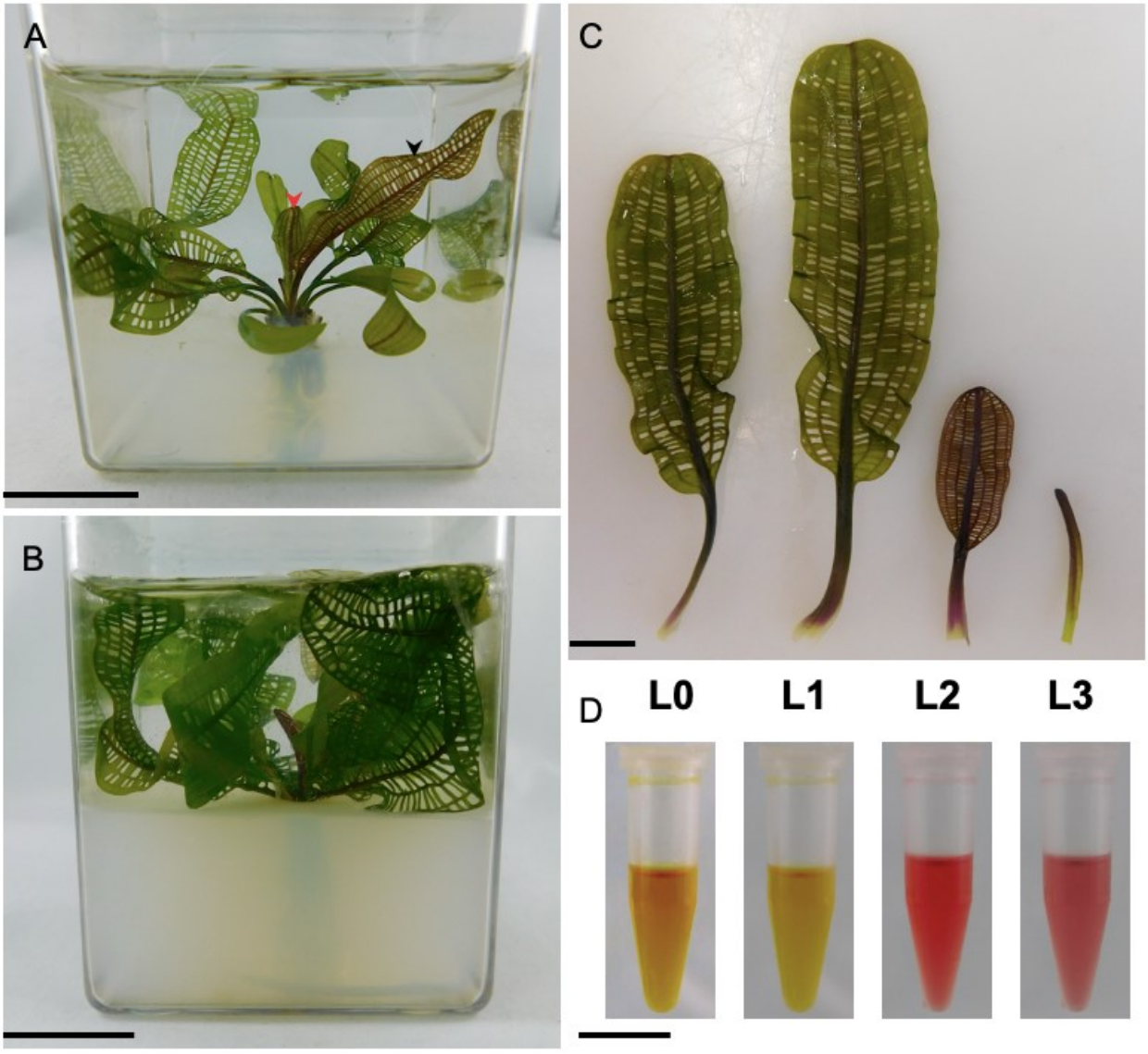

Figure 9. Whole plant experimentation using anthocyanin modulators. (A) Lace plants grown in sterile magenta box culture vessels that possessed a minimum of three fully perforated leaves were randomly assigned to a treatment group (control, methyl jasmonate, or phenidone). Black arrowhead = Leaf 0 (L0). Red arrowhead = Leaf 1 (L1). Control and treated plants were monitored for 14 days, and leaves were then harvested for morphological analysis. (B-D) An example of a leaf layout, and anthocyanin extraction of a control plant following 14 days of growth. (B) A control plant prior to leaf harvest. (C) Leaf 0 (L0) was designated as the last leaf to fully develop prior to treatment, and the leaves that emerged post-treatment (L1, L2 and L3) were organized chronologically. Leaf-blade length, leaf blade width, and number of perforations were measured in control and treated plants. (D) Relative anthocyanin abundance was compared in similar leaf stages of control and treated plants using spectrophotometry. Scale bars: A-B = 2.5 cm, C-D = 1 cm.

2.6.2.3. *Statistical analysis*

Statistical analyses were performed using GraphPad Prism 7 Software (GraphPad Software, San Diego, California, USA). Data are represented as mean ± standard error (SE). A two-tailed t-test was performed to compare the mean anthocyanin abundance between window and mature stage leaves. A two-way ANOVA and Dunnett's test were used for multiple comparisons for leaf length, width, perforation number and anthocyanin abundance.

CHAPTER 3: RESULTS

3.1. ANTHOCYANIN PROFILING IN LACE PLANT TISSUES

3.1.1. Ultra-pressure liquid chromatography analysis

UPLC-DAD was performed to determine the number of anthocyanin species present in lace plant tissues and to compare lace plant anthocyanins to six anthocyanin standards found in common fruits and vegetables. The six standards, including delphinidin 3-glucoside, cyanidin 3-glucoside, pelargonidin 3-glucoside, petunidin 3-glucoside, peonidin 3 glucoside, malvidin 3-glucoside, provided the various retention times presented in Table 3. Three unidentified impurities were also observed at 13.45, 15.21 and 16.52 min (Table 3).

Table 3. UPLC-DAD retention times for six common anthocyanins standards.

Anthocyanin Standard	**Retention time (min)**
Delphinidin 3-glucoside	3.78
Cyanidin 3-glucoside	5.50
Pelargonidin 3-glucoside	6.91
Petunidin 3-glucoside	7.43
Peonidin 3-glucoside	8.95
Malvidin 3-glucoside	10.70
Unidentified impurities	13.45, 15.21, 16.52

The retention times of the six anthocyanin standards (Table 3 and Fig. 10A) varied from the retention times observed in the lace plant crude anthocyanin from pre-perforated leaves (Fig. 10B), window stage leaves (Fig. 10C), mature leaves (Fig. 10D), and inflorescences (Fig. 10E). Comparison of the chromatograms (Fig. 10) showed that the absorbance peaks present in the anthocyanin standards chromatogram (Fig. 10A) were absent in the various lace plant tissue chromatograms (Fig. 10B-E). Absorbance peaks in the pre-perforated, window and mature stage leaf chromatograms were recorded at ~ 10, 15, 16, 19 and 19.5 min. However, the absorbance for

these retention times was lower in the pre-perforated leaves compared to window stage leaves. The chromatogram for mature leaves showed a lower absorbance peak at ~ 19.5 min compared to window stage leaves. The chromatogram for mature leaves also differed from window stage leaves at ~ 12 min and 18-19 min, where low to no absorbances were measured at these retention times. The chromatogram for lace plant inflorescences (Fig. 10E) had many peaks similar to in the leaf tissue chromatograms (e.g., ~ 10, 15, 16, 19 and 19.5 min) at higher absorbances, as well as additional smaller absorbance peaks at ~ 11-11.5, 16-17, and 18-19 min.

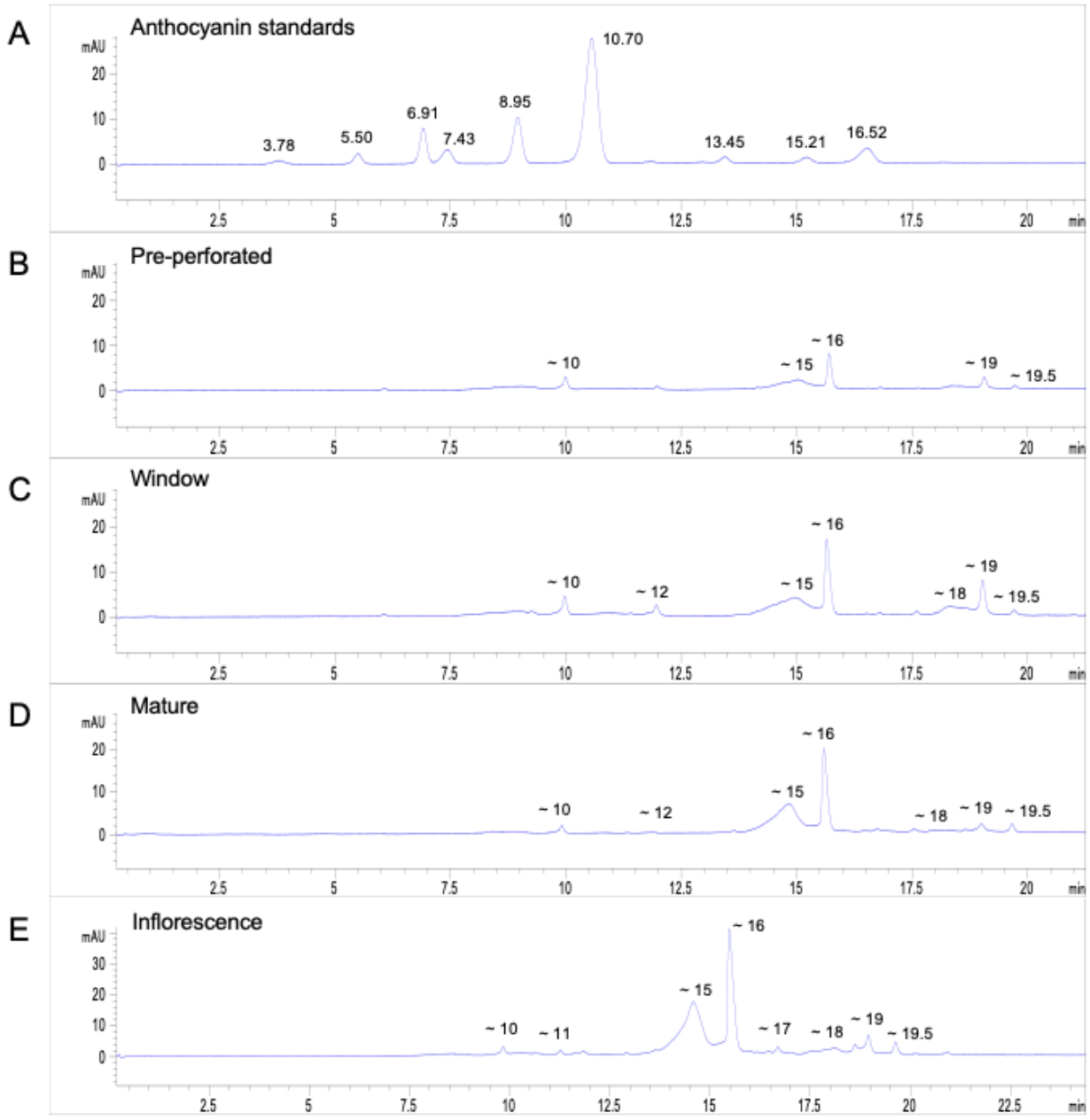

Figure 10. UPLC-DAD chromatograms for anthocyanin standards and lace plant tissues. Chromatogram for (A) six anthocyanin standards, and lace plant anthocyanin from (B) pre-perforated, (C) window, and (D) mature stage leaves, and (E) inflorescence with major peak times labelled.

3.1.2. Liquid-chromatography mass-spectrometry analysis

LC-MS/MS was performed to identify the anthocyanin species present in window and mature stage lace plant leaves. Three major peaks occurred in both window and mature chromatograms at 20.1 min, 24.6 min and 30.5 min, and the precursor/product mass transitions for these peaks and their potential anthocyanin identification are presented in Table 4. Two precursor/product mass transitions were observed at 20.1 min, 611/303 and 449/303. The potential anthocyanin assignments for these transitions were delphinidin 3-rutinoside and delphinidin 3-rhamnoside, respectively. The mass transition observed for 24.6 min was 433/287; kaempferol rhamnoside and cyanidin 3-rhamnoside were the proposed anthocyanin assignments in that particular instance. The mass transition observed for 30.5 min was 773/287, and cyanidin 3-sophoroside-5-glucoside was the proposed anthocyanin identification.

Commercial anthocyanin standards (delphinidin 3-rutinoside, delphinidin 3-rhamnoside, kaempferol rhamnoside, and cyanidin 3-rhamnoside) were purchased and run on the LC-MS/MS to use as references for the retention times of the proposed anthocyanins present in the window and mature stage leaf anthocyanin chromatograms (shown in Table 4). Although all the parent/product mass transitions for the commercially purchased anthocyanins matched the mass transitions from the lace plant anthocyanin LC-MS/MS chromatograms, none of the retention times for the commercially purchased anthocyanins matched the times for peaks exhibited in the lace plant anthocyanin LC-MS/MS chromatograms. The cyanidin 3-sophoroside-5-glucoside standard did not exhibit a peak for the 773/287 mass transition.

Table 4. LC-MS/MS results for lace plant anthocyanins and reference standards. Retention time, precursor/product ion transitions, and proposed anthocyanin identification of three major peaks from window and mature stage lace plant leaf LC-MS/MS chromatograms, and retention time and parent/product ion transitions of corresponding anthocyanin standards used to confirm lace plant anthocyanin identification.

Retention time of lace plant anthocyanin (min)	**Precursor/product ion ratio expressed as the m/z (mass/charge) ratio for each lace plant anthocyanin**	**Proposed lace plant anthocyanin identification**	**Retention time of anthocyanin standards (min)**	**Precursor/product ion ratio expressed as the m/z (mass/charge) ratio for each anthocyanin standards**
20.1	611/303	Delphinidin 3-rutinoside	12.3	611/303
20.1	449/303	Delphinidin 3-rhamnoside	14.1	449/303
24.6	433/287	Kaempferol rhamnoside	32.1	433/287
24.6	433/287	Cyanidin 3-rhamnoside	12.8	433/287
30.5	773/287	Cyanidin 3-sophoroside-5-glucoside	No peak	773/287

3.2. INVESTIGATION OF ANTHOCYANIN VACUOLAR INCLUSIONS IN LACE PLANT

3.2.1. Light microscope analysis of anthocyanin

The presence of anthocyanins was investigated in window and mature stage leaves via live-cell imaging and spectrophotometric analysis (Figs. 11-12). Window stage leaves exhibited an abundance of red/pink pigmentation localized throughout the leaf blade, excluding EPCD and LPCD cells (Figs. 11A and 12). Anthocyanin was abundant at the apex of window stage leaves, but it was not apparent at the leaf margins in the epidermal cell layer (Figs. 11B, 12B and D). AVIs were also visible in the leaf apex (Fig. 11). Cells in this region were predominantly

red/pink from soluble anthocyanin within the vacuolar lumen compared to AVI pigmentation, which was visible as small concentrated bodies (Fig. 12D). Cross sections of the window stage leaf apex showed anthocyanin localized in the mesophyll layers (Fig. 12C and E). The mid-region of the window stage leaves was also examined for the presence of AVIs (Fig. 12F-K). Although soluble anthocyanin was visible in the mid-vein (Fig. 12F and I) and NPCD cells (Fig. 12G and J), AVIs were not visible. A cross-section of the mid-region of window stage leaves showed soluble anthocyanin localized in the mesophyll cell layers and not in the epidermis (Fig. 12K). Anthocyanins and AVIs were not observable in the leaf apex of mature stage leaves (Fig. 11C-D). Spectrophotometry analysis (Fig. 11E) showed that window stage leaves have significantly more anthocyanin than mature leaves ($t = 2.964$, $df = 9$, $p = 0.0159$).

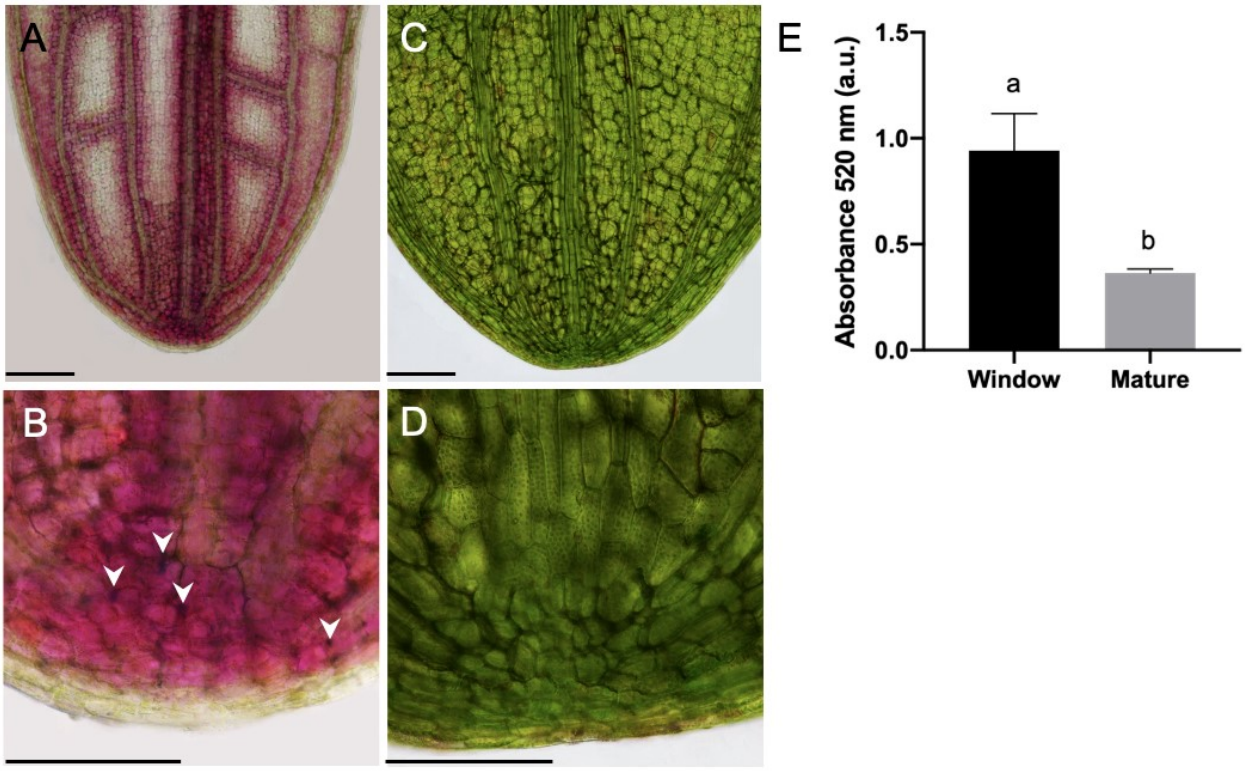

Figure 11. Presence of anthocyanins in window and mature stage lace plant leaves. (A) Window stage leaf apex at low and (B) higher magnification. Soluble anthocyanins and anthocyanin vacuolar inclusions (white arrowheads) were visible in window stage leaves at higher magnification. (C) Mature stage leaf apex at low and (D) high magnification. (E) Relative abundance ± SE of anthocyanin in window and mature stage lace plant leaves. $n \geq 5$. Scale bars: A and C = 0.2 cm B and D = 0.1 cm.

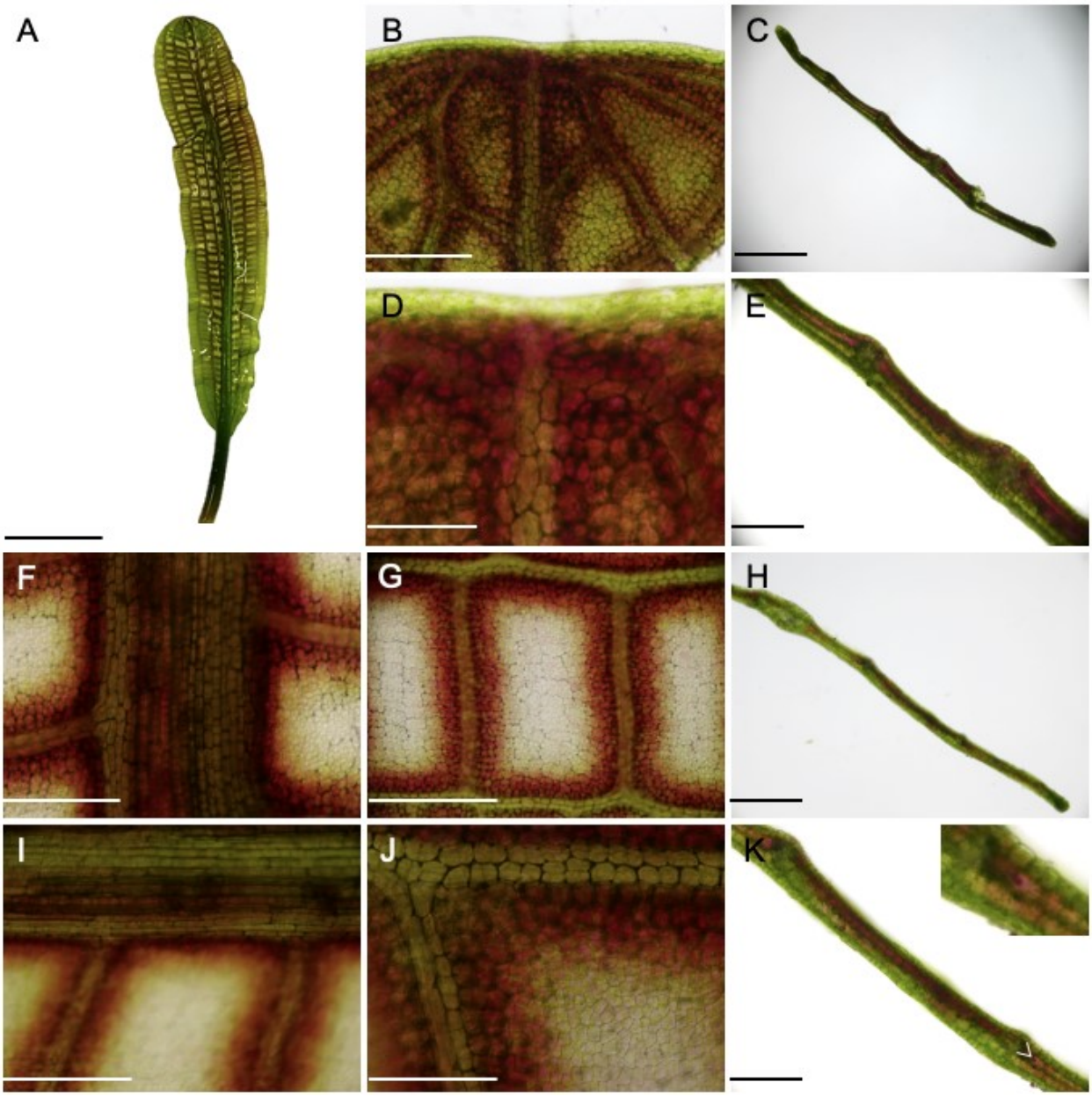

Figure 12. Investigation of anthocyanin in window stage lace plant leaves. (A) Whole window stage leaf obtained from sterile cultures. (B) Micrographs of the window stage leaf apex (top 10% of the total leaf blade length) and (C) corresponding cross-section at low magnification and (D-E) apex and cross section micrographs at higher magnification. (F-K) Micrographs of the mid-region of window stage leaves (top 10 to 25% of the total leaf blade length). (F) Window mid-vein, (G) areole, (H) cross-section at low magnification and (I-K) similar areas at higher magnification. (K) An anthocyanin vacuolar inclusion (white arrowhead) in the mid-leaf cross section is visible at higher magnification (enlarged in top-right corner). Scale bars: A = 1 cm, B, E-G, I, and K = 0.5 mm, C and H = 1 mm, D = 0.1 mm J = 0.2 mm.

3.2.2. Confocal microscope investigation of anthocyanin

Anthocyanin autofluorescence was examined in window stage leaves using confocal laser scanning microscopy (Fig. 13 and 14). The apex of window stage leaves exhibited anthocyanin autofluorescence in all mesophyll cells and vasculature tissues (Fig. 13A). The anthocyanin autofluorescence was absent in the epidermal cell layer at the apex leaf margin (Fig. 13B). Soluble anthocyanin was observable in cells as a solid red fluorescence that occupies the majority of the vacuolar space (Fig. 13C-F), whereas concentrated anthocyanin bodies were visible as spherical bodies that fluoresce more intensely than soluble anthocyanin. The anthocyanin bodies observed by confocal microscopy in the window stage leaf apex were approximately 1-2 μm in diameter, located within the vacuolar space, and typically limited to one per cell (Fig. 13C-F).

The mid-region of window stage leaves exhibited anthocyanin autofluorescence in the NPCD cells and vasculature (Fig. 14A). Autofluorescence was absent in the EPCD and LPCD cells in window areoles (Fig. 14A). Soluble anthocyanin was prominent in NPCD cells; however, few, small anthocyanin bodies were also observable (Fig. 14C and E). The anthocyanin bodies observed by confocal microscopy in the mid-regions of window stage leaves were smaller than those seen in the window stage leaf apex. They were approximately 500-800 nm in diameter, and many were found within one cell. A few of the concentrated bodies of anthocyanin were seen at the periphery of the vacuolar space, so it is possible they were localized in the lumen or cytosol. Therefore, two distinct morphologies of anthocyanin bodies were observed in the two areas of investigation (apex and mid-regions) in window stage leaves.

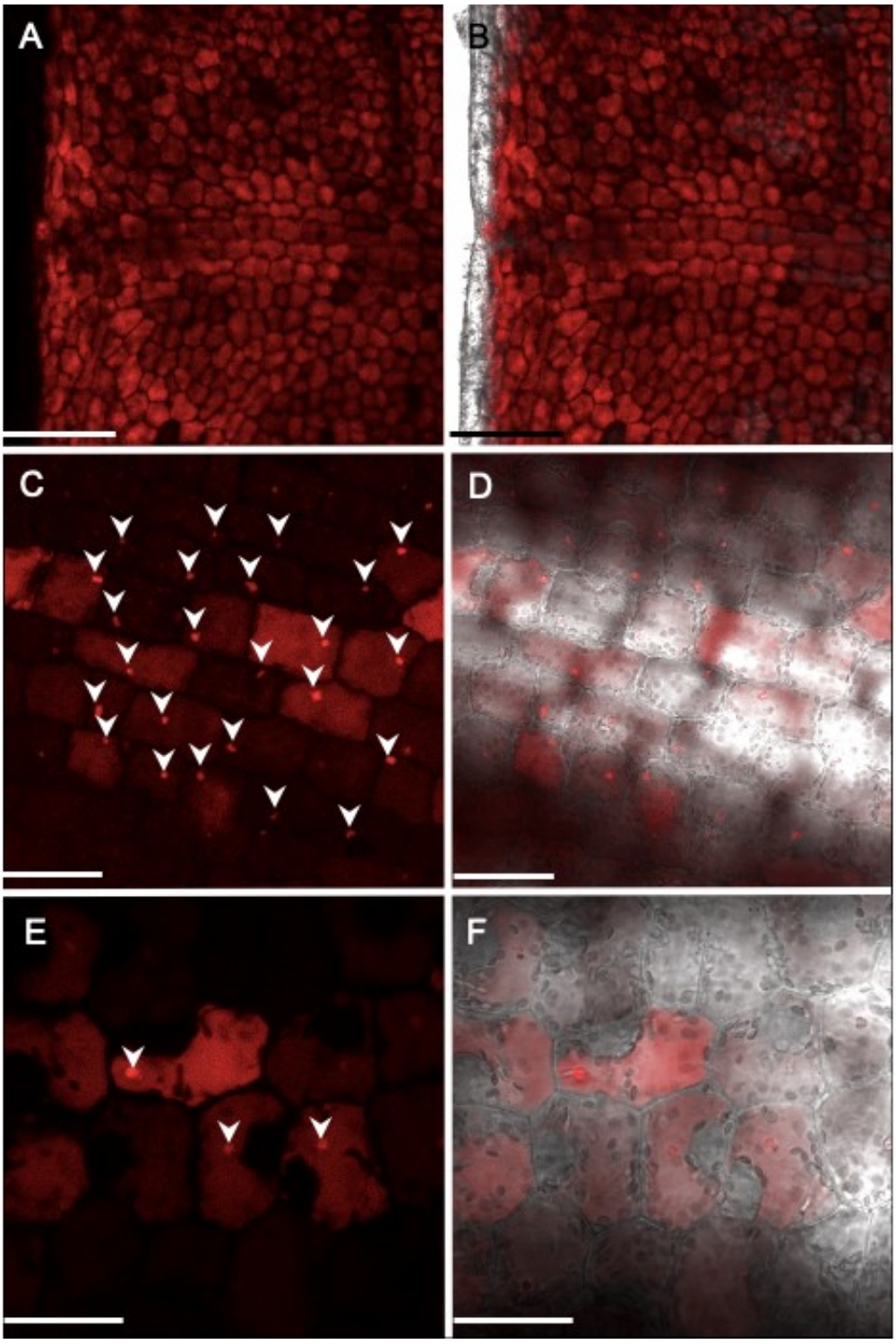

Figure 13. Anthocyanin autofluorescence in the apex of window stage leaves. (A) Window stage leaf apex at 20x, (C) 40x and (E) 100x magnification and (B, D, F) corresponding differential interference contrast (DIC) overlay image showing background cellular structure. Anthocyanin concentrated bodies (white arrowheads) are distinct from soluble anthocyanin localized in the vacuole. A and B = 200 µm, C and D = 50 µm, E and F = 20 µm.

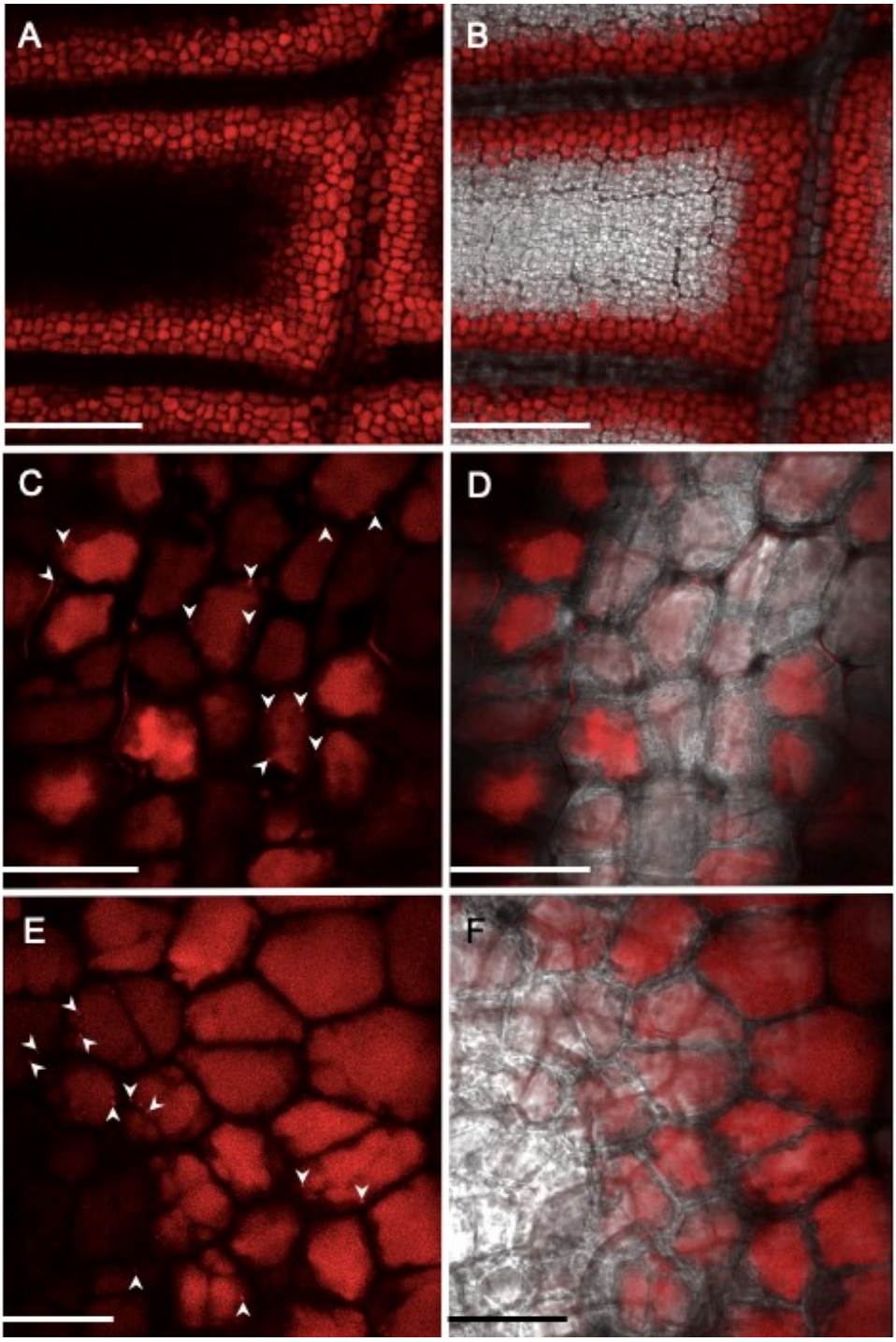

Figure 14. Anthocyanin autofluorescence in the mid-region (top 10 to 25% of the total leaf blade length) of window stage leaves. (A) A window stage leaf areole at 20x and (B) corresponding differential interference contrast overlay (DIC) image showing background cellular structure. (C) Micrographs of vasculature at 40x and (E) non-PCD (NPCD) cells at 100x magnification with (D, F) corresponding DIC overlay images. Anthocyanin vacuolar inclusions (white arrowheads) are distinct from soluble anthocyanin localized in the vacuole. A and B = 200 μm, C and D = 50 μm, E and F = 20 μm.

3.2.3. Transmission electron microscope analysis of anthocyanin transport

Anthocyanin and AVIs in window stage leaves were also examined using TEM to determine their structure, subcellular localization and transport method (Fig. 15). Anthocyanin aggregates contained in vesicles in the cytoplasm were termed anthocyanin bodies, whereas anthocyanin aggregates located in the vacuole were termed AVIs. Electron-dense, osmiophilic, spherical bodies that lacked an immediate enclosing membrane were visible in the cytoplasm and vacuole (Fig. 15A-F). The spherical bodies that were visible in the cytoplasm were enclosed in vesicles closely associated with ER networks (Fig. 15B–C). The anthocyanin containing vesicles were also observable in the cytoplasm near mitochondria and chloroplasts (Fig. 15C-E). Vesicles containing the electron-dense bodies were seen adjacent or conjoined to the tonoplast (Fig. 15D-E). The electron-dense bodies appear to enter the vacuole and were observed on the inner face of the tonoplast membrane (Fig. 15E). Inside the vacuole, some of the electron-dense bodies were shown to agglomerate (Fig 15F).

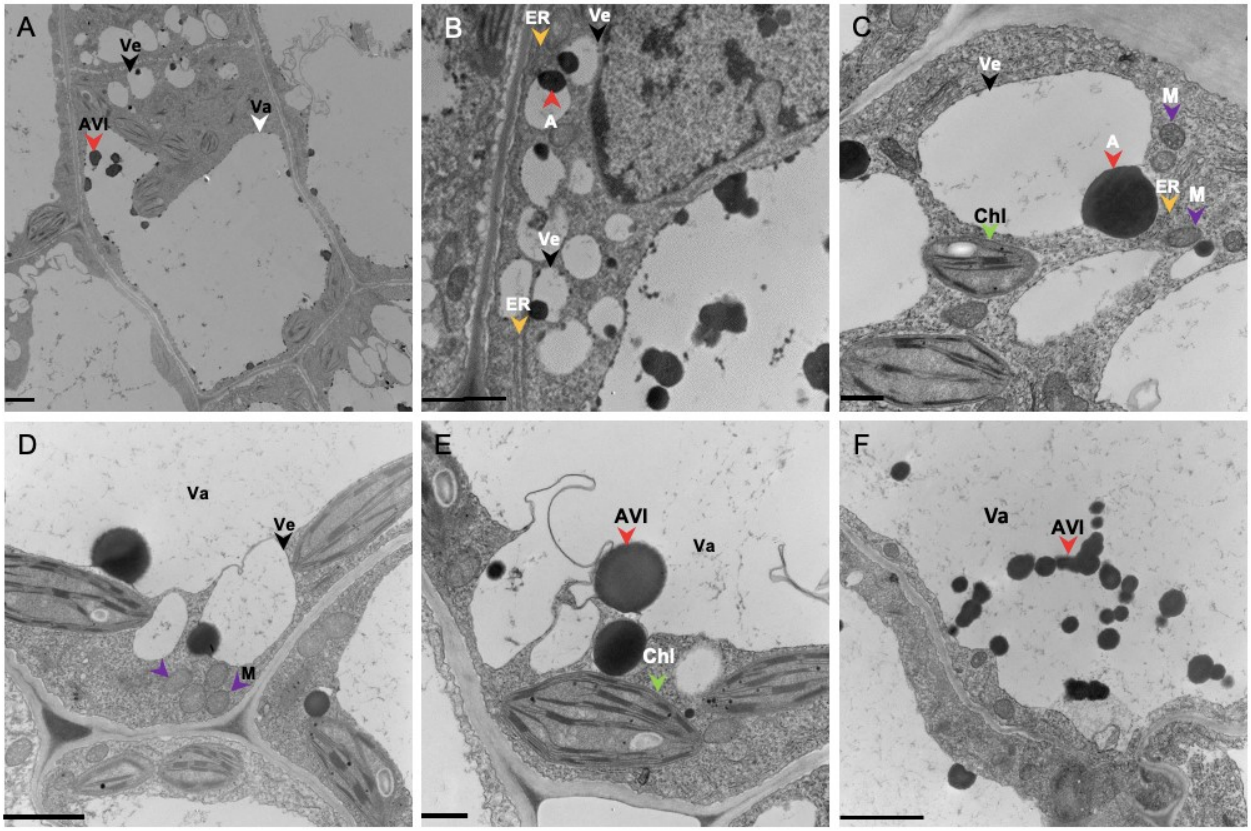

Figure 15. Transmission electron microscope (TEM) investigation of the intracellular transportation mechanism of anthocyanin in window stage lace plant leaves. (A) Micrograph of a window stage leaf cell. (B-C) Spherical, electron-dense anthocyanin bodies are present in vesicles in the cytoplasm closely associated with endoplasmic reticulum (ER) networks. (D) anthocyanin-containing vesicles are seen adjacent to the tonoplast. (E) Anthocyanin bodies enter the vacuole. (F) Within the vacuole, anthocyanin vacuolar inclusions (AVIs) may remain solitary or agglomerate. A (red arrowheads) = Anthocyanin bodies. AVI (red arrowhead) = Anthocyanin vacuolar inclusion. Chl (green arrowheads) = Chloroplast. ER (yellow arrowheads) = Endoplasmic reticulum. M (purple arrowheads) = Mitochondria. Va (white arrowheads) = Vacuole. Ve (black arrowheads) = Vesicle. Scale bars: A-B, D and F = 2 µm, C = 0.5 µm, E = 0.8 µm.

3.3. INVESTIGATION OF ENDOPLASMIC RETICULUM IN LACE PLANT LEAVES

3.3.1. Confocal analysis of endoplasmic reticulum

Lace plant leaves were stained with fluorescent green dye, DiOC6(3), to determine ER structure and dynamics within the various cell types (Fig. 16 and 17; Supplementary material 2-5). Window stage leaves stained with DiOC6(3) exhibited green fluorescence throughout areoles

(Fig. 16A-B). The DiOC6(3) staining was more noticeable in NPCD cells and leaf veins compared to EPCD and LPCD cells. Stained NPCD cells displayed green fluorescence uniformly distributed throughout the cytoplasm (Fig. 16C-D; Supplementary material 2). ER networks were visible as dynamic tubules and fluorescence was the most intense in the cytosol closest to the outer face of epidermal cells. EPCD cells stained with DiOC6(3) showed ER as dynamic puncta (Fig. 16E-F; Supplementary material 3). Networks of tubules were not observed in EPCD and LPCD cells. Stained LPCD cells exhibited limited fluorescence (Fig. 16G-H; Supplementary material 4). Few fluorescent puncta were recorded in the cytosol and as conglomerations with large aggregates in the vacuole in LPCD cells.

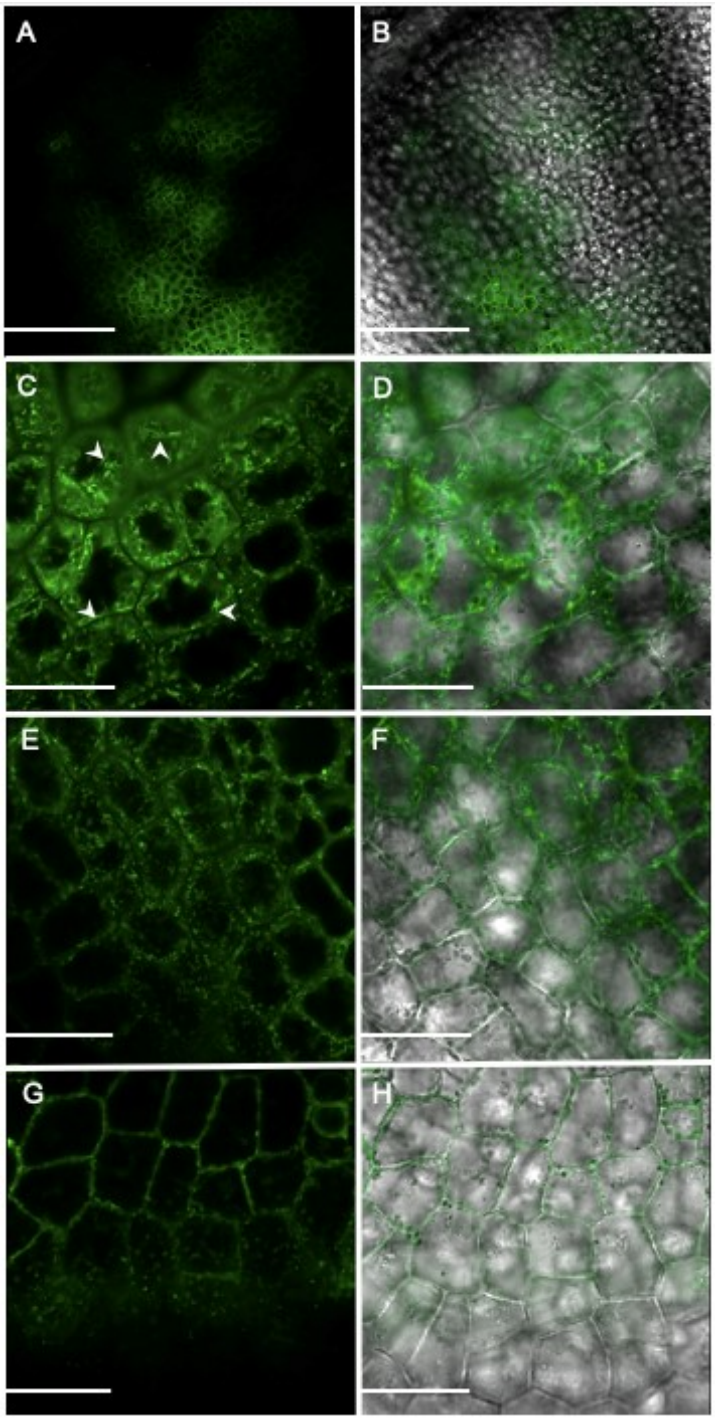

Figure 16. Confocal microscopy of structure of endoplasmic reticulum (ER) across the programmed cell death (PCD) gradient in window stage lace plant leaves. (A) An areole stained with ER dye, 3,3'-dihexyloxacarbocyanine iodide (DiOC6[3]), and (B) corresponding differential interference contrast (DIC) overlay image showing corresponding background cellular structure. (C) Non-PCD (NPCD), (E) early-PCD (EPCD), and (G) late-PCD (LPCD) cells stained with DiOC6(3). (D, F, H) Corresponding DIC overlay images. Scale bars: A and B = 200 µm, C-H = 50 µm.

Mature stage leaves stained with DiOC6(3) exhibited green fluorescence in all cells within the areoles (Fig. 17A-B). Similar to DiOC6(3)-stained NPCD cells in window stage leaves, mature cells had fluorescent ER uniformly distributed throughout the cytoplasm (Fig. 17C-F). ER fluorescence was the most intense in the cytosol closest to the outer face of epidermal cells. ER in mature leaves were visible as long, dynamic networks of polygonal tubules, lamellar sheets, as well as intensely stained puncta (Fig. 17E; Supplementary material 5). The network of tubules was brighter and had more distinct structures in the stained cells of mature leaves compared to NPCD cells in window stage leaves.

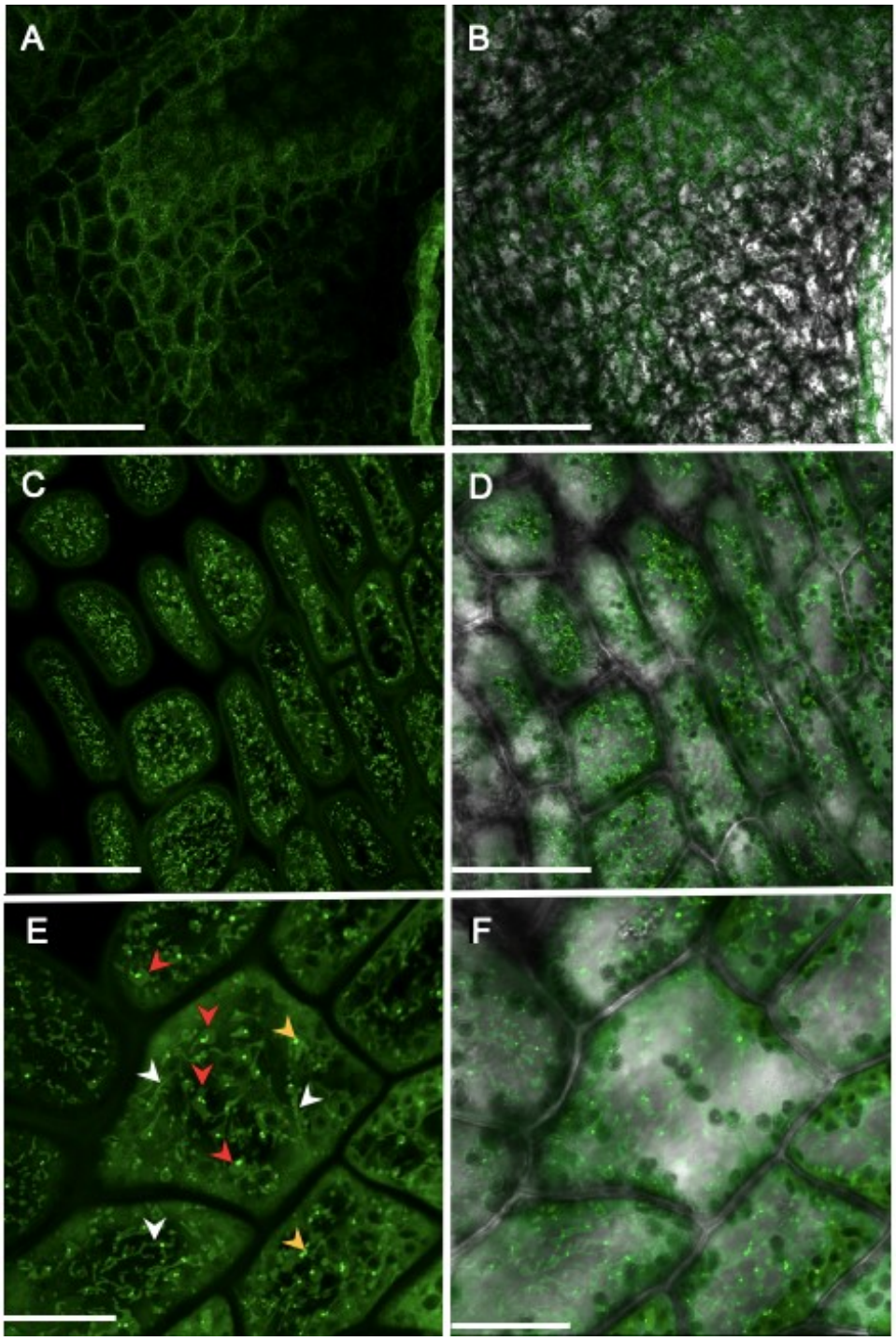

Figure 17. Confocal microscopy of structure of endoplasmic reticulum (ER) in mature stage lace plant leaves. (A) An areole stained with ER dye, 3,3'-dihexyloxacarbocyanine iodide (DiOC6[3]), and (B) corresponding differential interference contrast (DIC) overlay image showing background cellular structure. (C) Micrographs of mature cells at 40x and (E) 100x magnification. (D, F) Corresponding DIC overlay images. ER structures are visible as tubular networks (white arrowheads), cisternae sheets (red arrowheads) and spherical bodies (yellow arrowheads). Scale bars: A and B = 200 µm, = 50 µm, E and F = 20 µm.

3.3.2. Ultrastructural analysis of endoplasmic reticulum

Transmission electron microscopy was performed to examine the ER structure in NPCD and PCD cells in window stage lace plant leaves (Fig. 18). Healthy NPCD cells (Fig. 18A-D) possessed chromatin evenly distributed throughout the nucleus. The vacuole in NPCD cells was intact and contained numerous spherical, osmiophilic AVIs. Chloroplasts and mitochondria were intact (Fig. 18B-C). ER networks in NPCD were composed of long, interconnected tubules localized in the cytoplasm (Fig. 18 B-D, yellow arrowheads). ER tubules were often seen in close proximity to anthocyanin-containing vesicles (Fig. 18B and D). Cells that had initiated the PCD process (Fig. 18E-H) had misshapen chloroplasts (Fig. 18F), and inconspicuous thylakoid membranes (Fig. 18F-G). ER in PCD cells were fragmented and swollen (Fig. 18F-H).

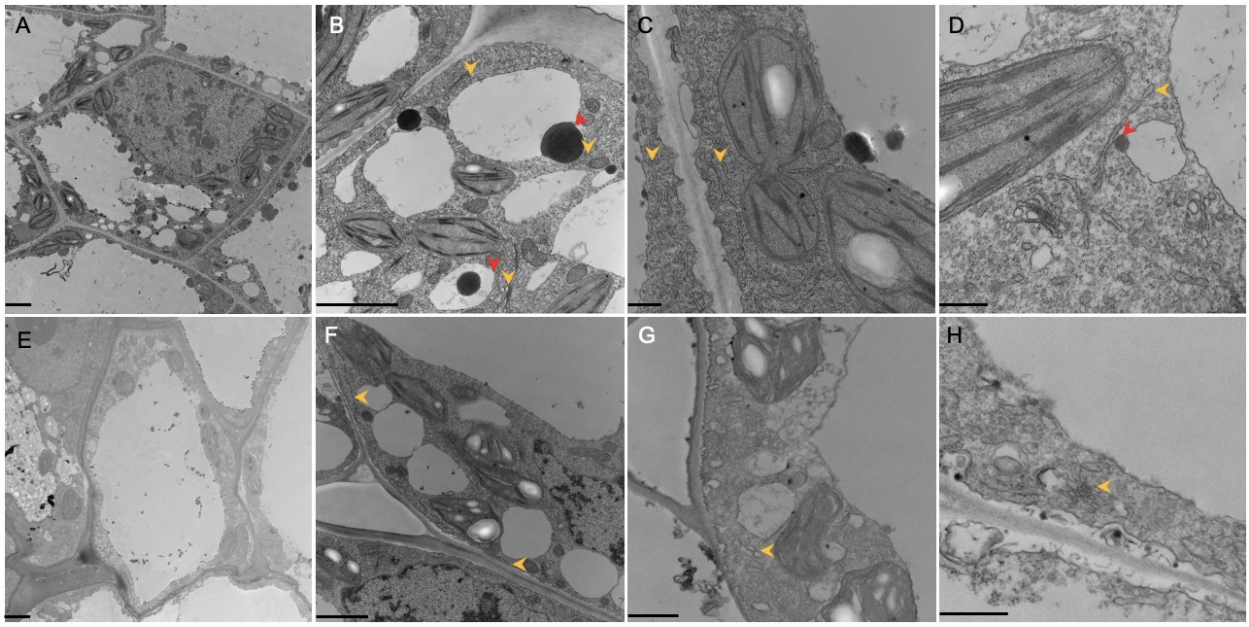

Figure 18. Transmission electron micrographs of endoplasmic reticulum (ER) in non-programmed cell death (NPCD) and programmed cell death (PCD) cells in window stage lace plant leaves. (A-D) ER in cells that will not undergo developmental PCD (non-PCD or NPCD cells) during perforation formation. (B-C) ER networks (yellow arrow heads) composed of long, interconnected tubules localized in the cytoplasm in NPCD cells. (D) Anthocyanin-containing vesicles (red arrowheads) closely associated with ER networks. (E-H) Micrographs of ER in cells that will undergo PCD (PCD cells) during perforation formation. (F-H) ER strands in PCD cells are fragmented and swollen (yellow arrowheads). Scale bars: A-B, E-F = 2 µm, C-D and H = 0.5 µm, G = 0.8 µm.

3.4. Pharmacological experiments with anthocyanin modulators

Whole plant treatment experiments with anthocyanin modulators, methyl jasmonate (MeJA) and phenidone, were performed to determine the role of anthocyanin in lace plant development (Figs. 19-20). Individual plants were treated with 0 (control), 1, 2.5, or 5 µM MeJA (Fig. 19). There were no significant differences in leaf length between control and treated plants when comparing similar leaf stages (Fig. 19B). The leaf width of L2 was significantly smaller in 2.5 µM MeJA plants ($P = 0.0171$) compared to control plants (Fig. 19C). Leaf width was not different for any other concentrations or leaf stages. The number of perforations did not differ between control and treated plants for all concentrations (Fig. 19D). Anthocyanin absorbance

was significantly higher in leaf 2 for 1 µM (P = 0.0197), 2.5 µM (P = 0.0131) and 5 µM treated plants (P = 0.0378).

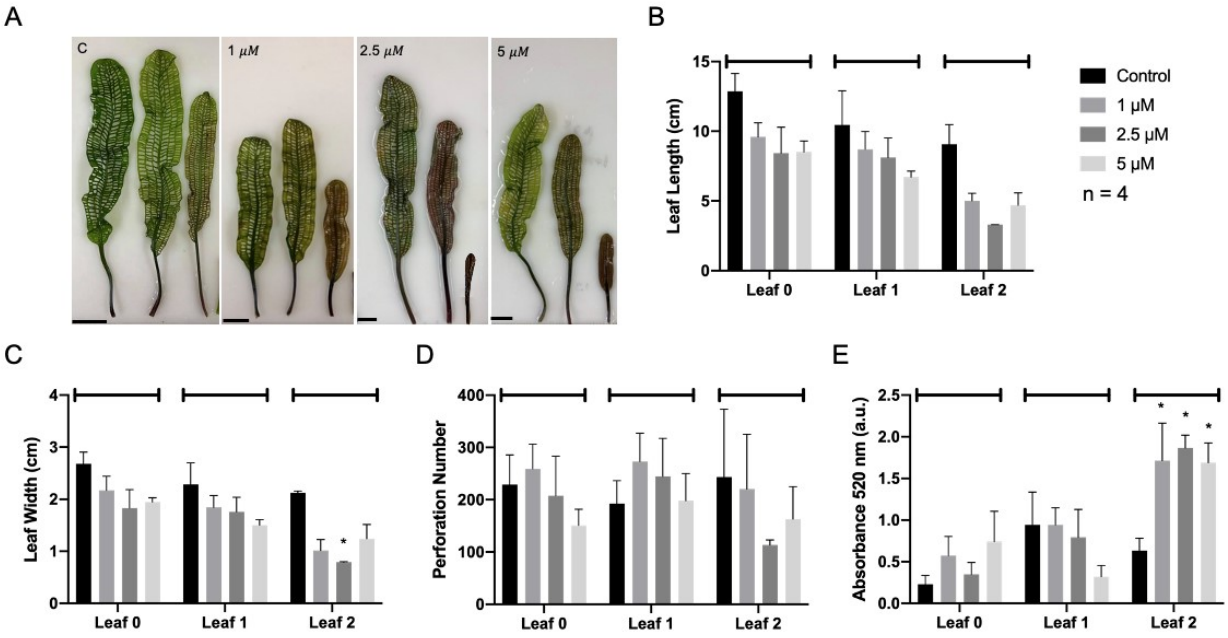

Figure 19. Whole plant treatment experiments using anthocyanin modulator, methyl jasmonate (MeJA), on lace plants. (A) Leaf layout of control and MeJA treated plants. A range of MeJA concentrations (control, 1 µM, 2.5 µM, or 5 µM) were used to determine its effects on lace plant leaf growth and development. Leaves are displayed in chronological order of emergence (leaf 0, leaf 1, and leaf 2) from left to right. (B) Leaf length, (C) leaf width, (D) number of perforations, and (E) relative anthocyanin abundance ± SE were compared in control and treated plants. (C-E) Bars above leaf stage (leaf 0, 1 or 2) indicate a group for Dunnett's multiple comparisons testing. C = Control. * = $p < 0.05$. Scale bars: A = 1 cm.

Individual plants were treated with 0 (control), 10, 100, or 200 µM phenidone (Fig. 20). There were no significant differences in leaf lengths, widths, or number of perforations between control and treated plants when comparing similar leaf stages (Fig. 19B-D). Anthocyanin absorbance was significantly lower in leaf 2 for 100 µM (P = 0.0197), and 200 µM treated plants (P = 0.0378).

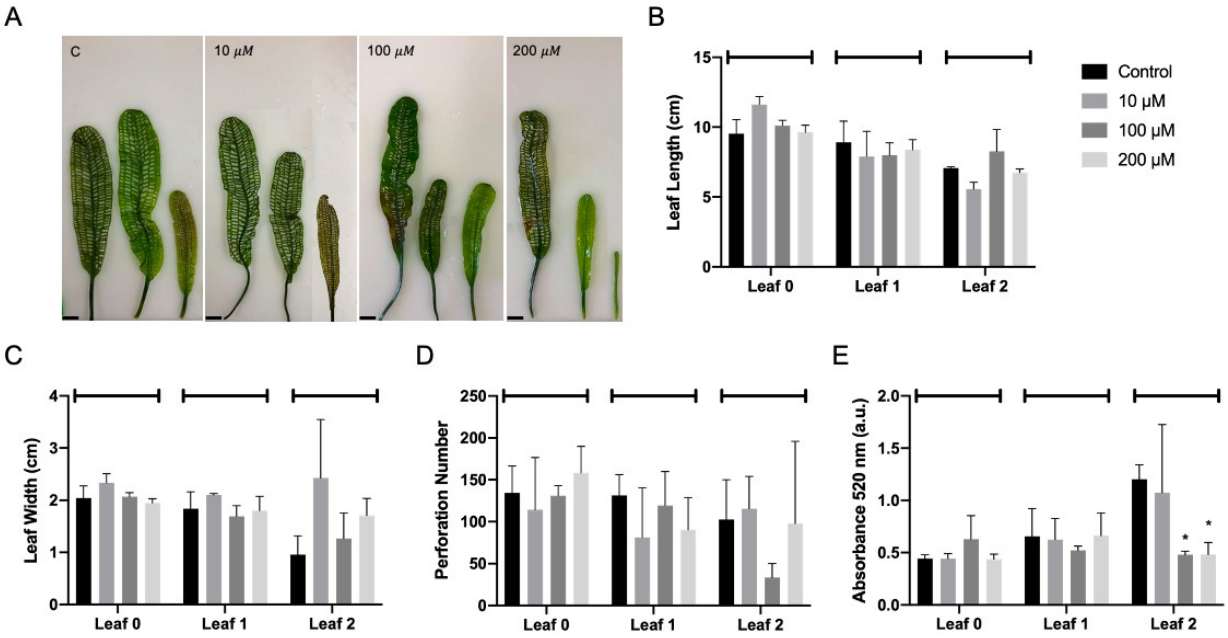

Figure 20. Whole plant treatment experiments using anthocyanin modulator, phenidone, on lace plants. (A) Leaf layout of control and phenidone treated plants. A range of phenidone concentrations (control, 10 µM, 100 µM, or 200 µM) were used to determine its effects on lace plant leaf growth and development. Leaves are displayed in chronological order of emergence (leaf 0, leaf 1, and leaf 2) from left to right. (B) Leaf length, (C) leaf width, (D) number of perforations, and (E) relative anthocyanin abundance ± SE were compared in control and treated plants. (C-E) Bars above leaf stage (leaf 0, 1 or 2) indicate a group for Dunnett's multiple comparisons testing C = Control. * = $p < 0.05$. Scale bars: A = 1 cm.

CHAPTER 4: DISCUSSION

4.1. ANTHOCYANIN PROFILING IN LACE PLANT TISSUES

4.1.1. UPLC of anthocyanin in lace plant tissues

The retention times of the common six anthocyanin standards (Table 3) used to compare to anthocyanins in lace plant tissues were not observed in any of the lace plant tissue chromatograms, suggesting that common anthocyanins are not present in lace plant leaves or inflorescences (Table 3 and Fig. 10). Cyanidin, delphinidin, pelargonidin, peonidin, malvidin, and petunidin are the most common anthocyanidins distributed in plants. The distribution of these anthocyanidins in fruits and vegetables is 50%, 12%, 12%, 12%, 7%, and 7%, respectively (Castañeda-Ovando et al. 2009; Khoo et al. 2017). The most common sugar in anthocyanidin 3-monosaccharides is glucose (Einbond et al. 2004; Zhang et al. 2014; Veberic et al. 2015). Cyanidin 3-glucoside is the most common anthocyanin in nature and is often used as a standard in anthocyanin profiling analyses (Wrolstad et al. 2005; Khoo et al. 2017). These findings indicate that lace plant tissues possess a unique profile of anthocyanins that are not common in nature.

Similar retention times for anthocyanin peaks were observed in pre-perforation, window and mature-stage leaf chromatograms. This indicates that the same anthocyanin species are present throughout the leaf stages, and these anthocyanins may be used for stress tolerance and managing normal cell signalling (Hatier and Gould 2008b; Landi et al. 2015). However, the relative abundance of these anthocyanins differed in the various developmental stages. Peaks were lower in pre-perforated and mature stage leaves compared to window, which shows the accumulation of certain anthocyanin species during this specific stage of perforation formation. During window-stage, anthocyanins are used to mitigate oxidative stress caused by ROS (a

signalling molecule for PCD) in cells destined to live (Dauphinee et al. 2017). The accumulation of certain anthocyanin species (indicated by the chromatogram peaks) during window stage suggests that these specific compounds might be crucial for regulating PCD.

Additionally, certain anthocyanin species observed in the chromatograms of pre-perforation stage and window stage leaves were not observed in mature-leaf chromatograms. Similar anthocyanins in both pre-perforation and window stage leaves may indicate the role these anthocyanins play in moderating developmental PCD in young lace plant leaves. Although there is no microscopic evidence of PCD initiation in pre-perforated leaves (Gunawardena et al. 2004), molecular analysis indicates that caspase (cysteine-aspartic proteases, PCD facilitators) activity is prompted at this early stage of perforation formation (Lord et al. 2013). Therefore, anthocyanin production for PCD signalling may be produced in both pre-perforated and window stage leaves. Alternatively, the anthocyanins might be used for their antioxidant properties to protect young leaves from light, temperature or other adverse conditions. Previous literature indicates that anthocyanins are common in young developing leaves to protect developing chloroplasts from the photo-inhibitory and photooxidative effects of strong light (Gould 2004; Hatier and Gould 2008b).

Numerous anthocyanin peaks were observed in the chromatogram of lace plant inflorescences, which were not observed or were less abundant in leaf chromatograms. The anthocyanin species present may be utilized to produce the distinct pink and purple colouration seen in the lace plant inflorescences (Fig. 5B). Various shades of pink/purple are observed in the petals, pistil, anther, filament, and spikes. Anthocyanin colour is influenced by chemical side groups, vacuolar pH, co-pigmentation with other molecules and metal ions (Kallam et al. 2017; Liu et al. 2018). Anthocyanidins differ in colour based on the number and position of the

hydroxyl group. An increase in the number of hydroxyl groups changes the colour of the anthocyanidin from orange to purple (Ananga et al. 2013; Liu et al. 2018). Addition of a glycosyl group results in reddening of anthocyanin pigment, whereas acylation causes a colour shift from red to blue (Liu et al. 2018). The various anthocyanin species presented in the lace plant inflorescence chromatogram may contribute of the diversity of colours observed in the floral structures.

The longer retention times of peaks observed in lace plant samples suggests that the anthocyanins are acylated. Acylation of a sugar hydroxyl reduces the polarity and increases the elution times (Young and Abdel-Aal 2009). Sugars are often acylated with aromatic or aliphatic acids, which increases their stability in solution (Ananga et al. 2013; Zhang et al. 2014; Liu et al. 2018). Anthocyanins are highly reactive and unstable, but acylation prevents degradative reactions and facilitates storage for future use (Zhang et al. 2014). The acylation of anthocyanins has also been shown to increase antioxidant activity (Hatier and Gould 2008b; Khoo et al. 2017). Additionally, AVIs contain a high proportion of acylated anthocyanins compared to total anthocyanin content in the cell (Conn et al. 2003; Grotewold and Davies 2008; Conn et al. 2010; Pourcel et al. 2010; Chanoca et al. 2015; Kallam et al. 2017). These results suggest that acylated anthocyanins may be abundant in lace plant tissues functioning as potent antioxidants and may be contained in AVI structures. Isolation and identification of the anthocyanin species present in AVIs in window stage lace plant leaves may elucidate the anthocyanins involved in perforation formation.

4.1.2. LC-MS/MS of anthocyanin in window and mature leaves

Based on the LC-MS/MS parent/product mass transitions, five anthocyanins identifications were proposed: delphinidin 3-rutinoside, delphinidin 3-rhamnoside, kaempferol

rhamnoside, cyanidin 3-rhamnoside and cyanidin 3-sophoroside-5-glucoside. The corresponding anthocyanin standards were purchased and used to confirm retention times of the proposed anthocyanin species, and although the precursor/product ion transitions were the same, the retention times were not. This demonstrates that the proposed identifications of lace plant anthocyanins were incorrect. The similarities in precursor/product ion mass transition could be due to the structural diversity of anthocyanin species (Crozier et al. 2008; de Brito Francisco and Martinoia 2018). Depending on the chemical moieties attached to the anthocyanin species, two structurally different compounds may result in similar masses. Interestingly, there was no peak for the reference anthocyanin cyanidin 3-sophoroside-5-glucoside, which suggests that the compound may have been degraded.

Reference compounds for LC-MS are often expensive and difficult to obtain, which presents an important drawback for LC-MS methods (Košir et al. 2004; Castañeda-Ovando et al. 2009). An alternative strategy to identify anthocyanin species present in lace plant leaves is nuclear magnetic resonance (NMR), which utilizes magnetic fields to determine the structure of organic molecules. This method would dictate the structure, sugar identification, position and angle of the sugar attachments (Wrolstad et al. 2005).

4.2. INVESTIGATION OF ANTHOCYANIN VACUOLAR INCLUSIONS IN LACE PLANT

4.2.1. Light microscope analysis of anthocyanin in window and mature leaves

Anthocyanins were abundant at the leaf apex of window stage leaves and was observable as two morphologies: soluble, and concentrated bodies (Fig. 11). Abundant soluble anthocyanins are visible in all cells within the apex, excluding the leaf margins (Fig 11A and B). The sharp contrast in anthocyanin abundance between the leaf margin and lamina may be explained by an auxin maximum and the canalization hypothesis. Auxin maxima are thought to be located within

the epidermal layers of the leaf margins in young, developing leaves, even after primary morphogenesis and formation of vascular tissues (Reinhardt et al. 2003; Hay et al. 2006; Scarpella et al. 2010; Bilsborough et al. 2011). The high concentration of auxin in these areas would prevent the accumulation of anthocyanins in cells. Previous studies have identified the antagonistic effect of auxin on anthocyanin biosynthesis in apple and carrot cells (Ozeki and Komamine 1986; Ji et al. 2015; Wang et al. 2018). Accumulation of auxin in lace plant leaves resulting from polar-auxin transport inhibition resulted in lower anthocyanin levels in window stage leaves (Denbigh et al. 2020). During vasculature formation, auxin maxima promote the formation of veins, which leads to subsequent depletion of auxin in surrounding cells (Reinhardt et al. 2003). This would facilitate the accumulation of auxin found in the laminar cells of the leaf apex, adjacent to the leaf margins that possessed no visible anthocyanins.

Although abundant anthocyanins in window stage leaves has been observed in previous studies (Denbigh et al. 2020), the presence of AVIs in leaves grown under normal conditions is not as obvious in lace plant leaves (Fletcher 2017). Numerous AVIs have been recorded in the apices of window stage leaves grown under stressful conditions, including low light, nutrient stress and high pH (Fletcher 2017). The morphology of AVIs in stressed window stage leaves is highlighted in Appendices 2 and 3 and resemble the two forms of AVI structures described in Grotewold and Davies (2008): spherical, liquid-like bodies and fibrous structures. Few AVIs were observable in window stage leaves grown in normal conditions (Fig. 11). However, no AVIs were visible in mature leaves using light microscopy. During this stage of development, PCD is completed and the need for anthocyanins to combat oxidative stress resulting from this developmental process would be limited. Quantification of anthocyanins in window and mature stage leaves concur with microscopic observations, confirming that anthocyanin levels are lower

in mature compared to window stage leaves (Fig. 11). Dauphinee et al. (2017) suggest that the limited amount of anthocyanins present in mature lace plant leaves is utilized in cell senescence or turnover. During cell senescence in leaves, anthocyanins are utilized to mitigate oxidative stress resulting from chloroplast degradation, thus allowing for effective nutrient recycling and redistribution (Lee et al. 2003).

4.2.2. Light microscope analysis of anthocyanin in various areas of the window stage leaf

Few AVIs were seen in the leaf apex of window stage leaves using light microscopy, whereas AVIs were rarely observed in the mid-regions, including the vasculature and NPCD cells (Fig. 12). Interestingly, AVIs were seen in both vasculature and NPCD cells of window stage leaves grown under stressful conditions (Appendices 2 and 4D, F-G and I-J; Supplementary material 1). The production of anthocyanins in NPCD cells in response to ROS accumulation and oxidative stress is recognized. However, the presence and accumulation of the pigment in the vasculature is less understood. Anthocyanins are typically act or function close to the site of synthesis and are not known to travel long distances through the plant (Landi et al. 2015). Anthocyanin precursors and other flavonoids have been found to travel long distances in *Arabidopsis* mainly through vascular tissue (Buer et al. 2007). Anthocyanins (or their precursors) may be transported via vasculature to facilitate the supply of antioxidants in cells combating oxidative stress. The transport mechanism of anthocyanins between cells requires further investigation (Landi et al. 2015).

Cross-sections of window stage leaves at the leaf apex and mid-region revealed anthocyanins localized within the mesophyll cells as opposed to the epidermal cells (Fig. 12C and E). Anthocyanins have been observed in the epidermal cell layers of young, developing leaves in various plant species, where they are thought to play a photoprotective role (Crozier et

al. 2008). The pigment absorbs harmful UV and filters visible light, preventing the photosystem from being overloaded with light and limiting the formation of ROS (Gould 2004; Hatier and Gould 2008b; Landi et al. 2015). Young chloroplasts are especially vulnerable to damage from high light, but anthocyanins are visible in mesophyll cells of window stage lace plant leaves instead of epidermal cells where the anthocyanins would be optimal for light and UV interception (Gould 2004). This highlights the role of anthocyanins in the developmental process of PCD in addition to photoprotection and stress response. Cross-sections of window stage leaves grown under stressful conditions have anthocyanins in the epidermis of mid-leaf regions (Appendix 4H and K), but not in the epidermis of the leaf apex. Similar to the leaf apex of window stage leaves grown under normal conditions, the sharp contrast in anthocyanin abundance may be due to the auxin maximum located within the epidermal layers of the leaf margins, which would prevent the accumulation of anthocyanins (Reinhardt et al. 2003; Hay et al. 2006; Bilsborough et al. 2011).

It is important to note that the dark pigmentation from soluble anthocyanins in stressed window stage leaves frequently concealed the presence AVIs using light microscopy (Appendix 4F and I). Therefore, AVIs may have also been present in window stage leaves grown under normal conditions and were merely masked by soluble anthocyanin pigmentation. Further investigation was performed in window stage leaves via confocal microscopy and TEM to verify the presence of AVIs.

4.2.3. Confocal microscope investigation of anthocyanin in window stage leaves

Two morphologies of anthocyanin were observable in the apex and mid-regions of window stage leaves, (i) a weakly-fluorescent mass that occupied the majority of the vacuolar space, and (ii) intensely fluorescent spherical bodies (Fig. 13 and 14). Similar anthocyanin

autofluorescence patterns were observed in *Arabidopsis*, lisianthus and tobacco cells, and were described as "diffuse vacuolar" anthocyanins and anthocyanin aggregates or bodies respectively (Poustka et al. 2007; Chanoca et al. 2015; Kallam et al. 2017). Previous literature defines the anthocyanin bodies as AVIs if they were observed within the vacuole (Zhang et al. 2006; Chanoca et al. 2015). At the window apex (Fig. 13), soluble (diffuse vacuolar) anthocyanin autofluorescence was observed in mesophyll cells, and the autofluorescence was absent in the epidermal layer of the leaf margins, which corresponds to the light microscopy observations (Fig. 12). However, in contrast to the light microscopy observations of few AVIs visible in the leaf apex, anthocyanin bodies (or AVIs) were detected as a single spherical aggregate within the vacuole in almost all cells (Fig. 13). This suggests that the AVIs may be concealed by the soluble anthocyanin pigmentation, thus making them unobservable using light microscopy.

Soluble anthocyanin was also detected in the vasculature and NPCD cells in the mid-regions of window stage leaves (Fig. 14), similar to the light microscopy observations (Fig. 12). Anthocyanin bodies were also visible in these cells, although the morphology of the bodies differed from the bodies observed in the apex of window stage leaves (summarized in Table 5). The bodies found within cells of the mid-region were smaller and more numerous. It was also less clear if some of the bodies were present within the vacuole or cytoplasm, and therefore, these bodies cannot be classified as an "AVI" or "anthocyanin body". Differences in AVI morphologies have been recorded in different plant organs, as well as within the same tissues or cells (Bae et al. 2006; Zhang et al. 2006). Irregular-shaped AVIs were observed within the abaxial surface of lisianthus petals, whereas vesicle-like AVIs were seen within the adaxial surface (Zhang et al. 2006).

The difference in the AVI morphologies between the leaf apex and mid-region could be due to different concentrations of anthocyanins. Anthocyanins are abundant at the leaf apex of window stage leaves (Denbigh et al. 2020), which would enable the formation of larger concentrated bodies, as the number of observable AVIs is correlated with anthocyanin abundance (Grotewold and Davies 2008; Conn et al. 2010). These AVIs could be used for the transportation of concentrated anthocyanins throughout the vascular system, as AVIs have been observed within the vasculature of stressed leaves (Appendix 2 and 4; Supplementary material 1; Fletcher 2017), however, the function of AVIs is still unclear. It has been suggested that AVIs are simply a storage mechanism as a result of excess anthocyanin abundance (Grotewold and Davies 2008) or are used to scatter intense light (Bae et al. 2006). The latter is less likely, as the AVIs are observable in the mesophyll cell layers as opposed to the epidermal layers where protection would be the most advantageous. It is also possible that anthocyanins are unable to accumulate to significant levels for AVI formation in NPCD cells as the anthocyanins are utilized to prevent PCD-related oxidative stress.

Table 5. Summary table of microscope observations of anthocyanin vacuolar inclusions (AVIs) in window and mature stage lace plant leaves grown under normal and stressed conditions.

Leaf stage	Growth conditions	Region examined	Light microscopy	Confocal laser scanning microscopy (CLSM)	Transmission electron microscopy (TEM)
Window	Normal	Apex	Few AVIs visible (Fig. 11). Often seen in the vascular tissues.	Present in all cells, including vascular tissues. 1-2 μm in diameter, located within the vacuolar space, and limited to one per cell (Fig. 13C-F).	Data not available.
	Normal	Mid-region	AVIs are rarely visible (Fig. 12F-K). Very few were visible in cross sections (Fig. 12K)	Present in vascular tissues and NPCD cells. 500-800 nm in diameter and multiple were found within one cell. It is possible some anthocyanins were localized in the lumen and cytosol.	Lacked an immediate enclosing membrane. Visible in the vacuole and cytoplasm (anthocyanin-containing bodies) in NPCD cells (Fig. 15). Few AVIs were visible in the vacuole of PCD cells (Fig. 18E).
	Stressful	Apex	Present in all cells, including vascular tissues (Appendix 2). Spherical, liquid-like bodies and fibrous structures (Appendix 3). Present in the upper epidermis (Appendix 4).	Data not available.	Data not available.

Leaf stage	Growth conditions	Region examined	Light microscopy	Confocal laser scanning microscopy (CLSM)	Transmission electron microscopy (TEM)
	Stressful	Mid-region	Present in vascular tissue and NPCD cells (Appendix 4).	Data not available.	Data not available.
Mature	Normal	Apex	AVIs are not visible (Fig. 11).	Data not available.	Data not available.

4.2.4. Anthocyanin trafficking in lace plant cells

Anthocyanin bodies were observable as electron-dense, osmiophilic bodies within the cytoplasm and vacuole of cells via TEM (Fig. 15). Osmiophilic bodies were also observed in the anthocyanin-containing vacuoles of sweet potato suspension cells, and were identified as AVIs (Nozue et al. 1993). The electron-dense bodies have also been observed in *Arabidopsis*, apple, carnation, and lisianthus (Bae et al. 2006; Zhang et al. 2006; Grotewold and Davies 2008; Conn et al. 2010). The chemical structure of anthocyanin has various functional groups, such as hydro, methyl, hydroxyl or phenol groups, that can be fixed with osmium tetroxide, resulting in high electron densities in TEM (Bae et al. 2006). A concentrated body of anthocyanins would therefore result in an extremely electron-dense structure in electron micrographs.

The anthocyanin bodies found in lace plant cells were not surrounded by an immediate enclosing membrane. This morphology has also been observed in sweet potato, apple, and lisianthus cells (Nozue et al. 1993; Markham et al. 2000; Bae et al. 2006; Zhang et al. 2006), whereas membrane-bound AVIs were recorded in red cabbage, *Arabidopsis* and grapes (Small and Pecket 1982; Conn et al. 2010; Pourcel et al. 2010). Even though no enclosing membrane was observed in the electron micrographs of lisianthus cells, membranous components were found within the chemical profile of the AVIs (Conn et al. 2010).

Anthocyanin bodies could be observed within the vacuole, as well as in the cytoplasm contained in vesicle-like structures. Within the vacuole, the anthocyanin bodies have been observed to accumulate on the inner side of the tonoplast membrane (Nozue et al. 1993; Bae et al. 2006) or within the vacuole lumen (Zhang et al. 2006; Poustka et al. 2007; Grotewold and Davis 2008; Pourcel et al. 2010). Very few studies have reported the presence of anthocyanin-containing membranous vesicles located within the cytoplasm adjacent to ER (Zhang et al. 2006; Pourcel et al. 2010).

The anthocyanin-containing vesicles in lace plant cells were also observed near ER networks and adjacent or conjoined to vacuoles. This system of anthocyanin transport is similar to the vesicular transport method that suggests anthocyanins are translocated into the ER lumen and are enclosed by an ER-derived membrane for delivery to the tonoplast and vacuolar sequestration (Poustka et al. 2007; Grotewold and Davies 2008; Conn et al. 2010; Chanoca et al. 2015). The vesicular transport model is also seen in *Arabidopsis*, sweet potato, and red cabbage (Small and Pecket 1982; Nozue et al. 1993).

Grotewold and Davies (2008) suggested that the anthocyanin-containing vesicles seen in the vesicular transport model are ER-derived pre-vacuolar vesicles (PVs). The anthocyanins are thought to "hitchhike" onto vesicles containing storage proteins that contribute to the formation and maturation of the vacuole. These vesicles by-pass the Golgi apparatus and are directly transported from the ER to the vacuole via the protein secretory pathway (Poustka et al. 2007). Therefore, vesicular transport of anthocyanin may contribute to the biogenesis of the vacuole in young, developing window-stage lace plant cells through the fusion of ER-derived PVs containing anthocyanin bodies.

It is unclear how anthocyanins and AVIs are re-mobilized or distributed after entering the vacuole. Soluble anthocyanins may be actively transported across the tonoplast membrane into the cytoplasm via ATP- or H^+DT-proteins (Poustka et al. 2007; Chanoca et al. 2015). Once translocated into the cytoplasm, the anthocyanins are highly bioactive and are degraded (Castañeda-Ovando et al. 2009). The acylation of anthocyanins within AVIs increases the stability of the pigment (Grotewold and Davies 2008; Pourcel et al. 2010; Kallam et al. 2017; Liu et al. 2018), which could allow for the controlled activity and optimal use of the antioxidant. Vesicles containing anthocyanin bodies were observed near the mitochondria and chloroplasts, which are major ROS producing organelles (Fig. 15C-E). These vesicles may be tonoplast-derived and may provide antioxidant activity in the cytoplasm.

4.3. INVESTIGATION OF ENDOPLASMIC RETICULUM IN LACE PLANT LEAVES

4.3.1. Confocal analysis of endoplasmic reticulum in window and mature leaves

Staining for ER was visualized throughout window and mature areoles (Fig. 16-17). The fluorescent stain has been used in previous research to investigate ER structures in animal, plant and fungal cells (McCauley and Hepler 1990; Cole et al. 2000). The morphologies of the fluorescent internal structures in cells stained with DiOC6(3) differed from those stained with CMXRos (Appendix 5). ER was seen as tubular, networks and lamellar sheets, whereas mitochondria were visible as distinct puncta, which suggests the DiOC6(3) dye is ER-specific at the concentrations used.

The ER stained with DiOC6(3) in lace plant leaves looked very similar to cortical ER in onion and *Funaria* moss cells (Hepler et al. 1990; McCauley and Hepler 1990). The ER in lace plant cells were observed as tubular networks adjacent to the plasma membrane (PM), and in mature cells, lamellar cisternae (ER sheets) were observed (Fig. 17E). Cortical ER is observed in

a large number of animal and plant cells, and is visible as smooth tubular networks joined by lamellar sheets positioned extremely close to the plasma membrane (Hepler et al. 1990). The exact function of cortical ER is unknown. However, various theories have been proposed. Cortical ER in adjacent cells are connected by plasmodesmata (canals located within cell walls); therefore, cell signalling molecules may be transported from the cell surface to the cortical ER, or between cells via symplastic transport as a form of communication (Hepler et al. 1990). A second hypothesis is that cortical ER plays a role in coordinating intracellular movement and secretion, due to its prevalent interaction with the cytoskeleton (Hepler et al. 1990). The networks are also seen to play an important role in growth and development (McCauley and Hepler 1990; Hepler and Gunning 1998; Stefano and Brandizzi 2018). The pattern of cortical ER corresponds to both cell type and developmental stage of the cell in *Funaria* gametophyte cells (McCauley and Hepler 1990). Similar to observations in mature-stage cells in lace plant leaves, older *Funaria* cells exhibited more widely spaced ER networks. In contrast, younger *Funaria* cells have a tighter network that is less defined using fluorescent microscopy, which is comparable to the cortical ER in young, developing window-stage cells.

Differences in ER morphology are also visible across the PCD gradient in window stage leaves (Fig. 16). ER in NPCD cells were visible as tubular networks, whereas in EPCD and LPCD cells, ER was fragmented and visible as distinct puncta. The differences in ER structure and dynamics across the various cell types could be due to cellular stress from PCD. Under stressful conditions resulting from environmental cues or developmental signals, the ER becomes saturated with unfolded or misfolded proteins. In response to the disturbance in cell homeostasis, the cell will either respond with adaptations to reduce the number of unfolded proteins (known as UPR) or promote factors that mediate and execute PCD (Cacas 2010). This leads to the eventual

systematic degradation of organelles and may explain the disruption of tubular ER networks observed in PCD cells in window stage leaf areoles. Similar observations of altered ER morphologies were observed in onion bulb cells subjected to cold treatments. In stressed cells, the ER networks, cisternae and tubular strands were difficult to distinguish, and "disintegrate" into short ER tubules, which exhibit rapid movements over short distances (Quader et al. 1989).

4.3.2. Endoplasmic reticulum ultrastructure in healthy and dying cells

The ultrastructural changes of ER in healthy (NPCD) and dying (PCD) cells was analyzed through TEM (Fig. 18). Healthy cells exhibited characteristics previously described in NPCD cell by Gunawardena et al. (2004). These included evenly distributed chromatin, intact chloroplast and mitochondria, as well as anthocyanin-containing vesicles localized in the cytoplasm as described in Figure 18. Dying lace plant (PCD) cells displayed misshapen chloroplasts and inconspicuous thylakoid membranes, which have been reported in previous research (Gunawardena et al. 2004; Wright et al. 2009; Dauphinee et al. 2019). Few studies have elucidated the morphological changes in ER during PCD in plants. During apoptosis in animals, the dynamic tubular network changes to enlarged and swollen bodies (Bottone et al. 2013). These findings in animal cells were similar to observations of ER in PCD cells in both TEM and confocal micrographs. The ER is also thought to physically attach to mitochondria to facilitate the propagation of death-signals. Although mitochondria were seen adjacent to ER in PCD cells in window stage leaves, attachment of the two organelle membranes was not observed (Fig. 18).

Anthocyanin bodies were also not visible adjacent to ER networks in PCD cells (Fig. 18). This could be due to the use and loss of anthocyanins resulting from the mitigation of overwhelming ROS accumulation during PCD (Dauphinee et al. 2017). Anthocyanins may also be actively downregulated or degraded to enable ROS accumulation and PCD signalling.

Enzymatic factors within the vacuole may be used to breakdown anthocyanins (Liu et al. 2018), overwhelm cellular systems with accumulating ROS, and promote PCD execution.

4.4. PHARMACOLOGICAL EXPERIMENTS WITH ANTHOCYANIN MODULATORS

Lace plants that were treated with MeJA did not exhibit significant differences in leaf length and number of perforations compared to the control, suggesting that the concentrations of the anthocyanin promoter did not affect normal leaf growth or perforation formation. Leaf widths did not significantly differ from the control for all leaf stages, except for leaf 2 of 2.5 μM-treated plants. This exception could be due to the low replicate number and variability in leaf morphology in the novel lace plant cultivar used for experimentation. Whole plant treatment experiments with anthocyanin modulators (MeJA and phenidone) were previously performed on the original cultivar (Fletcher 2017), but the new cultivar was utilized for this study to optimize parameters (i.e. corm size, volume of solid and liquid medium) for future pharmacological experimentation. The new cultivar often produced larger leaves that grew out of the medium and became desiccated and damaged. Therefore, the damaged leaves were omitted as replicates.

Spectrophotometric analysis of MeJA-treated plants determined that the concentration of anthocyanins was significantly higher in all leaf stages compared to control, which indicates that the compound enhanced anthocyanin biosynthesis. Methyl jasmonate is an organic compound derived from jasmonic acid and an endogenous regulator involved in plant growth, development, and homeostasis (Bennett and Wallsgrove 1994; Cao et al. 2009; Huang et al. 2015). Methyl jasmonate is known to induce anthocyanin accumulation in numerous plant species through the upregulation of various enzymes involved with the biosynthetic pathway (Bennett and Wallsgrove 1994; Saniewski et al. 2003; Shan et al. 2009; Qi et al. 2011; Jaakola 2013; Huang et al. 2015). Although anthocyanin levels increased with the addition of MeJA, perforation number

did not differ, which is similar to results seen in Fletcher (2017). This phenomenon was also seen in other experiments using anthocyanin biosynthesis enhancers in lace plants (e.g. ethylene biosynthesis promoter, ACC [Dauphinee et al. 2012]). Thus, the presence of additional endogenous anthocyanins in lace plant leaves at the beginning of leaf development and PCD initiation does not affect perforation formation.

Phenidone is a lipoxygenases inhibitor, which prevents the synthesis of jasmonates in plant cells (Cucurou et al. 1991). Leaf length and width were not significantly different in phenidone-treated plants at various concentrations compared to control plants, indicating that the concentrations did not alter normal growth. Spectrophotometric analysis of phenidone-treated plants showed that anthocyanin abundance was reduced in leaf 2 at higher concentrations (100 and 200 μM), although perforation formation was not significantly reduced compared to control. These results were similar to Fletcher (2017), however, perforation formation was inhibited in leaf 1 (i.e. the first leaf that developed immediately after treatment) of old cultivar plants. It is possible that the concentrations were not high enough for the new cultivar plants to elicit a reaction or that the phenidone treatment has a delayed effect. Plants were grown for two weeks following treatment before harvest and analysis. A longer treatment period may be necessary to see the full effect of lipoxygenase inhibition and subsequent anthocyanin decline.

4.5. CONCLUSIONS

Lace plants use PCD during development to form perforations throughout its leaf blade. The pattern of anthocyanin presence and eventual loss is linked to the PCD process, supporting a critical role for the pigments in lace plant PCD. UPLC data indicated that the most common naturally occurring anthocyanins were not present in lace plant profiles. Additionally, the lace plant anthocyanin profiles differed between the various stages of leaf development in support of the first hypothesis, suggesting a role for the specific anthocyanin species present. Inflorescences exhibited a complex profile of anthocyanins, which may reflect the role of anthocyanins in colouring the various floral structures. The retention times of anthocyanin peaks in lace plant chromatogram results suggest the presence of acylated anthocyanins, which are typically concentrated in AVIs. LC-MS/MS was used to identify the anthocyanins present in window and mature stage leaves, and five potential anthocyanin identifications were proposed based on precursor/product ion transitions. Reference compounds used to confirm the anthocyanin identifications indicated that the species present in window and mature stage leaves differ from the proposed identifications. Alternative methods for anthocyanin identification include NMR, which would provide detailed and accurate structural information of the organic compounds.

Using light microscopy, anthocyanins and AVIs were visible in window stage leaves, but were not seen in mature stage leaves, which supports the hypothesis that the presence of anthocyanin bodies varies across developmental leaf stages. Very few AVIs were visible at the leaf apex and none were seen in the mid-regions (leaf vasculature and areoles) of window stage leaves. Anthocyanins were restricted to mesophyll cells, which suggest a direct role in lace plant leaf development in addition to environmental stress response.

Confocal microscopy revealed the presence of two AVI morphologies in window stage leaves: singular, large anthocyanin bodies located in the apices, and multiple, small anthocyanin bodies located in mid-leaf regions (Fig. 13 and 14). The differences in morphologies within this developmental leaf stage could be due to differing anthocyanin concentrations, activity, or type. Specific anthocyanins are known to be selected for AVI formation via acylation, which suggests a specific function. Extraction and identification of anthocyanins contained within AVIs in various areas and cell types in window stage leaves could further elucidate the role of AVIs in lace plant development and PCD.

The mode of intracellular anthocyanin trafficking in plant cells is unclear. Three models have been proposed: the ligandin transporter, vesicular transport, and autophagic transport. According to TEM of window stage leaf cells, anthocyanin bodies are produced in the cytoplasm and are contained within ER-derived vesicles, which supports the vesicular transport model of anthocyanin trafficking, in accordance with the hypothesis. Anthocyanin-containing vesicles directly fused with the tonoplast membrane in young, developing window stage cells. This indicates that the anthocyanins "hitchhike" in pro-vacuolar compartments via the protein trafficking pathway, and contribute to the formation of the tonoplast and vacuolar lumen, and maturation of the vacuole. It is possible that multiple modes are utilized in lace plant cells. However, the vesicular transport mode is most evident in lace plant leaves based on the experimental observations. Confirmation of the mode of anthocyanin transport in lace plant cells could involve further histochemical staining, genetic transformation, or molecular investigation. Detection of vesicular membranes around anthocyanin bodies in lace plant leaves can be achieved using the FM1-43 membrane probe (Chanoca et al. 2015), which would further support the vesicular transport model. Genetic transformation of the lace plant using *Agrobacterium*

tumefaciens could also be used to detect ligandin transport, which involves GST-assisted trafficking of anthocyanins. This could be done by creating a construct containing *Arabidopsis* GST gene, *TRANSPARENT TESTA19 (TT19)*, and a GFP reporter gene (according to Chanoca et al. 2015). Autophagic transport of anthocyanins could also be investigated via molecular examination of autophagy-related proteins. AVI accumulation via biosynthesis modulators and subsequent immunoprobing of atg-family proteins may indicate the role of autophagy in AVI formation, translocation, and storage.

Limited research has been carried out on the role of ER in developmentally regulated plant PCD and the structural changes associated with the process. Fluorescent probing of ER using DiOC6(3) stain in window and mature stage lace plant leaves revealed morphologies structurally similar to cortical ER. This form of ER is thought to be involved in cell growth and development, intracellular movement, as well as signalling and communication. It is possible that the cortical ER in lace plant assists in propagating death signals or transporting anthocyanins across various cells. In agreement with the hypothesis, ER changes were visible across the PCD gradient using both confocal and TEM analysis. Colocalization of ER and AVIs would confirm the mode of intracellular anthocyanin transport and elucidate the connection between ER dynamics and anthocyanin production during lace plant PCD.

Anthocyanin abundance during the early stages of lace plant leaf development is crucial for the initiation of PCD. Anthocyanin biosynthesis modulators were used to further determine the role of anthocyanin in lace plant PCD. Methyl jasmonate was seen to increase anthocyanin abundance in treated lace plant leaves, whereas phenidone decreased anthocyanin abundance. Although anthocyanin presence was altered, there was no difference in perforation formation compared to control for both treatments. Consequently, based on the results, the hypothesis that

anthocyanin modulation affects perforation formation in lace plant leaves was rejected. This could be due to the limited number of replicates and the greater variability in leaf morphology of the new cultivar, as the inhibition of anthocyanin abundance in young lace plant leaves has been shown to limit perforation formation in numerous studies (Lord et al. 2011; Dauphinee et al. 2012; Fletcher 2017; Dauphinee et al. 2017; Dauphinee et al. 2019; Denbigh et al. 2020; Fraser et al. 2020; Rowarth et al. 2020).

4.5.1. Future directions

The results using UPLC identified differing anthocyanin species present at specific stages of leaf development and inflorescences. The identification of the five most abundant anthocyanins in window and mature stage leaves were proposed from LC-MS/MS results, however the retention times differed from anthocyanin references. Therefore, alternative methods should be used to verify the identification of the anthocyanin species, such as obtaining new anthocyanin references for LC-MS/MS analysis or determining structure of the compound via NMR.

Anthocyanins and AVIs were investigated using a combination of live-cell imaging and TEM techniques. AVIs are visible at the leaf apex and mid-regions as two distinct morphologies and are intracellularly transported from the ER to the vacuole via vesicular transport. The method of anthocyanin trafficking can be confirmed with further experimentation using transformation, histochemical, pharmacological, and/or molecular methods. Ultrastructural changes of the ER, the site of anthocyanin synthesis, were visible across the PCD gradient. Co-localization of ER and AVIs using confocal microscopy would further elucidate their interactions during the developmentally regulated process in lace plant. Extraction and identification of anthocyanins contained in AVIs would suggest its potential role in lace plant leaf development.

Anthocyanin biosynthesis modulation with methyl jasmonate and phenidone did not significantly affect perforation formation in lace plant leaves at the concentrations used. Therefore, further whole plant experiments with higher treatment concentrations and longer treatment periods are necessary to optimize the concentrations of the modulators.

REFERENCES

Akula R, Ravishankar GA. 2011. Influence of abiotic stress signals on secondary metabolites in plants. Plant Signaling and Behavior. 6(11):1720–1731. doi:10.4161/psb.6.11.17613.

Aldred E. 2009a. Introduction to plant pharmacology: Secondary metabolites. In: Pharmacology. Edinburgh; New York: Elsevier. p. 147–147.

Aldred EM. 2009b. Phenols. In: Pharmacology. Edinburgh; New York: Elsevier. p. 149–166.

Ananga A, Georgiev V, Ochieng J, Phills B, Tsolov V. 2013. Production of anthocyanins in grape cell cultures: A potential source of raw material for pharmaceutical, food, and cosmetic industries. In: Sladonja B, Poljuha D, editors. The Mediterranean Genetic Code - Grapevine and Olive. Books on Demand. p. 247–287.

Arimura G, Maffei M. 2016. Introduction to plant specialized metabolism. In: Arimura G, Maffei M, editors. Plant Specialized Metabolism: Genomics, Biochemistry, and Biological Functions. CRC Press. p. 376.

Bae R-N, Kim K-W, Kim T-C, Lee S-K. 2006. Anatomical observations of anthocyanin rich cells in apple skins. HortScience. 41(3):733–736.

Bassham DC. 2015. Pigments on the move. Nature. 526(7575):644–645. doi:10.1038/526644a.

Bennett RN, Wallsgrove RM. 1994. Tansley Review No. 72. Secondary metabolites in plant defence mechanisms. New Phytology. 127(4):617–633.

Bilsborough GD, Runions A, Barkoulas M, Jenkins HW, Hasson A, Galinha C, Laufs P, Hay A, Prusinkiewicz P, Tsiantis M. 2011. Model for the regulation of *Arabidopsis thaliana* leaf margin development. Proceedings of the National Academy of Sciences USA. 108(8):3424–3429. doi:10.1073/pnas.1015162108.

Bottone M, Santin G, Aredia F, Bernocchi G, Pellicciari C, Scovassi A. 2013. Morphological features of organelles during apoptosis: An overview. Cells. 2(2):294–305. doi:10.3390/cells2020294.

Buer CS, Muday GK, Djordjevic MA. 2007. Flavonoids are differentially taken up and transported long distances in *Arabidopsis*. Plant Physiology. 145(2):478–490. doi:10.1104/pp.107.101824.

Cacas J-L. 2010. Devil inside: Does plant programmed cell death involve the endomembrane system? Plant Cell Environment. 33(9):1453–1473. doi:10.1111/j.1365-3040.2010.02117.x.

Cao S, Zheng Y, Wang K, Jin P, Rui H. 2009. Methyl jasmonate reduces chilling injury and enhances antioxidant enzyme activity in postharvest loquat fruit. Food Chemistry. 115(4):1458–1463. doi:10.1016/j.foodchem.2009.01.082.

Castañeda-Ovando A, Pacheco-Hernández M de L, Páez-Hernández ME, Rodríguez JA, Galán-Vidal CA. 2009. Chemical studies of anthocyanins: A review. Food Chemistry. 113(4):859–871. doi:10.1016/j.foodchem.2008.09.001.

Chanoca A, Kovinich N, Burkel B, Stecha S, Bohorquez-Restrepo A, Ueda T, Eliceiri KW, Grotewold E, Otegui MS. 2015. Anthocyanin vacuolar inclusions form by a microautophagy mechanism. Plant Cell. 27(9):2545–2599. doi:10.1105/tpc.15.00589.

Chen LY, Grimm GW, Wang QF, Renner SS. 2015. A phylogeny and biogeographic analysis for the Cape-Pondweed family Aponogetonaceae (Alismatales). Molecular Phylogenetic Evolution. 82:111–117. doi:10.1016/j.ympev.2014.10.007.

Cole L, Davies D, Hyde GJ, Ashford AE. 2000. ER-tracker dye and BODIPY-brefeldin A differentiate the endoplasmic reticulum and Golgi bodies from the tubular-vacuole system in living hyphae of *Pisolithus tinctorius*. Journal of Microscroscopy. 197(3):239–248. doi:10.1046/j.1365-2818.2000.00664.x.

Coll NS, Epple P, Dangl JL. 2011. Programmed cell death in the plant immune system. Cell Death and Differentiation. 18(8):1247–1256. doi:10.1038/cdd.2011.37.

Conn S, Curtin C, Bézier A, Franco C, Zhang W. 2008. Purification, molecular cloning, and characterization of glutathione S-transferases (GSTs) from pigmented *Vitis vinifera* L. cell suspension cultures as putative anthocyanin transport proteins. Journal of Experimental Botany. 59(13):3621–3634. doi:10.1093/jxb/ern217.

Conn S, Franco C, Zhang W. 2010. Characterization of anthocyanic vacuolar inclusions in *Vitis vinifera* L. cell suspension cultures. Planta. 231(6):1343–1360. doi:10.1007/s00425-010-1139-4.

Conn S, Zhang W, Franco C. 2003. Anthocyanic vacuolar inclusions (AVIs) selectively bind acylated anthocyanins in *Vitis vinifera* L. (grapevine) suspension culture. Biotechnology Letters. 25:835–839.

Croteau R, Kutchan TM, Lewis NG. 2000. Natural products (secondary metabolites). In: Buchanan B, Gruissem W, Jones R, editors. Biochemistry & Molecular Biology of Plants. American Society of Plant Physiologists. p. 1250–1318.

Crozier A, Jaganath IB, Clifford MN. 2008. Phenols, polyphenols and tannins: An overview. In: Crozier A, Clifford MN, Ashihara H, editors. Plant Secondary Metabolites: Occurrence, Structure and Role in the Human Diet. John Wiley & Sons. p. 1–24.

Cucurou C, Battioni JP, Thang DC, Nam NH, Mansuy D. 1991. Mechanisms of inactivation of lipoxygenases by phenidone and BW755C. Biochemistry. 30(37):8964–8970. doi:10.1021/bi00101a008.

Daneva A, Gao Z, Van Durme M, Nowack MK. 2016. Functions and regulation of programmed cell death in plant development. Annual Review of Cell and Developmental Biology. 32(1):441–468. doi:10.1146/annurev-cellbio-111315-124915.

Das PK, Shin DH, Choi S-B, Park Y-I. 2012. Sugar-hormone cross-talk in anthocyanin biosynthesis. Molecules and Cells. 34:501–507. doi:10.1007/s10059-012-0151-x.

Dauphinee AN, Denbigh GL, Rollini A, Fraser M, Lacroix CR, Gunawardena AHLAN. 2019. The function of autophagy in lace plant programmed cell death. Frontiers in Plant Science. 10:1198. doi:10.3389/fpls.2019.01198.

Dauphinee AN, Fletcher JI, Denbigh GL, Lacroix CR, Gunawardena AHLAN. 2017. Remodelling of lace plant leaves: Antioxidants and ROS are key regulators of programmed cell death. Planta. 246(1):133–147. doi:10.1007/s00425-017-2683-y.

Dauphinee AN, Gunawardena Arunika N. 2015. An overview of programmed cell death research: From canonical to emerging model species. In: Gunawardena AN, McCabe PF, editors. Plant Programmed Cell Death. Springer, Cham. p. 1–31.

Dauphinee AN, Wright H, Rantong G, Gunawardena AHLAN. 2012. The involvement of ethylene in programmed cell death and climacteric-like behaviour during the remodelling of lace plant (*Aponogeton madagascariensis*) leaves. Botany. 90(12):1237–1244. doi:10.1139/b2012-093.

de Brito Francisco R, Martinoia E. 2018. The vacuolar transportome of plant specialized metabolites. Plant Cell Physiology. 59(7):1326–1336. doi:10.1093/pcp/pcy039.

Denbigh GL, Dauphinee AN, Fraser MS, Lacroix CR, Gunawardena AHLAN. 2020. The role of auxin in developmentally regulated programmed cell death in lace plant. American Journal of Botany. 107(4):577–586. doi:10.1002/ajb2.1463.

Drew KL, Harris MB, LaManna JC, Smith MA, Zhu XW, Ma YL. 2004. Hypoxia tolerance in mammalian heterotherms. Journal of Experimental Biology. 207(18):3155–3162. doi:10.1242/jeb.01114.

Eichmann R, Schäfer P. 2012. The endoplasmic reticulum in plant immunity and cell death. Frontiers in Plant Sciences. 3:200. doi:10.3389/fpls.2012.00200.

Einbond LS, Reynertson KA, Luo XD, Basile MJ, Kennelly EJ. 2004. Anthocyanin antioxidants from edible fruits. Food Chemistry. 84(1):23–28. doi:10.1016/S0308-8146(03)00162-6.

Feng W, Hao Z, Li M. 2017. Isolation and structure identification of flavonoids. In: Justino G, editor. Flavonoids - From Biosynthesis to Human Health. InTechOpen. doi: 10.5772/67810

Fletcher JL. 2017. Profiling phenolic compounds in *Aponogeton madagascariensis* and investigating their role in programmed cell death during leaf development, MSc thesis, Dalhousie University, Halifax, NS.

Fraser MS, Dauphinee AN, Gunawardena AHLAN. 2020. Determining the effect of calcium on cell death rate and perforation formation during leaf development in the novel model system, the lace plant (*Aponogeton madagascariensis*). Journal of Microscopy. 278(3):132–144. doi:10.1111/jmi.12859.

Fuchs Y, Steller H. 2015. Live to die another way: Modes of programmed cell death and the signals emanating from dying cells. Nature Reviews Molecular Cell Biology. 16(6):329–344. doi:10.1038/nrm3999.

Gomez C, Conejero G, Torregrosa L, Cheynier V, Terrier N, Ageorges A. 2011. In vivo grapevine anthocyanin transport involves vesicle-mediated trafficking and the contribution of anthoMATE transporters and GST. The Plant Journal. 67(6):960–970. doi:10.1111/j.1365-313X.2011.04648.x.

Gould KS. 2004. Nature's Swiss army knife: The diverse protective roles of anthocyanins in leaves. Journal of Biomedicine and Biotechnology. 2004(5):314–320. doi:10.1155/S1110724304406147.

Grotewold E, Davies K. 2008. Trafficking and sequestration of anthocyanins. Natural Product Communications. 3(8):1251–1258. doi:10.1177/1934578x0800300806.

Guerriero G, Berni R, Muñoz-Sanchez JA, Apone F, Abdel-Salam EM, Qahtan AA, Alatar AA, Cantini C, Cai G, Hausman JF, et al. 2018. Production of plant secondary metabolites: Examples, tips and suggestions for biotechnologists. Genes. 9(6):309. doi:10.3390/genes9060309.

Gunawardena AHLAN, Greenwood JS, Dengler NG. 2004. Programmed cell death remodels lace plant leaf shape during development. The Plant Cell. 16(1):60–73. doi:10.1105/tpc.016188.

Gunawardena AHLAN, Navachandrabala C, Kane M, Dengler NG. 2006. Lace plant: A novel system for studying developmental programmed cell death. In: Teixeira da Silva JA, editor. Floriculture, Ornamental and Plant Biotechnology: Advances and Topical Issues. 1st ed. Global Science Books. p. 157–162.

Gunawardena AHLAN, Pearce DM, Jackson MB, Hawes CR, Evans DE. 2001. Characterisation of programmed cell death during aerenchyma formation induced by ethylene or hypoxia in roots of maize (*Zea mays* L.). Planta. 212(2):205–214. doi:10.1007/s004250000381.

Hanson BJR. 2003. Natural Products: The Secondary Metabolites. Abel EW, editor. Royal Society of Chemistry.

Harborne JB. 2007. Role of secondary metabolites in chemical defence mechanisms in plants. In: Chadwick DJ, Marsh J, editors. Ciba Foundation Symposium: Bioactive Compounds from Plants. Vol. 154. John Wiley & Sons, Ltd. p. 126–139.

Hatier J-HB, Gould KS. 2008a. Anthocyanin function in vegetative organs. In: Anthocyanins. Springer New York. p. 1–19.

Hatier J-HB, Gould KS. 2008b. Foliar anthocyanins as modulators of stress signals. Journal of Theoretical Biology. 253(3):625–627. doi:10.1016/J.JTBI.2008.04.018.

Hay A, Barkoulas M, Tsiantis M. 2006. ASYMMETRIC LEAVES1 and auxin activities converge to repress *BREVIPEDICELLUS* expression and promote leaf development in *Arabidopsis*. Development. 133(20):3955–3961. doi:10.1242/dev.02545.

Hepler PK, Gunning BES. 1998. Confocal fluorescence microscopy of plant cells. Protoplasma. 201:121–157. doi:10.1007/BF01287411.

Hepler PK, Palevitz BA, Lancelle SA, Mccauley MM, Lichtschidl L. 1990. Cortical endoplasmic reticulum in plants. Journal of Cell Science. 96(3).

Hodges DM, Nozzolillo C. 1996. Anthocyanin and anthocyanoplast content of cruciferous seedlings subjected to mineral nutrient deficiencies. Journal of Plant Physiology. 147(6):749–754. doi:10.1016/S0176-1617(11)81488-4.

Howell SH. 2013. Endoplasmic reticulum stress responses in plants. Annual Review of Plant Biology. 64(1):477–499. doi:10.1146/annurev-arplant-050312-120053.

Huang X, Li J, Shang H, Meng X. 2015. Effect of methyl jasmonate on the anthocyanin content and antioxidant activity of blueberries during cold storage. Journal of the Science of Food and Agriculture. 95(2):337–343. doi:10.1002/jsfa.6725.

Jaakola L. 2013. New insights into the regulation of anthocyanin biosynthesis in fruits. Trends in Plant Sciences. 18(9):477–483. doi:10.1016/j.tplants.2013.06.003.

Jamwal K, Bhattacharya S, Puri S. 2018. Plant growth regulator mediated consequences of secondary metabolites in medicinal plants. Journal of Applied Research on Medical and Aromatic Plants. 9:26–38. doi:10.1016/j.jarmap.2017.12.003.

Ji XH, Zhang R, Wang N, Yang L, Chen X Sen. 2015. Transcriptome profiling reveals auxin suppressed anthocyanin biosynthesis in red-fleshed apple callus (*Malus sieversii* f. niedzwetzkyana). Plant Cell, Tissue and Organ Culture. 123(2):389–404. doi:10.1007/s11240-015-0843-y.

Kabera J, Semana E, Mussa A, He X. 2014. Plant secondary metabolites: Biosynthesis, classification, function and pharmacological properties. Journal of Pharmacy and Pharmacology. 2:377–392.

Kallam K, Appelhagen I, Luo J, Albert N, Zhang H, Deroles S, Hill L, Findlay K, Andersen ØM, Davies K, et al. 2017. Aromatic decoration determines the formation of anthocyanic vacuolar inclusions. Current Biology. 27(7):945–957. doi:10.1016/j.cub.2017.02.027.

Katerova Z, Todorova D, Tasheva K, Sergiev I. 2012. Influence of ultraviolet radiation on plant secondary metabolite production. Genetics and Plant Physiology. 2(3–4):113–144.

Khoo HE, Azlan A, Tang ST, Lim SM. 2017. Anthocyanidins and anthocyanins: Colored pigments as food, pharmaceutical ingredients, and the potential health benefits. Food & Nutrition Research. 61(1):1361779. doi:10.1080/16546628.2017.1361779.

Kim R, Emi M, Tanabe K, Murakami S. 2006. Role of the unfolded protein response in cell death. Apoptosis. 11(1):5–13. doi:10.1007/s10495-005-3088-0.

Košir IJ, Lapornik B, Andrenšek S, Wondra AG, Vrhovšek U, Kidrič J. 2004. Identification of anthocyanins in wines by liquid chromatography, liquid chromatography-mass spectrometry and nuclear magnetic resonance. Analytica Chimica Acta. 513(1):277–282. doi:10.1016/j.aca.2003.12.013.

Kovinich N, Arnason JT, De Luca V, Miki B. 2011. Coloring soybeans with anthocyanins? In: Gang DR, editor. The Biological Activity of Phytochemicals. Vol. 41. Springer New York. p. 47–57.

Landi M, Tattini M, Gould KS. 2015. Multiple functional roles of anthocyanins in plant-environment interactions. Environmental and Experimental Botany. 119:4–17. doi:10.1016/j.envexpbot.2015.05.012.

Lee DW, O'Keefe J, Holbrook NM, Feild TS. 2003. Pigment dynamics and autumn leaf senescence in a New England deciduous forest, eastern USA. Ecological Research. 18(6):677–694. doi:10.1111/j.1440-1703.2003.00588.x

Li Z, Pan Q, Cui X, Duan C. 2010. Optimization on anthocyanins extraction from wine grape skins using orthogonal test design. Food Science and Biotechnology 19(4):1047-53.

Liu JX, Howell SH. 2010. Endoplasmic reticulum protein quality control and its relationship to environmental stress responses in plants. The Plant Cell. 22(9):2930–2942. doi:10.1105/tpc.110.078154.

Liu Y, Tikunov Y, Schouten RE, Marcelis LFM, Visser RGF, Bovy A. 2018. Anthocyanin biosynthesis and degradation mechanisms in Solanaceous vegetables: A review. Frontiers in Chemistry. 6:52. doi:10.3389/fchem.2018.00052.

Lord CE, Wertman JN, Lane S, Gunawardena AH. 2011. Do mitochondria play a role in remodelling lace plant leaves during programmed cell death? BMC Plant Biology. 11(1):102. doi:10.1186/1471-2229-11-102.

Maizel A. 2015. A view to a kill: Markers for developmentally regulated cell death in plants. Plant Physiology. 169(4):2341. doi:10.1104/pp.15.01608.

Markham KR, Gould KS, Winefield CS, Mitchell KA, Bloor SJ, Boase MR. 2000. Anthocyanic vacuolar inclusions - Their nature and significance in flower colouration. Phytochemistry. 55(4):327–336. doi:10.1016/S0031-9422(00)00246-6.

Marrs KA, Alfenito MR, Lloyd AM, Walbot V. 1995. A glutathione S-transferase involved in vacuolar transfer encoded by the maize gene Bronze-2. Nature. 375(6530):397–400. doi:10.1038/375397a0.

McCauley MM, Hepler PK. 1990. Visualization of the endoplasmic reticulum in living buds and branches of the moss *Funaria hygrometrica* by confocal laser scanning microscopy. Development. 109(4).

Mueller LA, Goodman CD, Silady RA, Walbot V. 2000. AN9, a petunia glutathione S-transferase required for anthocyanin sequestration, is a flavonoid-binding protein. Plant Physiology. 123(4):1561–1570. doi:10.1104/pp.123.4.1561.

Namdeo A. 2007. Plant cell elicitation for production of secondary metabolites: A review. Pharmacognosy Reviews. 1(3):69–79.

Nozue M, Kubo H, Nishimura M, Katou A, Hattori C, Usuda N, Nagata T, Yasuda H. 1993. Characterization of intravacuolar pigmented structures in anthocyanin-containing cells of sweet potato suspension cultures. Plant Cell Physiology. 34(6):803–808. doi:10.1093/oxfordjournals.pcp.a078487.

Nozzolillo C, Amiguet VT, Bily AC, Harris CS, Saleem A, Andersen ØM, Jordheim M. 2010. Novel aspects of the flowers and floral pigmentation of two Cleome species (Cleomaceae), *C. hassleriana and C. serrulata*. Biochemical Systematics and Ecology. 38(3):361–369. doi:10.1016/j.bse.2010.03.005.

Ougham HJ, Morris P, Thomas H. 2005. The colours of autumn leaves as symptoms of cellular recycling and defenses against environmental stresses. In: Schatten GP, editor. Current Topics in Developmental Biology. Vol. 66. California; London: Elsevier Academic Press.

Ozeki Y, Komamine A. 1986. Effects of growth regulators on the induction of anthocyanin synthesis in carrot suspension cultures. Plant Cell Physiology. 27(7):1361–1368. doi:10.1093/oxfordjournals.pcp.a077234.

Pourcel L, Irani NG, Lu Y, Riedl K, Schwartz S, Grotewold E. 2010. The formation of

anthocyanic vacuolar inclusions in *Arabidopsis thaliana* and implications for the sequestration of anthocyanin pigments. Molecular Plant. 3(1):79–90.

Poustka F, Irani NG, Feller A, Lu Y, Pourcel L, Frame K, Grotewold E. 2007. A trafficking pathway for anthocyanins overlaps with the endoplasmic reticulum-to-vacuole protein-sorting route in *Arabidopsis* and contributes to the formation of vacuolar inclusions. Plant Physiology. 145(4):1323–1335. doi:10.1104/pp.107.105064.

Qi T, Song S, Ren Q, Wu D, Huang H, Chen Y, Fan M, Peng W, Ren C, Xiea D. 2011. The jasmonate-ZIM-domain proteins interact with the WD-repeat/bHLH/MYB complexes to regulate jasmonate-mediated anthocyanin accumulation and trichome initiation in *Arabidopsis thaliana*. The Plant Cell. 23(5):1795–1814. doi:10.1105/tpc.111.083261.

Quader H, Hofmann A, Schnepf E. 1989. Reorganization of the endoplasmic reticulum in epidermal cells of onion bulb scales after cold stress: Involvement of cytoskeletal elements. Planta. 177(2):273–280. doi:10.1007/BF00392816.

Quader H, Schnepf E. 1986. Endoplasmic reticulum and cytoplasmic streaming: Fluorescence microscopical observations in adaxial epidermis cells of onion bulb scales. Protoplasma. 131(3):250-2.

Reinhardt D, Pesce ER, Stieger P, Mandel T, Baltensperger K, Bennett M, Traas J, Friml J, Kuhlemeier C. 2003. Regulation of phyllotaxis by polar auxin transport. Nature. 426(6964):255–260. doi:10.1038/nature02081.

Rhodes MJC. 1994. Physiological roles for secondary metabolites in plants: Some progress, many outstanding problems. Plant Molecular Biology. 24(1):1–20. doi:10.1007/BF00040570.

Rowarth NM, Dauphinee AN, Denbigh GL, Gunawardena AHLAN. 2020. Hsp70 plays a role in programmed cell death during the remodelling of leaves of the lace plant (*Aponogeton madagascariensis*). Journal of Experimental Botany. 71(3):907–918.

Rudell DR, Fellman JK, Mattheis JP. 2005. Preharvest application of methyl jasmonate to “Fuji” apples enhances red coloration and affects fruit size, splitting, and bitter pit incidence. Journal of the American Society for Horticultural Science. 40(6):1760–1762.

Saniewski M, Horbowicz M, Puchalski J, Ueda J. 2003. Methyl jasmonate stimulates the formation and the accumulation of anthocyanin in *Kalanchoe blossfeldiana*. Acta Physiolgiae Plantarum. 25(2):143–149.

Santos EL, Maia BHLNS, Ferriani AP, Teixeira SD. 2017. Flavonoids: Classification, biosynthesis and chemical ecology. In: Justino G, editor. Flavonoids - From Biosynthesis to Human Health. InTech. p. 1–17.

Scarpella E, Barkoulas M, Tsiantis M. 2010. Control of leaf and vein development by auxin.

Cold Spring Harbor Perspectives in Biology. 2(a001511):1–17. doi:10.1101/cshperspect.a001511.

Shan X, Zhang Y, Peng W, Wang Z, Xie D. 2009. Molecular mechanism for jasmonate-induction of anthocyanin accumulation in *Arabidopsis*. Journal of Experimental Botany. 60(13):3849–3860. doi:10.1093/jxb/erp223.

Shitan N. 2016. Secondary metabolites in plants: Transport and self-tolerance mechanisms. Bioscience, Biotechnology, and Biochemistry. 80(7):1283–1293. doi:10.1080/09168451.2016.1151344.

Small CJ, Pecket RC. 1982. The ultrastructure of anthocyanoplasts in red-cabbage. Planta. 154:97–99.

Solfanelli C, Poggi A, Loreti E, Alpi A, Perata P. 2006. Sucrose-specific induction of the anthocyanin biosynthetic pathway in *Arabidopsis*. Plant Physiology. 140:637–646. doi:10.1104/pp.105.072579.

Srivastava R, Li Z, Russo G, Tang J, Bi R, Muppirala U, Chudalayandi S, Severin A, He M, Vaitkevicius SI, et al. 2018. Response to persistent ER stress in plants: A multiphasic process that transitions cells from prosurvival activities to cell death. The Plant Cell. 30(6):1220–1242. doi:10.1105/tpc.18.00153.

Stefano G, Brandizzi F. 2018. Advances in plant ER architecture and dynamics. Plant Physiology. 176(1):178–186. doi:10.1104/pp.17.01261.

Sun Y, Li H, Huang J-R. 2012. *Arabidopsis* TT19 functions as a carrier to transport anthocyanin from the cytosol to tonoplasts. Molecular Plant. 5(2):387–400.

Tanaka Y, Sasaki N, Ohmiya A. 2008. Biosynthesis of plant pigments: Anthocyanins, betalains and carotenoids. The Plant Journal. 54(4):733–749. doi:10.1111/j.1365-313X.2008.03447.x.

Taylor LP, Grotewold E. 2005. Flavonoids as developmental regulators. Current Opinion in Plant Biology. 8:317–323. doi:10.1016/j.pbi.2005.03.005.

Tian D, Wang J, Zeng X, Gu K, Qiu C, Yang X, Zhou Z, Goh M, Luo Y, Murata-Hori M, et al. 2014. The rice TAL effector-dependent resistance protein XA10 triggers cell death and calcium depletion in the endoplasmic reticulum. The Plant Cell. 26(1):497–515. doi:10.1105/tpc.113.119255.

Tiwari R, Rana CS. 2015. Plant secondary metabolites: A review. International Journal of Engineering Research and General Science. 3(5):661–670.

van Bruggen, H W E. 1985. Monograph of the genus *Aponogeton* (Aponogetonaceae). Stuttgart: Schweizerbart′sche Verlagsbuchhandlung.

Van Hautegem T, Waters AJ, Goodrich J, Nowack MK. 2015. Only in dying, life: Programmed cell death during plant development. Trends in Plant Science. 20(2):102–113. doi:10.1016/J.TPLANTS.2014.10.003.

Veberic R, Slatnar A, Bizjak J, Stampar F, Mikulic-Petkovsek M. 2015. Anthocyanin composition of different wild and cultivated berry species. Food Science and Technology. 60(1):509–517. doi:10.1016/j.lwt.2014.08.033.

Wang Y, Wang N, Xu H, Jiang S, Fang H, Su M, Zhang Z, Zhang T, Chen X. 2018. Auxin regulates anthocyanin biosynthesis through the Aux/IAA–ARF signaling pathway in apple. Horticulture Research. 5(1):59. doi:10.1038/s41438-018-0068-4.

Watanabe N, Lam E. 2008. BAX inhibitor-1 modulates endoplasmic reticulum stress-mediated programmed cell death in *Arabidopsis*. The Journal of Biological Chemistry. 283(6):3200–3210. doi:10.1074/jbc.M706659200.

Wright H, van Doorn WG, Gunawardena AHLAN. 2009. In vivo study of developmental programmed cell death using the lace plant (*Aponogeton madagascariensis*; Aponogetonaceae) leaf model system. American Journal of Botany. 96(5):865–876. doi:10.3732/ajb.0800343.

Wrolstad RE, Durst RW, Lee J. 2005. Tracking color and pigment changes in anthocyanin products. Trends in Food Science and Technology. 16(9):423–428. doi:10.1016/j.tifs.2005.03.019.

Young JC, Abdel-Aal ESM. 2009. Anthocyanins. In: Shewry PR, Ward JL, editors. Healthgrain Methods: Analysis of Bioactive Components in Small Grain Cereals. Elsevier Inc. p. 141–165.

Zhang Y, Butelli E, Martin C. 2014. Engineering anthocyanin biosynthesis in plants. Current Opinion in Plant Biology. 19:81–90. doi:10.1016/j.pbi.2014.05.011.

Zhang H, Wang L, Deroles S, Bennett R, Davies K. 2006. New insight into the structures and formation of anthocyanic vacuolar inclusions in flower petals. BMC Plant Biology. 6(1):1–14. doi:10.1186/1471-2229-6-29.

Zuppini A, Baldan B, Millioni R, Favaron F, Navazio L, Mariani P. 2004. Chitosan induces Ca^{2+} -mediated programmed cell death in soybean cells. New Phytology. 161(2):557–568. doi:10.1046/j.1469-8137.2003.00969.x.

APPENDICES

Appendix 1. Window and mature stage leaf anthocyanin extraction data. Percent extracted from window stage leaves is significantly more than mature stage leaves ($t = 2.890$, $df = 18$, $P = 0.0098$).

Window stage leaf weight (mg)	Window stage leaf extract weight (mg)	% Extracted from window stage leaves	Mature stage leaf weight (mg)	Mature stage leaf extract weight (mg)	% Extracted from mature stage leaves
820	23.6	2.878	13830	352	2.545
2920	102	3.493	8190	199.7	2.438
1400	43.5	3.107	3180	59.8	1.881
3180	78.5	2.469	13000	267.3	2.056
860	24.5	2.849	4790	123.5	2.578
1690	42.5	2.515	3130	72.3	2.309
2500	77.9	3.116	3430	82.6	2.408
2542.7	51.4	2.021	3885	97.8	2.517
940	24.5	2.606	5030	119.6	2.378
2541	81.3	3.199	22221	586.4	2.639

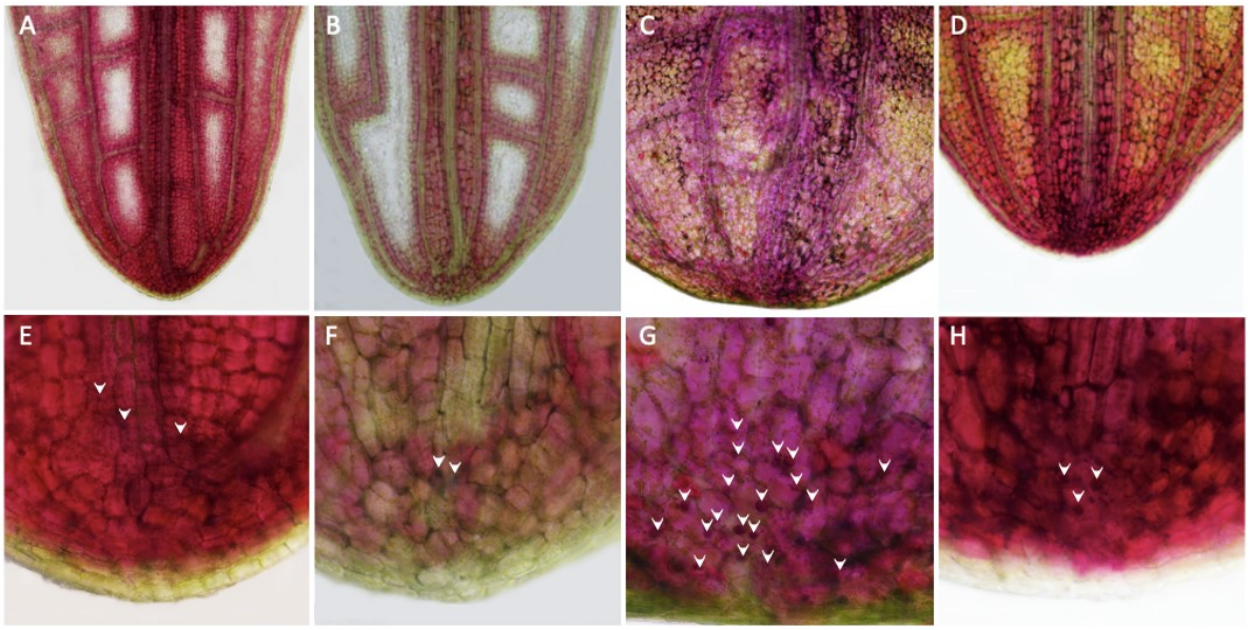

Appendix 2. Presence of anthocyanins in window stage leaves grown under normal and stressful conditions. Leaf apex of window stage leaves grown under normal (A-B) and stressful (C-D) conditions at low magnification. (E-H) Corresponding images at higher magnification. Anthocyanin vacuolar inclusions (AVIs; white arrowheads) are visible at the leaf apex at higher magnification.

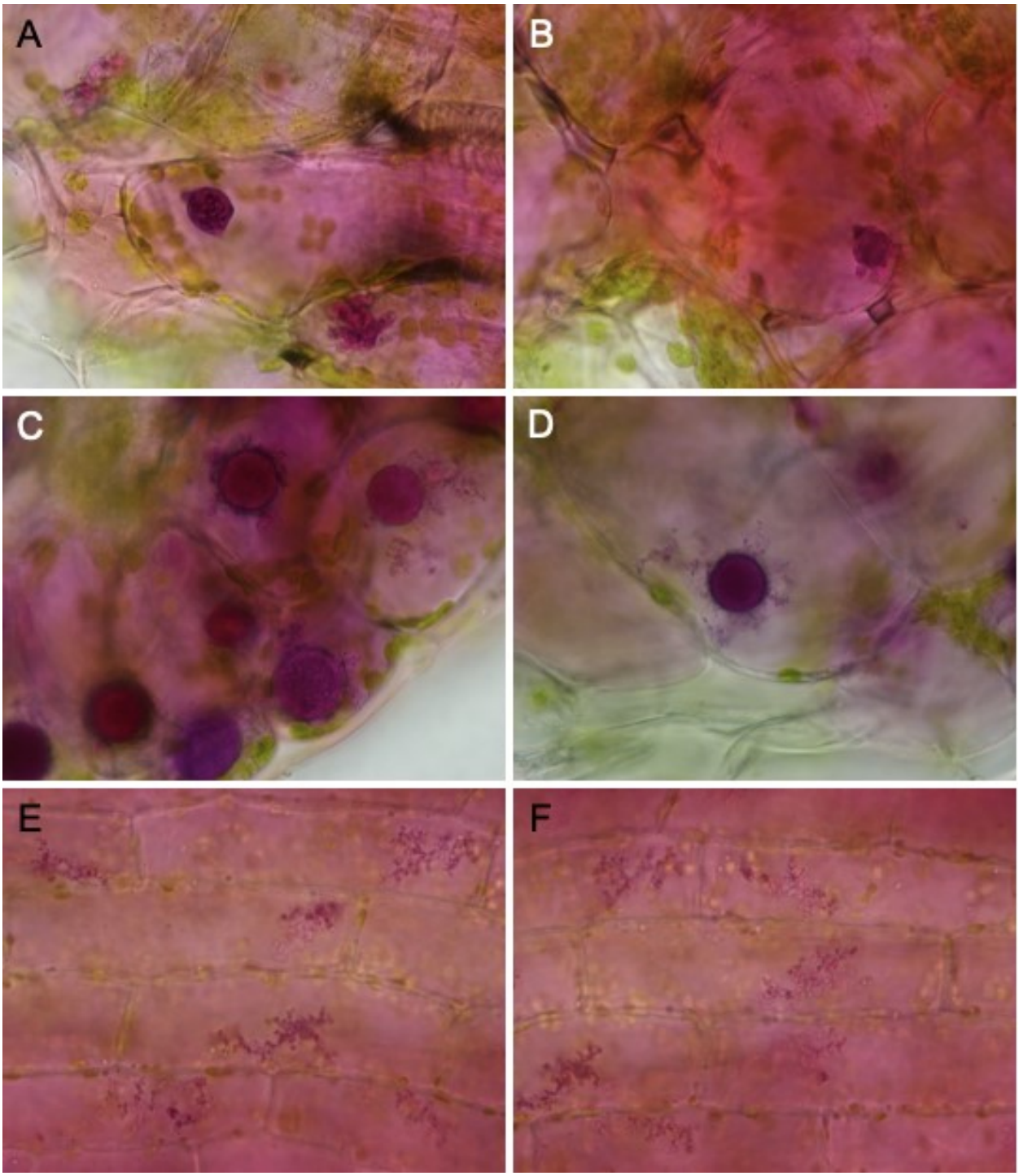

Appendix 3. Anthocyanin vacuolar inclusions (AVIs) in window stage leaves grown in stressful conditions. (A-B) AVIs can be seen as globular bodies, (C-D) spherical bodies that exhibit a liquid-like behavior, and (E-F) fibrous aggregates.

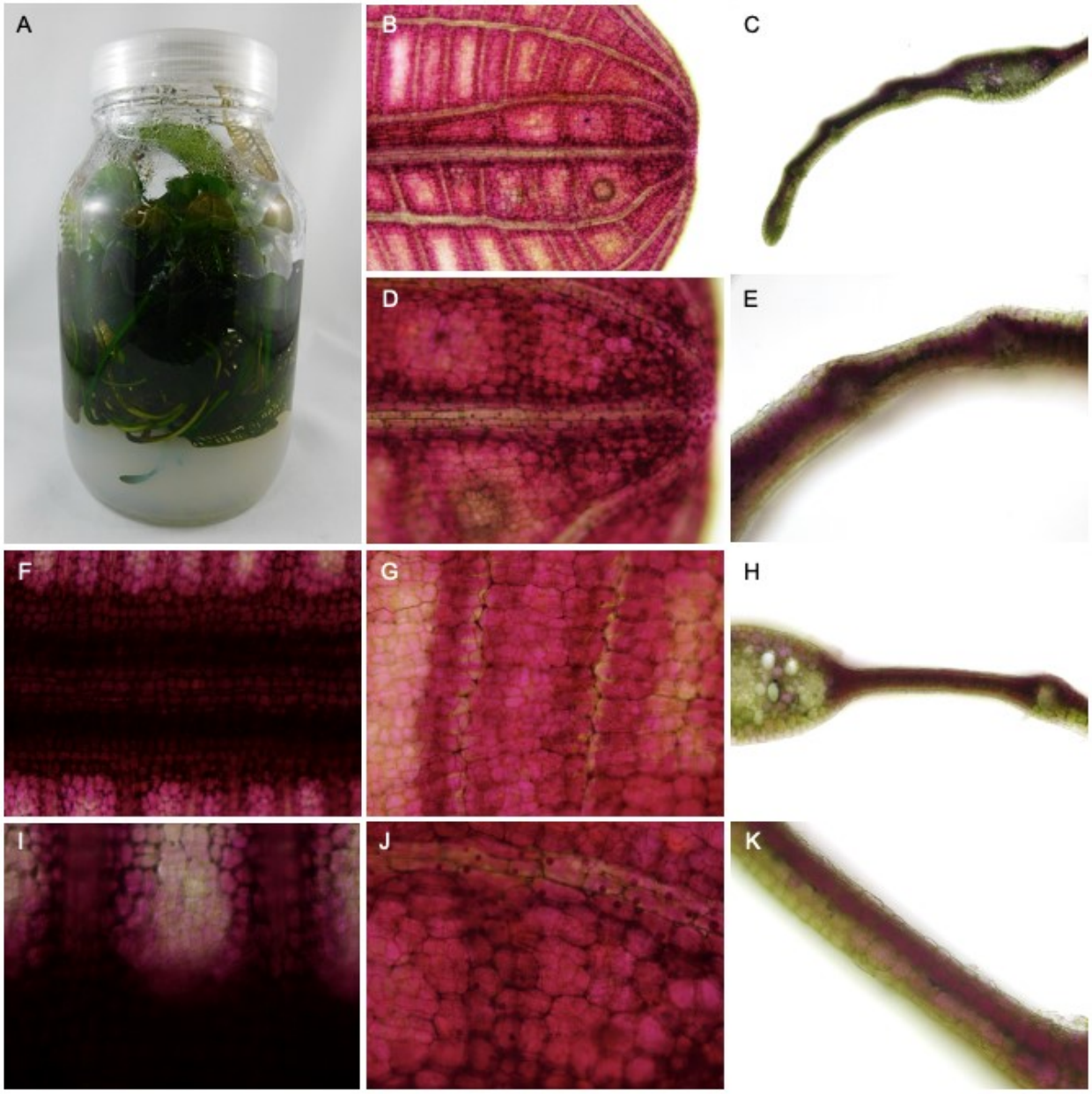

Appendix 4. Investigation of anthocyanin in window stage lace plant leaves grown in stressful conditions. (A) Window stage leaves were obtained from sterile cultures that were overgrown and limited in light and nutrients. (B) Micrographs of the stressed window-leaf apex (top 10% of the total leaf blade length) and (C) corresponding cross-section at low magnification and (D-E) apex micrographs at higher magnification. (F-K) Micrographs of the mid-region of stressed window stage leaves (top 10 to 25% of the total leaf blade length). (F) Window mid-vein, (G) areole, (H) cross-section at low magnification and (I-K) corresponding areas at higher magnification.

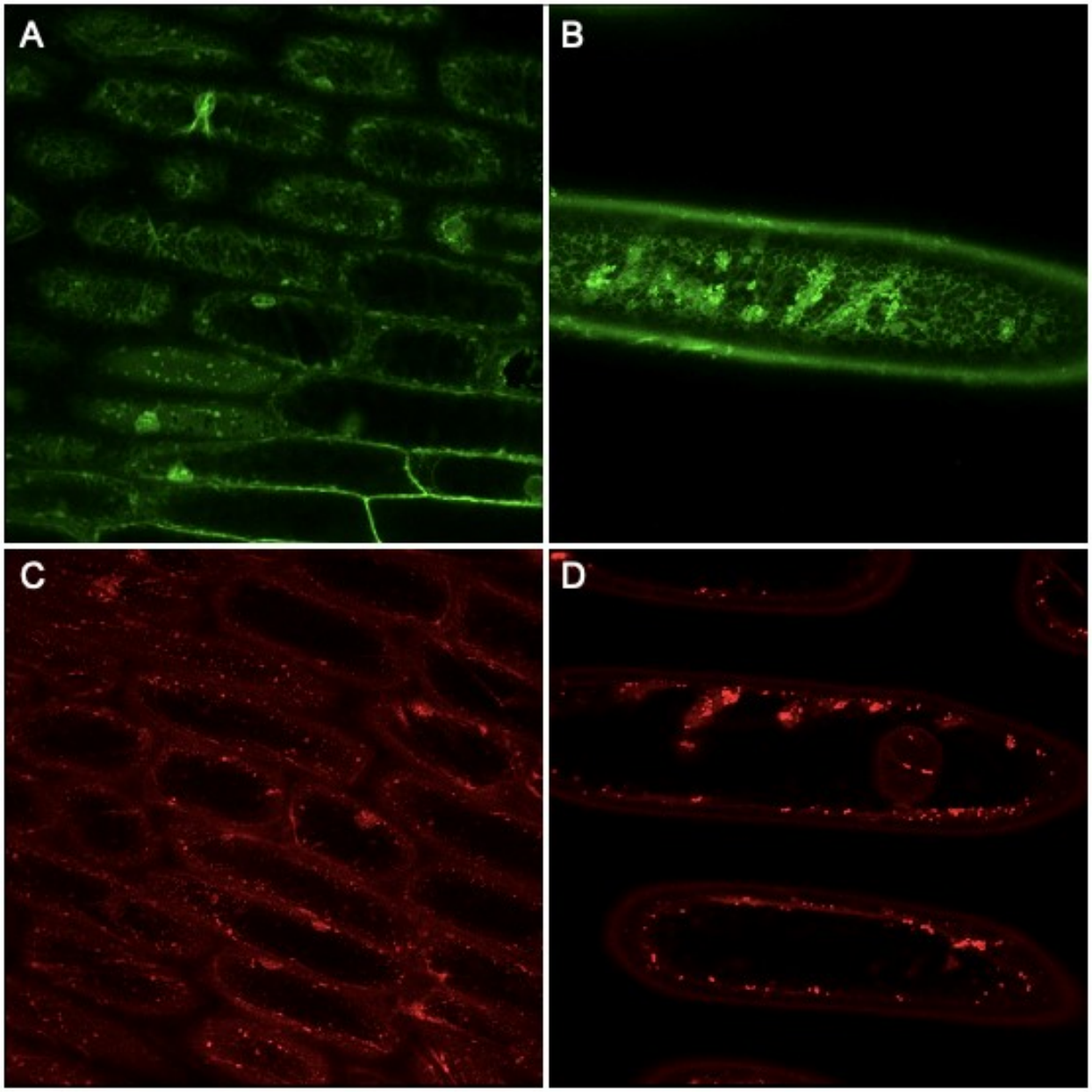

Appendix 5. Morphology of endoplasmic reticulum and mitochondria in onion bulb cells. (A) Onion cells stained with stained with ER dye, 3,3'-dihexyloxacarbocyanine iodide (DiOC6[3]), at low magnification and (B) higher magnification. (C) Onion cells stained with mitochondria dye, Mitotracker Red CMXRos, at low magnification and (D) higher magnification.

Appendix 6. Data and statistical analysis for whole plant experiments using anthocyanin biosynthesis promoter, methyl jasmonate (MeJA). Leaf length, leaf width, number of perforations, and relative anthocyanin abundance was recorded in plants treated with various concentrations of MeJA (0, 1, 2.5 or 5 µM).

Replicate Number		Leaf 0	Leaf 1	Leaf 2
Leaf length (cm)				
Control	Rep 1	10.55	12.194	7.652
	Rep 2	12.898	14.66	10.48
	Rep 3	11.589	11.589	
	Rep 4	16.422	3.379	
1 µM MeJA	Rep 1	8.643	12.33	
	Rep 2	7.297	7.988	5.557
	Rep 3	10.687	6.372	
	Rep 4	11.782	8.129	4.48
2.5 µM MeJA	Rep 1	4.03	5.089	3.312
	Rep 2	6.646	7.68	3.298
	Rep 3	11.16	7.847	
	Rep 4	11.877	11.877	
5 µM MeJA	Rep 1	6.919	6.126	2.985
	Rep 2		6.046	5.53
	Rep 3	9.202	6.892	6.8
	Rep 4	9.417	7.831	3.457
Leaf width (cm)				
Control	Rep 1	2.307	2.659	2.159
	Rep 2	2.794	3	2.09
	Rep 3	2.369	2.369	
	Rep 4	3.26	1.115	
1 µM MeJA	Rep 1	1.837	2.395	1.226
	Rep 2	1.774	1.71	
	Rep 3	2.956	1.961	0.807
	Rep 4	2.117	1.31	
2.5 µM MeJA	Rep 1	1.224	1.334	0.807
	Rep 2	1.214	1.448	0.778
	Rep 3	2.313	1.685	0.793
	Rep 4	2.569	2.569	
5 µM MeJA	Rep 1	2.165	1.596	0.742
	Rep 2	1.889	1.189	1.352
	Rep 3	1.778	1.601	1.967
	Rep 4	1.959	1.625	0.906

Perforation number					
Control	Rep 1	108	196		114
	Rep 2	275	309		373
	Rep 3	168	171		
	Rep 4	365	98		
1 μM MeJA	Rep 1	259	330		
	Rep 2	132	172		116
	Rep 3	284	193		
	Rep 4	361	397		325
2.5 μM MeJA	Rep 1	63	94		123
	Rep 2	164	265		104
	Rep 3	420	436		
	Rep 4	184	183		
5 μM MeJA	Rep 1	172	174		100
	Rep 2	58	87		120
	Rep 3	190	194		348
	Rep 4	183	338		84
Relative anthocyanin absorbance (a.u.)					
Control	Rep 1	0.0905	0.09		0.282
	Rep 2	0.01766	0.595		0.5435
	Rep 3	0.4185	1.157		0.711
	Rep 4	0.3966	1.928		0.994
1 μM MeJA	Rep 1	0.108	0.396		1.417
	Rep 2	0.403	1.13		0.589
	Rep 3	0.59166	0.884		2.629
	Rep 4	1.192	1.357		2.2156
2.5 μM MeJA	Rep 1	0.2305	0.312		1.895
	Rep 2	0.10966	0.1496		1.588
	Rep 3	0.7575	1.5355		2.115
	Rep 4	0.3006	1.176		
5 μM MeJA	Rep 1	0.3103	0.1315		1.924
	Rep 2	0.0896	0.145		
	Rep 3	1.7135	0.294		1.2136
	Rep 4	0.858	0.709		1.929

Two-way ANOVA table for leaf length in control and MeJA-treated plants.

ANOVA table	SS (Type III)	DF	MS	F (DFn, DFd)	P value
Interaction	11.50	6	1.917	F (6, 29) = 0.2663	P=0.9482
Row Factor	106.8	2	53.42	F (2, 29) = 7.419	P=0.0025
Column Factor	107.4	3	35.81	F (3, 29) = 4.973	P=0.0066

Residual	208.8	29	7.200		

Dunnett's multiple comparisons test for leaf length in control and MeJA-treated plants.

Dunnett's multiple comparisons test	Predicted (LS) mean diff.	95.00% CI of diff.	Significant?	Summary	Adjusted P Value
Leaf 0					
Control vs. 1 µM	3.263	-1.450 to 7.975	No	ns	0.2277
Control vs. 2.5 µM	4.437	-0.2757 to 9.149	No	ns	0.0685
Control vs. 5 µM	4.352	-0.7376 to 9.442	No	ns	0.1068
Leaf 1					
Control vs. 1 µM	1.751	-2.952 to 6.453	No	ns	0.6827
Control vs. 2.5 µM	2.332	-2.370 to 7.035	No	ns	0.4780
Control vs. 5 µM	3.732	-0.9708 to 8.434	No	ns	0.1433
Leaf 2					
Control vs. 1 µM	4.048	-2.569 to 10.66	No	ns	0.3094
Control vs. 2.5 µM	5.761	-0.8550 to 12.38	No	ns	0.0977
Control vs. 5 µM	4.373	-1.357 to 10.10	No	ns	0.1630

Two-way ANOVA table for leaf width in control and MeJA-treated plants.

ANOVA table	SS (Type III)	DF	MS	F (DFn, DFd)	P value
Interaction	0.8109	6	0.1352	F (6, 31) = 0.5380	P=0.7752
Row Factor	4.629	2	2.314	F (2, 31) = 9.212	P=0.0007
Column Factor	4.757	3	1.586	F (3, 31) = 6.312	P=0.0018
Residual	7.789	31	0.2512		

Dunnett's multiple comparisons test for leaf width in control and MeJA-treated plants.

Dunnett's multiple comparisons test	Predicted (LS) mean diff.	95.00% CI of diff.	Significant?	Summary	Adjusted P Value
Leaf 0					
Control vs. 1 µM	0.5115	-0.3638 to 1.387	No	ns	0.3516

Control vs. 2.5 µM	0.8525	-0.02283 to 1.728	No	ns	0.0576
Control vs. 5 µM	0.7348	-0.1406 to 1.610	No	ns	0.1154
Leaf 1					
Control vs. 1 µM	0.4418	-0.4336 to 1.317	No	ns	0.4664
Control vs. 2.5 µM	0.5268	-0.3486 to 1.402	No	ns	0.3290
Control vs. 5 µM	0.7830	-0.09233 to 1.658	No	ns	0.0875
Leaf 2					
Control vs. 1 µM	1.108	-0.1189 to 2.335	No	ns	0.0830
Control vs. 2.5 µM	1.332	0.2119 to 2.452	Yes	*	0.0171
Control vs. 5 µM	0.8828	-0.1797 to 1.945	No	ns	0.1184

Two-way ANOVA table for number of perforations in control and MeJA-treated plants.

ANOVA table	SS (Type III)	DF	MS	F (DFn, DFd)	P value
Interaction	26853	6	4476	F (6, 30) = 0.3337	P=0.9137
Row Factor	10295	2	5147	F (2, 30) = 0.3838	P=0.6846
Column Factor	37977	3	12659	F (3, 30) = 0.9439	P=0.4318
Residual	402349	30	13412		

Dunnett's multiple comparisons test for number of perforations in control and MeJA-treated plants.

Dunnett's multiple comparisons test	Predicted (LS) mean diff.	95.00% CI of diff.	Significant?	Summary	Adjusted P Value
Leaf 0					
Control vs. 1 µM	-30.00	-232.6 to 172.6	No	ns	0.9676
Control vs. 2.5 µM	21.25	-181.3 to 223.8	No	ns	0.9878
Control vs. 5 µM	78.25	-124.3 to 280.8	No	ns	0.6602
Leaf 1					
Control vs. 1 µM	-80.25	-282.8 to 122.3	No	ns	0.6436
Control vs. 2.5 µM	-52.00	-254.6 to 150.6	No	ns	0.8614

Control vs. 5 µM	-5.500	-208.1 to 197.1	No	ns	0.9999
Leaf 2					
Control vs. 1 µM	23.00	-262.0 to 308.0	No	ns	0.9939
Control vs. 2.5 µM	130.0	-155.0 to 415.0	No	ns	0.5336
Control vs. 5 µM	80.50	-166.3 to 327.3	No	ns	0.7501

Two-way ANOVA table for relative anthocyanin abundance in control and MeJA-treated plants.

ANOVA table	SS (Type III)	DF	MS	F (DFn, DFd)	P value
Interaction	3.816	6	0.6359	F (6, 34) = 2.231	P=0.0638
Row Factor	7.759	2	3.880	F (2, 34) = 13.61	P<0.0001
Column Factor	1.555	3	0.5182	F (3, 34) = 1.818	P=0.1624
Residual	9.691	34	0.2850		

Dunnett's multiple comparisons test for relative anthocyanin abundance in control and MeJA-treated plants.

Dunnett's multiple comparisons test	Predicted (LS) mean diff.	95.00% CI of diff.	Significant?	Summary	Adjusted P Value
Leaf 0					
Control vs. 1 µM	-0.3429	-1.271 to 0.5853	No	ns	0.6921
Control vs. 2.5 µM	-0.1188	-1.047 to 0.8094	No	ns	0.9789
Control vs. 5 µM	-0.5120	-1.440 to 0.4161	No	ns	0.3988
Leaf 1					
Control vs. 1 µM	0.0007500	-0.9274 to 0.9289	No	ns	>0.9999
Control vs. 2.5 µM	0.1492	-0.7789 to 1.077	No	ns	0.9600
Control vs. 5 µM	0.6226	-0.3055 to 1.551	No	ns	0.2508
Leaf 2					
Control vs. 1 µM	-1.080	-2.012 to -0.1483	Yes	*	0.0197
Control vs. 2.5 µM	-1.233	-2.240 to -0.2270	Yes	*	0.0131
Control vs. 5 µM	-1.056	-2.063 to -0.04986	Yes	*	0.0378

Appendix 8. Data and statistical analysis for whole plant experiments using anthocyanin biosynthesis inhibitor, pheidone. Leaf length, leaf width, number of perforations, and relative anthocyanin abundance was recorded in plants treated with various concentrations of phenidone (0, 10, 100 or 200 μM).

	Replicate Number	Leaf 0	Leaf 1	Leaf 2
Leaf length (cm)				
Control	Rep 1	8	8.02	
	Rep 2	7.857	5.072	
	Rep 3	10.133	11.546	7.163
	Rep 4	12.148	11.065	7
10 μM Phenidone	Rep 1	10.81	9.553	5.11
	Rep 2	12.734	4.307	
	Rep 3	11.316	9.864	6.053
	Rep 4			
100 μM Phenidone	Rep 1	10.965	5.999	6.704
	Rep 2	10.486	7.011	
	Rep 3	9.691	9.737	
	Rep 4	9.355	9.224	9.837
200 μM Phenidone	Rep 1	10.401	8.14	7.005
	Rep 2	10.55	6.406	
	Rep 3	8.374	9.675	
	Rep 4	9.177	9.281	6.5
Leaf width (cm)				
Control	Rep 1	1.667	1.69	
	Rep 2	1.607	1	0.6
	Rep 3	2.531	2.469	1.318
	Rep 4	2.355	2.211	
10 μM Phenidone	Rep 1	2.048	2.13	1.304
	Rep 2	2.281		
	Rep 3	2.661	2.073	3.55
	Rep 4			
100 μM Phenidone	Rep 1	2.116	1.333	1.279
	Rep 2	2.258	1.381	0.406
	Rep 3	2	1.893	
	Rep 4	1.899	2.165	2.108
200 μM Phenidone	Rep 1	2.165	1.501	1.384
	Rep 2	1.889	1.185	
	Rep 3	1.778	2.212	2.034
	Rep 4	1.959	2.306	

Perforation number				
Control	Rep 1	80	82	
	Rep 2	103	103	150
	Rep 3	226	150	55
	Rep 4	129	192	
10 μM Phenidone	Rep 1	12	34	77
	Rep 2	104	11	
	Rep 3	227	199	154
	Rep 4			
100 μM Phenidone	Rep 1	100	63	50
	Rep 2	139	37	0
	Rep 3	158	177	
	Rep 4	127	200	52
200 μM Phenidone	Rep 1	67	104	
	Rep 2	202	0	0
	Rep 3	199	185	196
	Rep 4	165	73	
Relative anthocyanin absorbance (a.u.)				
Control	Rep 1	0.3885	1.447	1.011
	Rep 2	0.555	0.315	1.122
	Rep 3	0.43666	0.364	
	Rep 4	0.387	0.497	1.4733
10 μM Phenidone	Rep 1	0.379	0.322	0.423
	Rep 2	0.5375	1.01	1.726
	Rep 3	0.4115	0.54	
	Rep 4			
100 μM Phenidone	Rep 1	1.276	0.4755	0.42433
	Rep 2	0.595	0.448	0.481
	Rep 3	0.324	0.54	
	Rep 4	0.324	0.628	0.538
200 μM Phenidone	Rep 1	0.444	1.2985	0.803
	Rep 2	0.5685	0.514	0.2735
	Rep 3	0.333	0.5113	0.469
	Rep 4	0.4035	0.32666	0.3855

Two-way ANOVA table for leaf length in control and phenidone-treated plants.

ANOVA table	SS (Type III)	DF	MS	F (DFn, DFd)	P value
Interaction	18.14	6	3.023	F (6, 26) = 0.9006	P=0.5094
Row Factor	61.92	2	30.96	F (2, 26) = 9.224	P=0.0009
Column Factor	1.471	3	0.4902	F (3, 26) = 0.1461	P=0.9313

Residual	87.27	26	3.356	

Dunnett’s multiple comparisons test for leaf length in control and phenidone-treated plants.

Dunnett's multiple comparisons test	Predicted (LS) mean diff.	95.00% CI of diff.	Significant?	Summary	Adjusted P Value
Leaf 0					
Control vs. 10 µM	-2.085	-5.582 to 1.412	No	ns	0.3339
Control vs. 100 µM	-0.5895	-3.827 to 2.648	No	ns	0.9427
Control vs. 200 µM	-0.09075	-3.328 to 3.147	No	ns	0.9997
Leaf 1					
Control vs. 10 µM	1.013	-2.484 to 4.510	No	ns	0.8152
Control vs. 100 µM	0.9282	-2.309 to 4.166	No	ns	0.8196
Control vs. 200 µM	0.5455	-2.692 to 3.783	No	ns	0.9536
Leaf 2					
Control vs. 10 µM	1.500	-3.069 to 6.069	No	ns	0.7520
Control vs. 100 µM	-1.189	-5.758 to 3.380	No	ns	0.8539
Control vs. 200 µM	0.3290	-4.240 to 4.898	No	ns	0.9958

Two-way ANOVA table for leaf width in control and phenidone-treated plants.

ANOVA table	SS (Type III)	DF	MS	F (DFn, DFd)	P value
Interaction	1.315	6	0.2192	F (6, 26) = 0.7034	P=0.6495
Row Factor	1.429	2	0.7146	F (2, 26) = 2.293	P=0.1210
Column Factor	2.081	3	0.6935	F (3, 26) = 2.225	P=0.1091
Residual	8.103	26	0.3117		

Dunnett’s multiple comparisons test for leaf width in control and phenidone-treated plants.

Dunnett's multiple comparisons test	Predicted (LS) mean diff.	95.00% CI of diff.	Significant?	Summary	Adjusted P Value
Leaf 0					

Control vs. 10 µM	-0.2900	-1.356 to 0.7756	No	ns	0.8403
Control vs. 100 µM	-0.02825	-1.015 to 0.9583	No	ns	0.9997
Control vs. 200 µM	0.09225	-0.8943 to 1.079	No	ns	0.9913
Leaf 1					
Control vs. 10 µM	-0.2648	-1.476 to 0.9468	No	ns	0.9098
Control vs. 100 µM	0.1438	-0.8455 to 1.133	No	ns	0.9702
Control vs. 200 µM	0.03575	-0.9535 to 1.025	No	ns	0.9995
Leaf 2					
Control vs. 10 µM	-1.468	-2.856 to -0.07992	Yes	*	0.0366
Control vs. 100 µM	-0.3053	-1.572 to 0.9618	No	ns	0.8752
Control vs. 200 µM	-0.7500	-2.138 to 0.6381	No	ns	0.4031

Two-way ANOVA table for number of perforations in control and phenidone-treated plants.

ANOVA table	SS (Type III)	DF	MS	F (DFn, DFd)	P value
Interaction	16217	6	2703	F (6, 27) = 0.5082	P=0.7967
Row Factor	13396	2	6698	F (2, 27) = 1.259	P=0.3000
Column Factor	4563	3	1521	F (3, 27) = 0.2860	P=0.8351
Residual	143599	27	5318		

Dunnett's multiple comparisons test for number of perforations in control and phenidone-treated plants.

Dunnett's multiple comparisons test	Predicted (LS) mean diff.	95.00% CI of diff.	Significant?	Summary	Adjusted P Value
Leaf 0					
Control vs. 10 µM	20.17	-118.7 to 159.1	No	ns	0.9695
Control vs. 100 µM	3.500	-125.1 to 132.1	No	ns	0.9999
Control vs. 200 µM	-23.75	-152.3 to 104.8	No	ns	0.9408
Leaf 1					
Control vs. 10 µM	49.92	-88.98 to 188.8	No	ns	0.7060

Control vs. 100 µM	12.00	-116.6 to 140.6	No	ns	0.9914
Control vs. 200 µM	40.75	-87.84 to 169.3	No	ns	0.7748
Leaf 2					
Control vs. 10 µM	-13.00	-193.9 to 167.9	No	ns	0.9957
Control vs. 100 µM	69.17	-95.99 to 234.3	No	ns	0.5961
Control vs. 200 µM	4.500	-176.4 to 185.4	No	ns	0.9999

Two-way ANOVA table for relative anthocyanin abundance in control and phenidone-treated plants.

ANOVA table	SS (Type III)	DF	MS	F (DFn, DFd)	P value
Interaction	1.149	6	0.1915	F (6, 30) = 1.653	P=0.1673
Row Factor	0.6658	2	0.3329	F (2, 30) = 2.872	P=0.0722
Column Factor	0.4602	3	0.1534	F (3, 30) = 1.324	P=0.2851
Residual	3.477	30	0.1159		

Dunnett's multiple comparisons test for relative anthocyanin abundance in control and phenidone-treated plants.

Dunnett's multiple comparisons test	Predicted (LS) mean diff.	95.00% CI of diff.	Significant?	Summary	Adjusted P Value
Leaf 0					
Control vs. 10 µM	-0.0008767	-0.6454 to 0.6437	No	ns	>0.9999
Control vs. 100 µM	-0.1880	-0.7847 to 0.4088	No	ns	0.7806
Control vs. 200 µM	0.004540	-0.5922 to 0.6013	No	ns	>0.9999
Leaf 1					
Control vs. 10 µM	0.03175	-0.6128 to 0.6763	No	ns	0.9987
Control vs. 100 µM	0.1329	-0.4639 to 0.7296	No	ns	0.9049
Control vs. 200 µM	-0.006865	-0.6036 to 0.5899	No	ns	>0.9999
Leaf 2					
Control vs. 10 µM	0.1276	-0.6419 to 0.8971	No	ns	0.9560

Control vs. 100 µM	0.7210	0.03270 to 1.409	Yes	*	0.0384
Control vs. 200 µM	0.7194	0.07551 to 1.363	Yes	*	0.0257

SUPPLEMENTARY MATERIAL

Supplementary material 1. Movement of anthocyanin vacuolar inclusions (AVIs) in the vasculature of window stage leaves grown under stressful conditions. Total magnification = 200x.

Supplementary material 2. Time-lapse video (20 sec) of non-PCD (NPCD) cells in window stage leaves stained with fluorescent ER dye, DiOC6(3). Total magnification = 400x.

Supplementary material 3. Time-lapse video (20 sec) of early-PCD (EPCD) cells in window stage leaves stained with fluorescent ER dye, DiOC6(3). Total magnification = 400x.

Supplementary material 4. Time-lapse video (20 sec) of late-PCD (LPCD) cells in window stage leaves stained with fluorescent ER dye, DiOC6(3). Total magnification = 400x.

Supplementary material 5. Time-lapse video (20 sec) of cells in mature stage leaves stained with fluorescent ER dye, DiOC6(3). Total magnification = 1000x.

Supplementary material 6. Time-lapse video (20 sec) of onion cells stained with stained with fluorescent ER dye, DiOC6(3). Total magnification = 600x.

Supplementary material 7. Time-lapse video (20 sec) of onion cells stained with stained with fluorescent mitochondria dye, mitotracker red CMXRos Total magnification = 600x.